CANADIAN THESES

THÈSES CANADIENNES

NOTICE

The quality of this microfiche is heavily dependent upon the quality of the original thesis submitted for microfilming. Every effort has been made to ensure the highest quality of reproduction possible.

If pages are missing, contact the university which granted the degree.

Some pages may have indistinct print especially if the original pages were typed with a poor typewriter ribbon or if the university sent us an inferior photocopy.

Previously copyrighted materials (journal articles, published tests, etc.) are not filmed.

Reproduction in full or in part of this film is governed by the Canadian Copyright Act, R.S.C. 1970, c. C-30. Please read the authorization forms which accompany this thesis.

AVIS

La qualité de cette microfiche dépend grandement de la qualité de la thèse soumise au microfilmage. Nous avons tout fait pour assurer une qualité supérieure de reproduction.

S'il manque des pages, veuillez communiquer avec l'université qui a conféré le grade.

La qualité d'impression de certaines pages peut laisser à désirer, surtout si les pages originales ont été dactylographiées à l'aide d'un ruban usé ou si l'université nous a fait parvenir une photocopie de qualité inférieure.

Les documents qui font déjà l'objet d'un droit d'auteur (articles de revue, examens publiés, etc.) ne sont pas microfilmés.

La reproduction, même partielle, de ce microfilm est soumise à la Loi canadienne sur le droit d'auteur, SRC 1970, c. C-30. Veuillez prendre connaissance des formules d'autorisation qui accompagnent cette thèse.

THIS DISSERTATION
HAS BEEN MICROFILMED
EXACTLY AS RECEIVED

LA THÈSE A ÉTÉ
MICROFILMÉE TELLE QUE
NOUS L'AVONS REÇUE

EXPERIMENTS ON UNIFORMLY SHEARED TURBULENCE

by

UMESH KARNIK

A thesis
presented to the University of Ottawa
in partial fulfillment of the
requirements for the degree of
MASTER OF APPLIED SCIENCE
in
DEPARTMENT OF MECHANICAL ENGINEERING

OTTAWA, Ontario, 1983

UNIVERSITÉ D'OTTAWA
UNIVERSITY OF OTTAWA

ABSTRACT

Turbulent flows with uniform mean velocity gradients and transversely homogeneous statistical features have been generated in a specially designed wind tunnel. Values of mean shear in the range of 13.4 s-1 84 s-1 were achieved by adjusting the centreline mean speed and by inserting grids of different mesh sizes. In all cases, the uniform mean shear exhibited near downstream constancy.

A search for universal asymptotic features of uniformly sheared turbulence using past and present data revealed that the Reynolds stresses and the turbulent kinetic energy grew exponentially in the cases of sufficiently strong shear with the rate of growth depending on the strength of the shear. In the cases of relatively weak shear these parameters reached constant asymptotic values. The streamwise velocity integral length scales grew exponentially at a rate which was nearly independent of the mean shear and different from that of the turbulent kinetic energy. It was also noticed that in all cases the dimensionless Reynolds stress tensor attained quasi-universal asymptotic values.

ACKNOWLEDGEMENTS

Words are inadequate to express my gratitude to Prof. Stavros Tavoularis for his thought provoking guidance and constant encouragement which have proved to be the key factors in completing the task in hand. His quick editing and comments during the writing of this dissertation were invaluable.

Thanks are due to Lancen Boukhriss and George Spak for completing the construction of the wind tunnel and to Don Seaman for providing general assistance when needed.

The financial support provided by NSERC and the University of Ottawa Rector's fund for conducting this research is greatly appreciated as also is the monetary assistance provided by the R.D.Sethna, Purshottamdas Narottamdas, Godrej and N.M.Wadia trusts, which supported me initially.

To my fiancee Padmaja, for her consistent morale boosting letters, I am greatly indebted.

NOMENCLATURE

h	height of test section
K_{ij}	normalized Reynolds stress tensor
L_{in}	initial length scale
L_{1f}	streamwise velocity integral length scale
ℓ	characteristic length
M	grid mesh size
P	turbulent kinetic energy production rate
q^2	turbulent kinetic energy ($= \overline{u_i u_i}$)
u_c	"characteristic velocity"
u_i	velocity fluctuation in i-direction
$\overline{U}_1$	streamwise mean velocity
$\overline{U}_c$	centreline mean velocity
x_g	downstream position of grid
x_i	co-ordinate axes; x_1 is parallel to the flow, x_2 is panallel to the mean shear and x_3 is perpendicular to the above

Greek symbols

ε	turbulent kinetic energy dissipation rate
ν	kinematic viscosity

Suffixes

$(\ )'$	root-mean-square value
$(\overline{\ })$	time averaged quantity
$(\ )_r$	reference value

CONTENTS

LIST OF TABLES

LIST OF FIGURES

Chapter I

INTRODUCTION

1.1 A BRIEF REVIEW OF TURBULENCE

Historically, the first detailed observations and descriptions of turbulence in the form of drawings by Leonardo da Vinci can be traced back to the 15th century. However the first detailed experiments on turbulent flow were probably performed by Hagen (1839), who studied the flow of water through round tubes and observed two distinct kinds of flow which are now known as laminar (Hagen-Poiseuille) and turbulent. Hagen (1854) later observed that viscosity and velocity influenced the occurrence of one or the other flow regimes. Reynolds (1883) confirmed this theory by introducing a parameter now known as the Reynolds number, which is defined as the product of the characteristic velocity and the characteristic length divided by the kinematic viscosity of the flow medium. In those studies, the adjective 'sinuous' was prevalent but the term 'turbulent flow' was introduced by Lord Kelvin in 1887.

Turbulent flows and their effects are encountered in nature and in almost every case where fluid motion is involved. Over the years, the study of turbulence has been

directed towards understanding its occurrence and structure and towards formulating practical procedures for its prediction.

Turbulence, arising from flow instabilities at large Reynolds numbers, is a feature of fluid flow and not a property of any particular fluid. Turbulence is characterized by its properties of randomness and irregularity, high diffusivity, rapid mixing and increased rates of momentum, heat and mass transfer and energy dissipation into heat. Turbulence is treated as continuum phenomenon, governed by the basic equations of mechanics and not described by molecular motion.

Turbulence cannot maintain itself and depends on its environment to obtain energy. A common source of energy is shear i.e. non-uniformities in the mean flow. Thus turbulent flows are generally shear flows. In the absence of shear or other maintainence mechanism, turbulence decays and the flow becomes laminar again. A familiar example of such an occurence is turbulence produced behind a grid placed across a uniform stream in a wind tunnel.

Reynolds (1894) introduced statistical methods in the description of turbulence by decomposing the velocity into mean and fluctuating parts. The statistical approach, necessary to study turbulence because of its random nature, introduced fundamental difficulties caused by the non-linearity of the Navier-Stokes equation, and is known as the

'closure problem' of turbulence theory. This problem could be solved approximately with the use of semi-empirical relations between various turbulent quantities. The study of turbulence can be further simplified by assuming certain symmetry relations in the statistical sense e.g. 'isotropy', viz. invariance under translation , reflection and rotation of the co-ordinate axes, a concept introduced by Taylor (1935).

Experimental techniques have provided the most reliable results for turbulent flows. However most of the known results have been collected in simplified cases of turbulent flows, since they can be easily reproduced and controlled in the laboratory. It is evident that the more complex turbulent flows contain several elements of these simplified cases. Although turbulence research has been intensive in the last thirty years, it appears that complicated technological flows are still far from being completely understood and modeled.

1.2 LITERATURE REVIEW

Traditional turbulent shear flows such as boundary layers, pipe flows, jets and wakes, were found to have shear carrying eddies which were comparable in size to the distance between the flow boundaries and would probably be affected by the boundary conditions (Corrsin, 1957). Homogene-

ous turbulence maintained by a uniform mean shear seemed to be the simplest conceivable shear flow in which the relation between shear stress and the mean velocity gradient could be studied without the complicating effects of the boundary conditions.

Analytical insight to the problem of exactly homogeneous turbulent shear flow has been provided by several investigators. Assuming that a stationary asymptotic state is possible, Reis (1952), Burgers & Mitchner (1953) and Craya (1958) have traced the symmetry properties of various velocity correlations.

The idea that a transversely homogeneous shear flow could be generated in the laboratory was introduced by Corrsin (1963). Rose (1966) first generated such a flow with the use of a plane grid with parallel rods of uniform diameter but non-uniform spacing. His attempt resulted in turbulent shear flow with a fairly uniform mean shear (velocity gradient) of about 13.7 s-1, as well as nearly homogeneous transverse distributions of turbulent intensities and shear stress. However the transverse profiles of the integral length scales were quite non-uniform, because of the non-uniform rod spacing.

Later other techniques were used by different researchers to produce turbulent flows with improved transverse homogeneity. Champagne et al.(1970) used a row of parallel

equal width channels having adjustable internal resistances in the form of screens to generate a shear of 12.9 s-1, at a centreline mean speed of 12.2 m/s ; Rose(1970) used combinations of uniform grids and a honeycomb with a hexagonal cross-section, uniform cell cross-section and non-uniform cell length ; Mulhearn & Luxton (1970) used a combination of a non-uniform grid and a uniform honeycomb which resulted in a mean shear of 5.45 s-1, at a centreline mean speed of 4.5 m/s.

In all these investigations the Reynolds stress tensor components and the turbulent kinetic energy were found to decrease from their initially imposed levels to seemingly constant asymptotic values . This was contradicted by the development of the integral length scales and the Taylor microscales which exhibited a continuous growth. Harris et al(1977) attributed these contradicting observations to the insufficient development time of the flows which corresponds to a small value of the total strain.

In subsequent experiments, Harris, Graham and Corrsin (1977) and later Tavoularis & Corrsin (1981) generated nearly homogeneous turbulent shear flows with an imposed mean shear which was nearly four times that of most previous experiments and found that the Reynolds shear stresses and the turbulent kinetic energy decayed initially and then grew monotonically. The integral length scales also exhibited a

continuous growth but the Taylor microscales appeared to reach constant asymptoitc values. In all reported experiments the shear stress correlation coefficient approached an asymptotic value of about 0.45.

Numerical simulations of homogeneous turbulent shear flow made by Shaanan (1975), Rogallo (1977) and Feiereisen et al (1982) have shown, among others, that the shear stress correlation coefficient was approximately constant, consistently with experimental results.

1.3 RESEARCH OBJECTIVE

Although several experiments have been conducted on transversely homogeneous turbulent shear flows, there has been no systematic study of the effects of parameters such as mean shear, initial turbulence level and initial length scale. This has prevented a conclusive study of uniformly sheared turbulence.

The present study aims at generating homogeneous turbulent shear flows spanning sufficiently wide ranges of mean shear, Reynolds number, dimensionless strain and length scales for a quantitative parametrization of possible universal features of uniformly sheared flow to be attempted.

The interaction of grid and uniformly sheared turbulence was also be investigated. The results will be analysed

systematically in an attempt to establish experimental stability criteria for uniformly sheared flows based on Hasen's (1967) stability analysis.

Chapter II

ANALYTICAL DESCRIPTION OF THE FLOW

The velocity field for an incompressible fluid flow with negligible body forces and constant viscosity is described by the Navier-Stokes equations, which in the Cartesian co-ordinate system (x_1, x_2, x_3) have the form

$$\frac{\partial U_i}{\partial t} + U_j \frac{\partial U_i}{\partial x_j} = -\frac{1}{\rho}\frac{\partial P}{\partial x_i} + \nu \frac{\partial^2 U_i}{\partial x_j \partial x_j} \qquad (Momentum) \qquad (2.1)$$

$$\frac{\partial U_i}{\partial x_i} = 0 \qquad (Continuity) \qquad (2.2)$$

where i=1,2,3 and repeated indices are summed.

In the following analysis the Reynolds decomposition procedure (Reynolds, 1894) has been used, i.e. the instantaneous velocity and pressure have been decomposed into mean (designated by overbars) and fluctuating (designated by lower case letters) components as follows

$$U_i = \overline{U}_i + u_i \qquad (2.3)$$

and

$$P = \overline{P} + p \tag{2.4}$$

where $\overline{u_i} = 0$ and $\overline{p} = 0$ by definition.

Thus, the mean continuity equation is

$$\frac{\partial \overline{U}_i}{\partial x_i} = 0 \tag{2.5}$$

the mean momentum equation is

$$\frac{\partial \overline{U}_i}{\partial t} + \overline{U}_j \frac{\partial \overline{U}_i}{\partial x_j} = -\frac{1}{\rho}\frac{\partial \overline{P}}{\partial x_i} + \nu \frac{\partial^2 \overline{U}_i}{\partial x_j \partial x_j} - \frac{\partial \overline{u_i u_j}}{\partial x_j} \tag{2.6}$$

the equation for the mean Reynolds stresses is

$$\begin{aligned} \frac{\partial \overline{u_i u_j}}{\partial t} + \overline{U}_k \frac{\partial \overline{u_i u_j}}{\partial x_k} = & -\overline{u_j u_k}\frac{\partial \overline{U}_i}{\partial x_k} - \overline{u_i u_k}\frac{\partial \overline{U}_i}{\partial x_k} \\ & -\frac{1}{\rho}\left(\overline{u_i \frac{\partial p}{\partial x_j}} + \overline{u_j \frac{\partial P}{\partial x_i}}\right) - \frac{\partial \overline{u_i u_j u_k}}{\partial x_k} \\ & +\nu\left[\overline{u_i \frac{\partial^2 u_j}{\partial x_k \partial x_k}} + \overline{u_j \frac{\partial^2 u_i}{\partial x_k \partial x_k}}\right] \end{aligned} \tag{2.7}$$

and the mean turbulent kinetic energy $\frac{1}{2}q^2 = \frac{1}{2}\overline{u_i u_i}$ is given by

$$\frac{\partial \frac{1}{2}q^2}{\partial t} + U_k \frac{\partial \frac{1}{2}q^2}{\partial x_k} = -\overline{u_i u_k}\frac{\partial U_i}{\partial x_k} - \frac{1}{\rho}\frac{\partial \overline{u_k p}}{\partial x_k} - \frac{\partial \overline{u_k u_i u_i}}{\partial x_k} + \nu\left[\frac{\partial^2 q^2}{\partial x_k \partial x_k} + \frac{\partial^2 \overline{u_i u_i}}{\partial x_i \partial x_k}\right] - \frac{1}{2}\nu\left[\frac{\partial u_i}{\partial x_k} + \frac{\partial u_k}{\partial x_i}\right]^2 \qquad (2.8)$$

where

(a) the terms on the left hand side of the equation represent the total rate of change of turbulent kinetic energy.

On the right hand side of the equation

(b) the first term, being usually positive, represents the production of turbulent kinetic energy.

(c) the second term represents work done due to pressure fluctuation gradients

(d) the third term symbolizes turbulent diffusion of kinetic energy

(e) the fourth term is work done by viscous stresses or viscous dissipation

(f) the final term being always negative represents dissipation of turbulent kinetic energy by viscous forces.

Assume that the flow has the following properties

(a) it is a rectilinear mean flow, parallel to the x_1 -axis imposed with a constant mean velocity gradient in the x_2 -direction. Hence

$$\bar{U}_2 = \bar{U}_3 = 0, \quad \frac{d\bar{U}_1}{dx_2} = constant, \quad \frac{d\bar{U}_1}{dx_3} = 0 \tag{2.9}$$

(b) all turbulence moments are transversely homogeneous, i.e.

$$\frac{\partial(\overline{\ })}{\partial x_2} = \frac{\partial(\overline{\ })}{\partial x_3} = 0 \tag{2.10}$$

(c) the flow is stationary, i.e.

$$\frac{\partial(\overline{\ })}{\partial t} = 0 \tag{2.11}$$

The consequences of the above assumptions are

(1)the mean continuity equation reduces to

$$\frac{\partial \bar{U}_1}{\partial x_1} = 0 \tag{2.12}$$

implying that U_1 is a function of x_2 only.

(2) the mean momentum equation (2.6) becomes

$$\frac{\partial P}{\partial x_i} = -\rho \frac{\partial \overline{u_i u_1}}{\partial x_1} \tag{2.13}$$

(3) the equations for the Reynolds stresses (2.7) are simplified to

$$U_1 \frac{d\frac{1}{2}\overline{u^2_1}}{dx_1} = -\overline{u_1 u_2} \frac{dU_1}{dx_2} + \frac{1}{\rho} \overline{p \frac{\partial u_1}{\partial x_1}} - \nu \overline{\frac{\partial u_1}{\partial x_k} \frac{\partial u_1}{\partial x_k}} \tag{2.14}$$

$$U_1 \frac{d\frac{1}{2}\overline{u^2_2}}{dx_1} = \frac{1}{\rho} \overline{p \frac{\partial u_2}{\partial x_2}} - \nu \overline{\frac{\partial u_2}{\partial x_k} \frac{\partial u_2}{\partial x_k}} \tag{2.15}$$

$$U_1 \frac{d\frac{1}{2}\overline{u^2_3}}{dx_1} = \frac{1}{\rho} \overline{p \frac{\partial u_3}{\partial x_3}} - \nu \overline{\frac{\partial u_3}{\partial x_k} \frac{\partial u_3}{\partial x_k}} \tag{2.16}$$

$$U_1 \frac{d\overline{u_1 u_2}}{dx_1} = -\overline{u^2_2} \frac{dU_1}{dx_2} + \frac{1}{\rho} \left(\overline{p \frac{\partial u_1}{\partial x_2}} + \overline{p \frac{\partial u_2}{\partial x_1}}\right) - 2\nu \overline{\frac{\partial u_1}{\partial x_k} \frac{\partial u_2}{\partial x_k}} \tag{2.17}$$

(4) the simplified form of the turbulent kinetic energy equation is

$$U_1 \frac{d(\frac{1}{2}q^2)}{dx_1} = -\overline{u_1 u_2} \frac{dU_1}{dx_2} - \nu \overline{\frac{\partial u_i}{\partial x_j} \frac{\partial u_i}{\partial x_j}} \tag{2.18}$$

In equation (2.18) the first term represents transport term (T), the second term production (P) and the third term viscous dissipation (ϵ) of kinetic energy.

Assuming that in the asymptotic state the dimensionless Reynolds stress tensor K_{ij} is constant

$$K_{ij} = \frac{\overline{u_i u_j}}{q^2} = constant \tag{2.19}$$

and the ratio P:ϵ is also constant, equation (2.18) can be further simplified (Tavoularis, 1983) as

$$\frac{dq}{dx} - \frac{q}{l} = 0 \tag{2.20}$$

where 'l' is a characteristic length given by

$$l = \left[\frac{-K_{12}}{U_1}\frac{dU_1}{dx_2} - \frac{\epsilon}{U_1 q^2}\right]^{-1} \tag{2.21}$$

Equation (2.20) has the solution

$$q(x_1) = q_r\, e^{(x_1 - x_r)/l} \tag{2.22}$$

where q^2_r is the turbulent kinetic energy at a reference location $x_1 = x_r$.

In flows where production dominates dissipation ("strongly sheared" flows) $\mathcal{I}$ is positive and the turbulent kinetic energy q^2 grows exponentially downstream.

Harris et al (1970) and Tavoularis and Corrsin (1980) have observed that

$$\frac{q^2}{(d\bar{U}_1/dx_2)^2 \times L^2_{11}} = constant \tag{2.23}$$

where L_{11}, the streamwise velocity integral length scale, is defined as the integral of the autocorrelation coefficient.

$$L_{11} = \int_0^\infty R_{11}(\tau)\, d\tau$$

$$R_{11}(\tau) = \frac{\overline{u_1(t)\, u_1(t+\tau)}}{\overline{u_1^2}}$$

This observation along with equation (2.22) imply that the streamwise velocity integral length scale L_{11} should also grow exponentially and at the same rate as the turbulent kinetic energy. Hence

$$L_{11}(x_1) = L_{11,r}\, e^{(x_1 - x_r)/l} \tag{2.24}$$

where L_{11_Y} is the streamwise velocity integral length scale at some reference position $x_1 = x_Y$.

Hasen (1967) predicts the existence of a stability barrier $\bar{A}(R)$ for the initial amplitude of turbulent fluctuations in a uniformly sheared turbulent flow; fluctuations decay or grow depending on whether the initial amplitude is less than or greater than the stability barrier, which is bound by the inequalities

$$L_{in}(\partial\bar{U}_1/\partial x_2)K_2/R^{2/3} \leq \bar{A}(R) \leq L_{in}(\partial\bar{U}_1/\partial x_2)K_1/R^{2/3}$$

where R is the Reynolds number $(\partial\bar{U}_1/\partial x_2)L_{in}^2/\nu$ and K_1 & K_2 are proper undefined constants. As $R \to \infty$, obviously $\bar{A}(R) \to 0$.

Chapter III

FLOW FACILITIES

3.1 THE WIND TUNNEL

The wind tunnel (Figure 1) used in the present experiments was designed and constructed at the University of Ottawa. The air flow was produced by two centrifugal blowers in parallel (Canadian Blower and Forge) rated at 6000 cfm, 1711 rpm, 4.15 bhp. The blowers were driven by a 5 hp, 1750 rpm D.C. motor (Baldor Electric Co.) and the motor speed was controlled by a Torqmatic solid state variable drive. An earlier facility (Shaw and Lee, 1976) using the same blowers also included heating and cooling systems, but these were now disconnected.

The air intake was filtered by a set of pleated, non-woven cotton fabric filters (Farr 30/30). The air streams from the two blower outlets passed through aluminium honeycombs (cell width 0.79 cm, length 1.27 cm) and merged into a rectangular duct (45.7 cm x 122 cm) equipped with a curved transition section to facilitate smooth convergence of the two streams. The duct led to a rectangular diffuser (wall angles 7.12 and 3.84), a settling chamber (213.4 cm x 183 cm x 122 cm) and

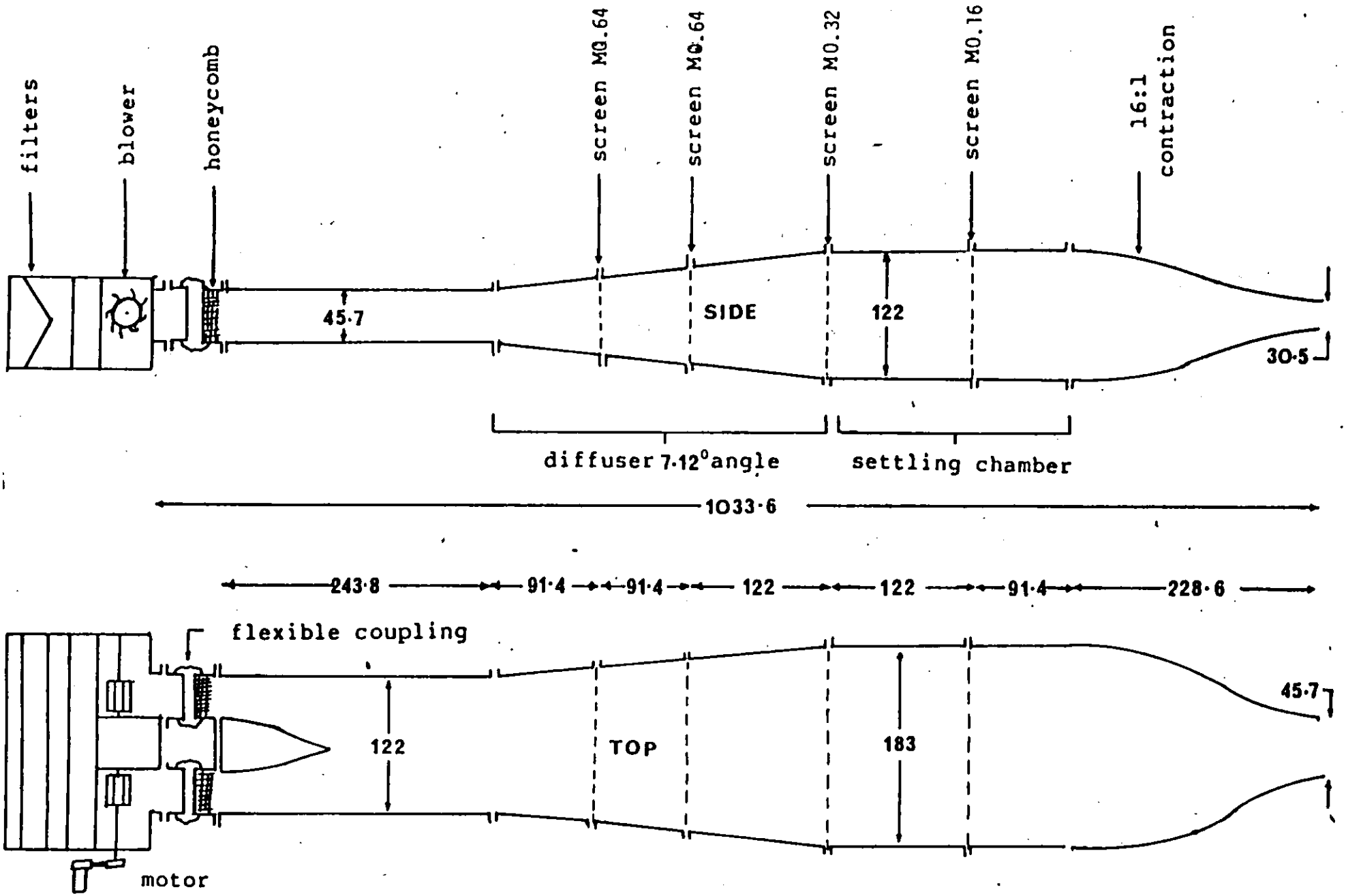

all dimension in cm

scale 1 cm = 40.53 cm

Figure 1. Upstream section of the Wind Tunnel

a 16:1 contraction. Four wire screens (with solidity of about 0.365 and mesh sizes 0.64, 0.64, 0.32 and 0.16 cm respectively) were streched across the diffuser and the settling chamber in order to reduce the possibility of seperation and to decrease the levels of mean speed inhomogeneity and of free stream turbulence. The relatively large contraction ratio further reduced the level of free stream velocity fluctuations.

3.2 THE TEST SECTION AND TRAVERSING MECHANISM

The final section was nominally 30.5 cm high, 45.7 cm wide and 518 cm long. The shear generator took up the first 15.2 cm, while the next 61 cm were occupied by the flow separator. The remaining length of about 441.8 cm was used as the test section.

The test section had its vertical walls made of plexiglass and was made in two parts. The first part was 137.2 cm long with fixed walls and had four slots for inserting grids or other flow obstructions (see Figure 2). The vertical walls of the remaining test section were moveable to account for boundary layer growth along the walls.

The bottom wall of the entire test section had a centreline slot to accomodate the belt which moved the traversing mechanism longitudinally. It was also provided with five transverse slots to allow transverse motion of the probe.

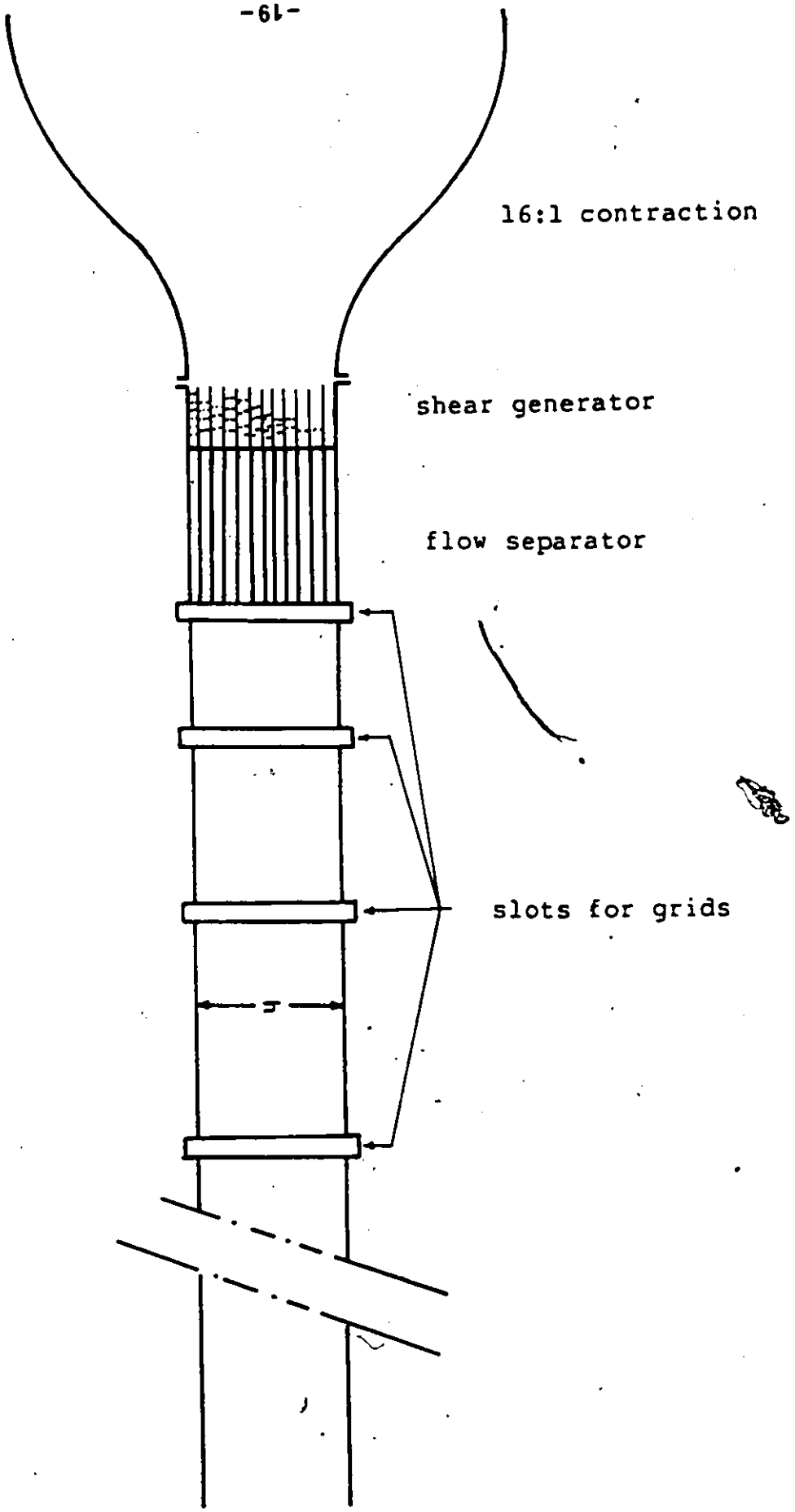

Figure 2. Downstream section of the Wind Tunnel

The traversing mechanism (Figures 3 & 4) consisted of a rectangular aluminium carriage (58.42 cm x 25.4 cm) mounted on four axial pillow blocks (Thomson SPB-16-OPN) sliding along two parallel shafts spanning the entire test section. A similar but smaller carriage (mounted on Thomson SPB-8-OPN pillow blocks) provided transverse motion with a total span of about 30 cm. Finally, a lead screw mechanism (UNISLIDE A2515 BE) with scale and vernier permitted the vertical positioning of the probes for a total traverse of about 30 cm and a position resolution of about 0.02 mm.

The probes were mounted through a probe holder on a hollow shaft which protruded inside the wind tunnel through a gap in the driving belt. The electrical leads were passed through the shaft to minimize flow induced vibrations and flow obstruction.

3.3 SHEAR GENERATOR AND FLOW SEPARATOR

The shear generator, shown in Figure 5, could be inserted in a slot immediately after the contraction. Its main purpose was to generate the shear necessary for the production of turbulence. The shear generator frame had dimensions 33.0 cm x 50.8 cm x 15.2 cm and was provided with 12 slots (0.635 cm x 0.317 cm) accomodating twelve 0.317 cm thick, 15.2 cm x 49.5 cm aluminium plates thus parting the flow into 12 seperate channels.

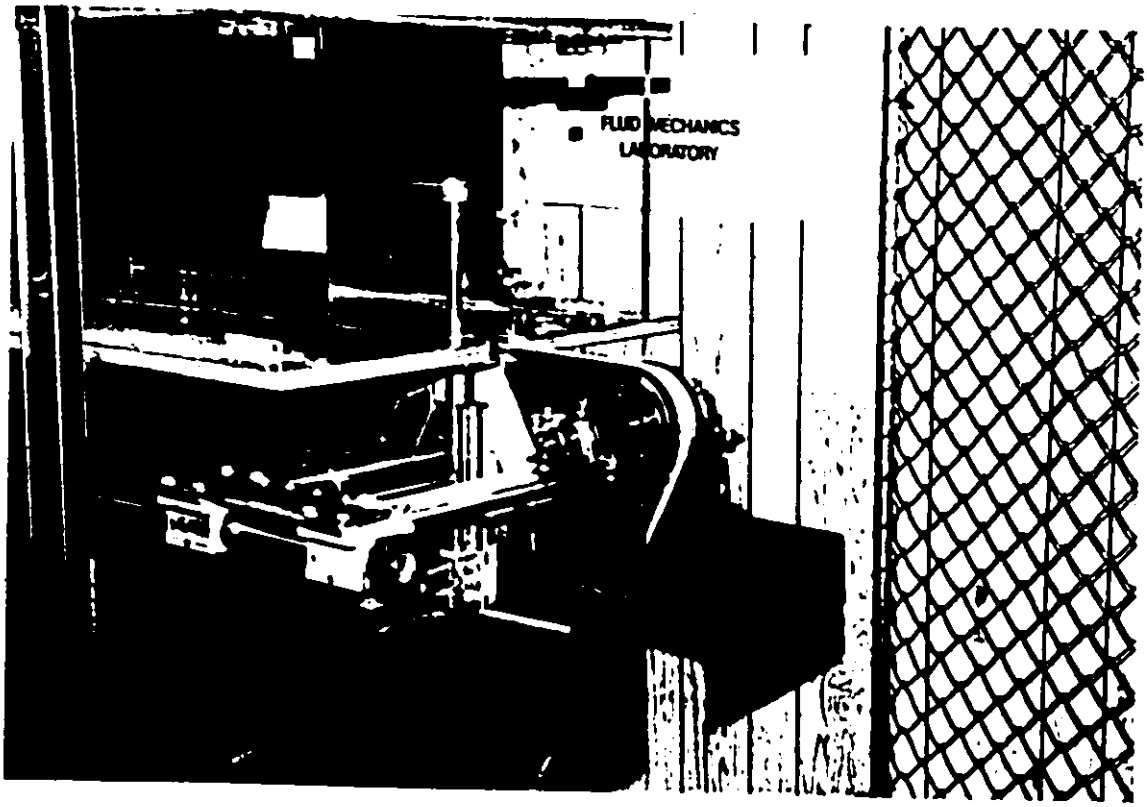

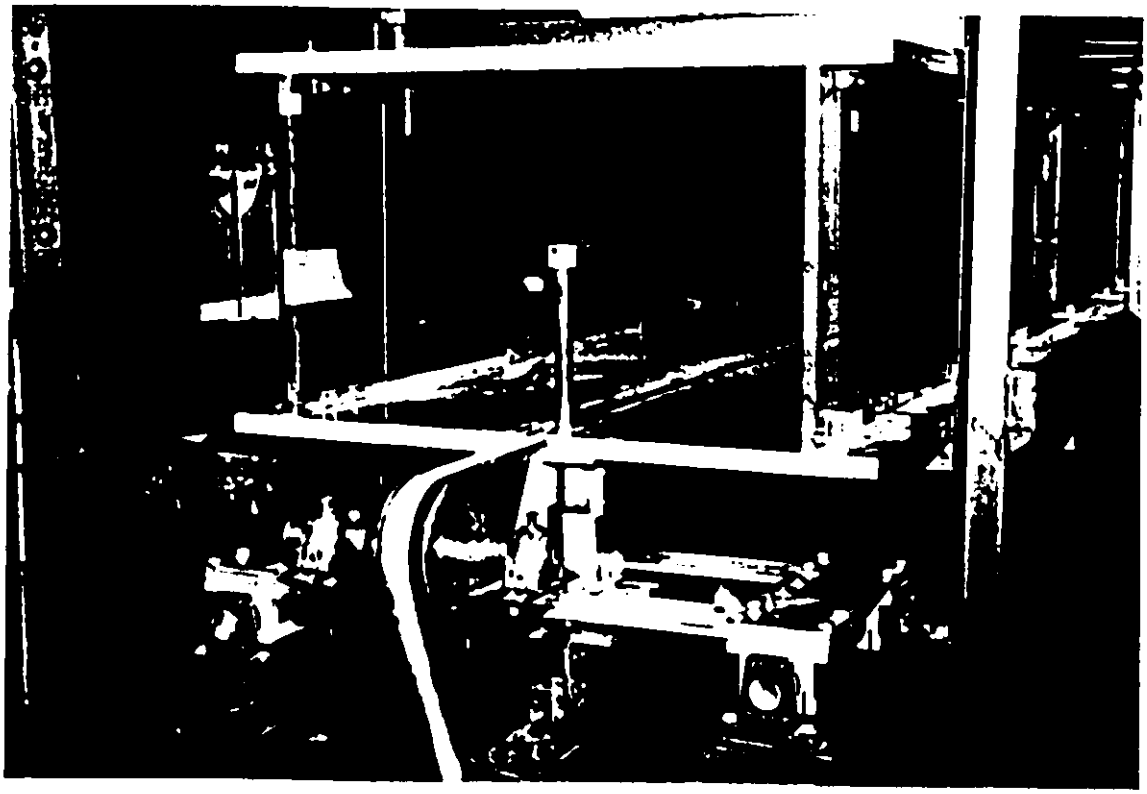

Figure 3. Photographs of two views of the traversing mechanism

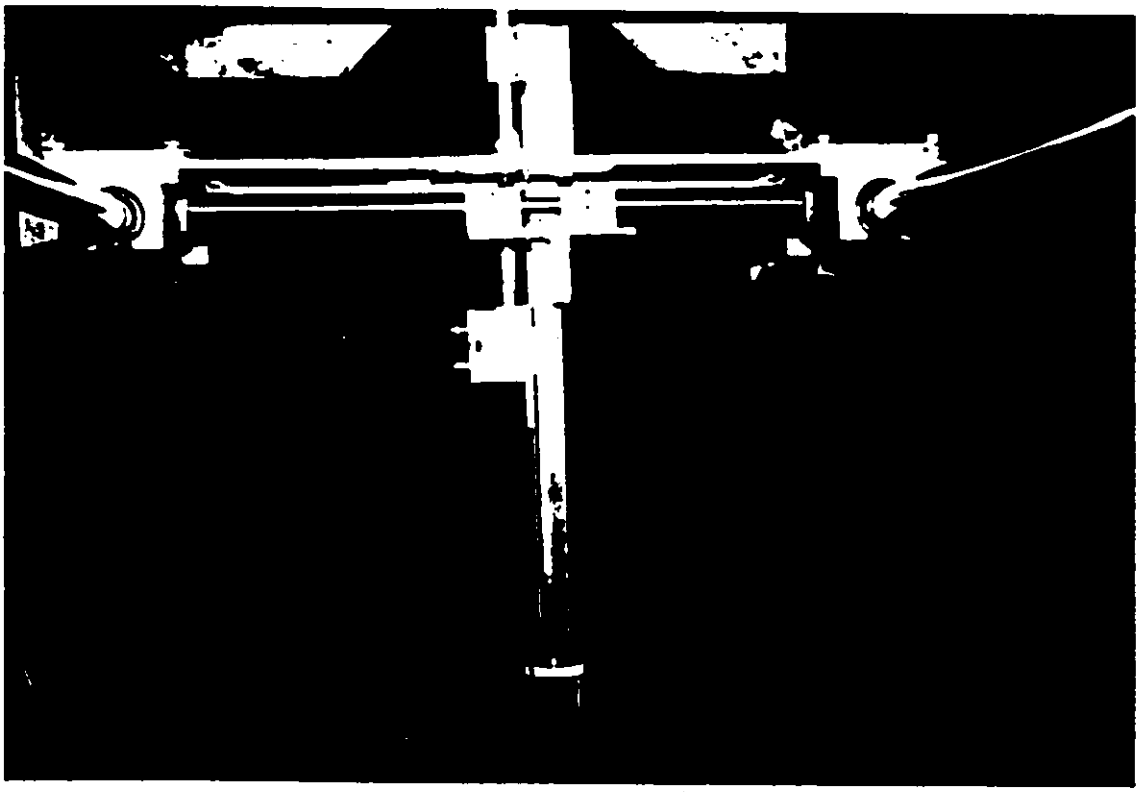

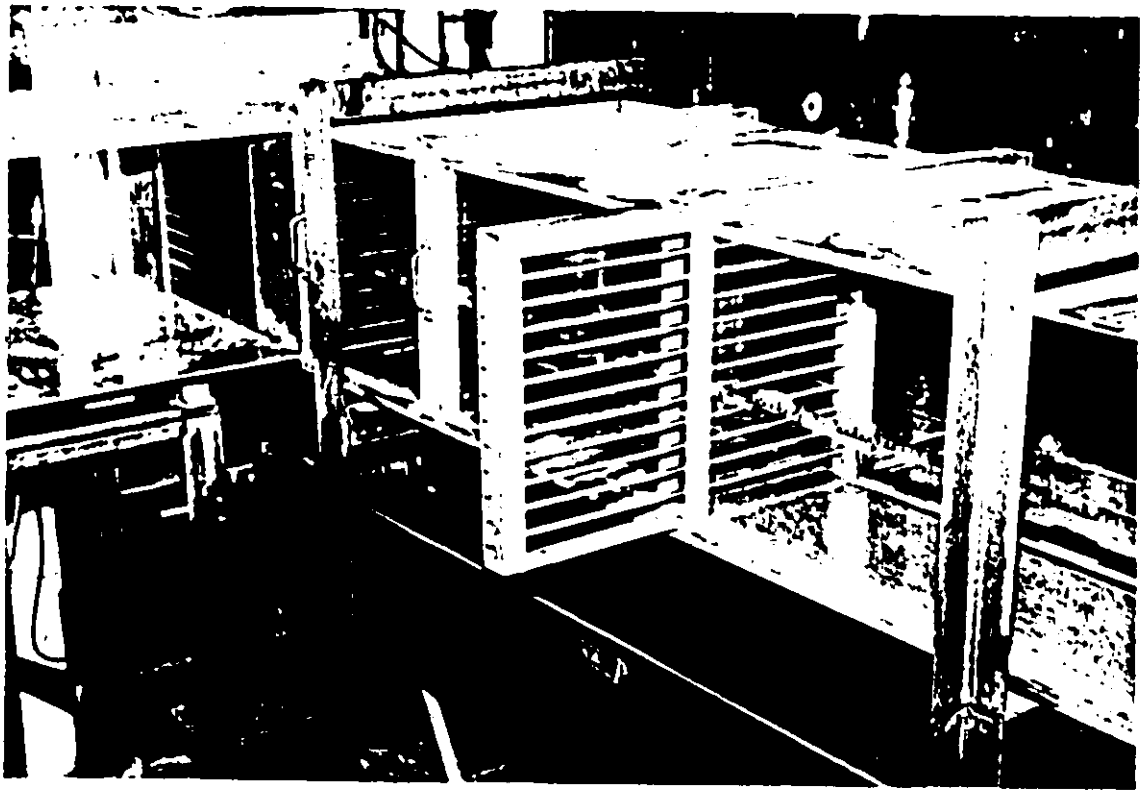

Figure 4. (a) photograph of the traversing mechanism as seen from below the wimd tunnel.
(b) photograph showing insertion of grid into a slot provided in the test section.

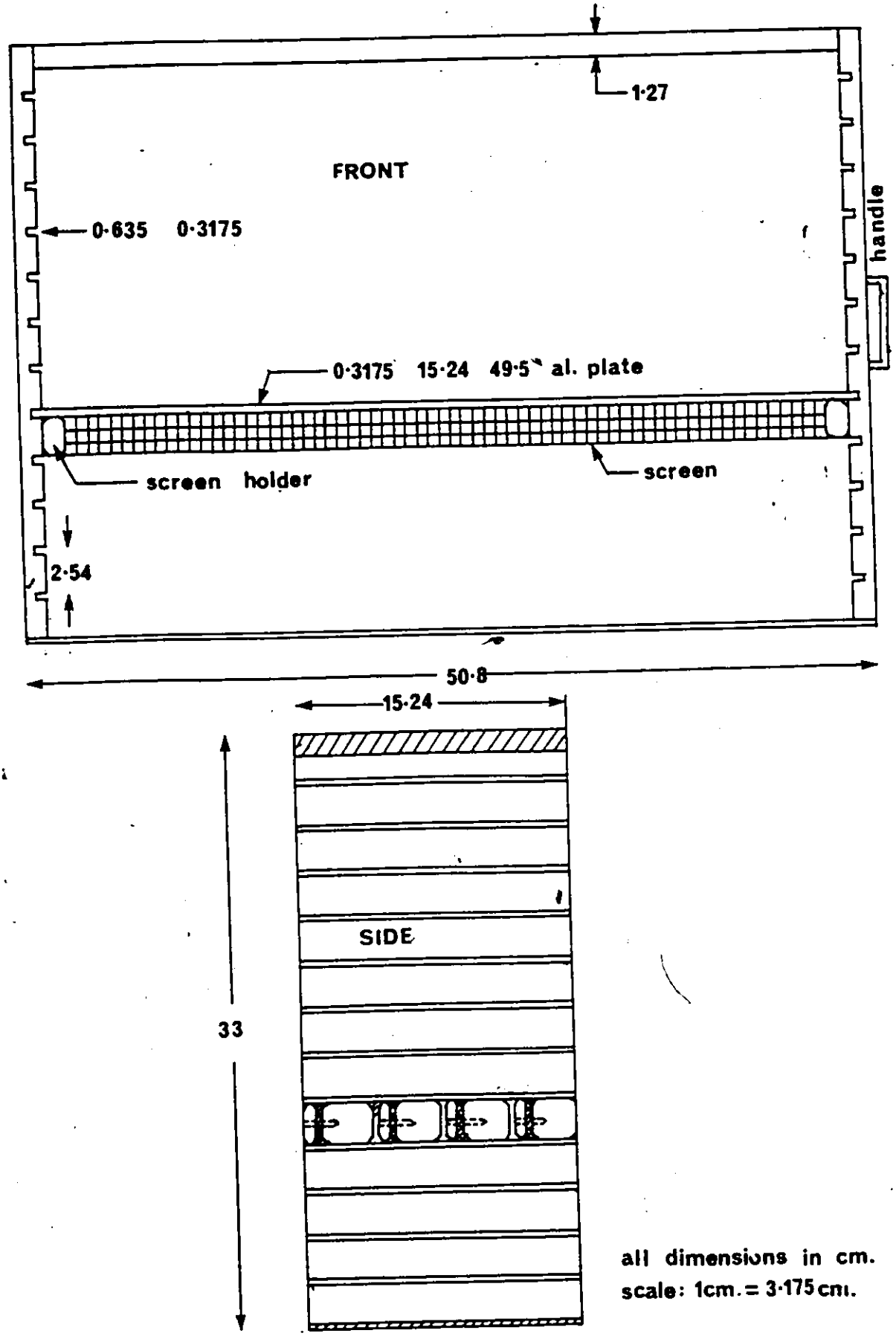

Figure 5. Shear Generator

A system of blocks mounted on the plates enabled the stretching of up to four wire screens across each channel. The shear generator could be replaced by an empty wooden frame whenever an undisturbed flow was desired in the test section.

The flow separator (Figure 6,) consisted of a set of 12 parallel aluminium plates, 61.0 cm long, that were aligned with those in the shear generator. Its function was to produce transverse uniformity of the turbulent scales. An empty section was attached to the flow separator and the entire assembly was mounted on axial pillow blocks sliding along shafts for convenient insertion of the desired section in the wind tunnel.

3.4 SHEAR GENERATION

Generation of the uniform mean shear involved proper selection of screen combinations to be stretched across each channel of the shear generator. An attempt was made to generate a maximum possible shear within the wind tunnel limitations.

Velocities necessary in each of the 12 channels to achieve a uniform shear were calculated by assuming a shear of 100 s-1 at a centreline mean speed of 13 m/s. The available screens were tested individually and in combinations in the central channel of the shear generator to attain each pre-

determined channel velocity (see Table 1).These combinations of screens were stretched across the different channels and were found to provide a reasonable approximation to the desired velocity distribution. Furthermore, certain screens were finely adjusted by removing a number of strands, which improved the uniformity of the mean shear. The final value obtained was 84 s-1 at a centreline mean speed of 13 m/s.

The screen combinations used in the present experiments as well as in similar previous investigations are shown in Table 2.

3.5 GRIDS

The grids used in the ensuing experiments (Figure 7) consisted of straight parallel cylindrical rods mounted on frames which could be inserted into any of the four slots across the test of the wind tunnel such that the rod axes were perpendicular to the flow and the direction of the shear. Three grids were constructed using rods with diameters 0.48 cm, 0.96 cm, 1.92 cm and distances between the axes of successive rods 1.25 cm, 2.54 cm and 5.08 cm respectively. Thus, in all cases the grid solidity (ratio of blocked area to the total area) was about 0.36. Such grids have been found (for instance, see review by Corrsin 1963) to generate stable nearly isotropic turbulence, when placed across a uniform stream.

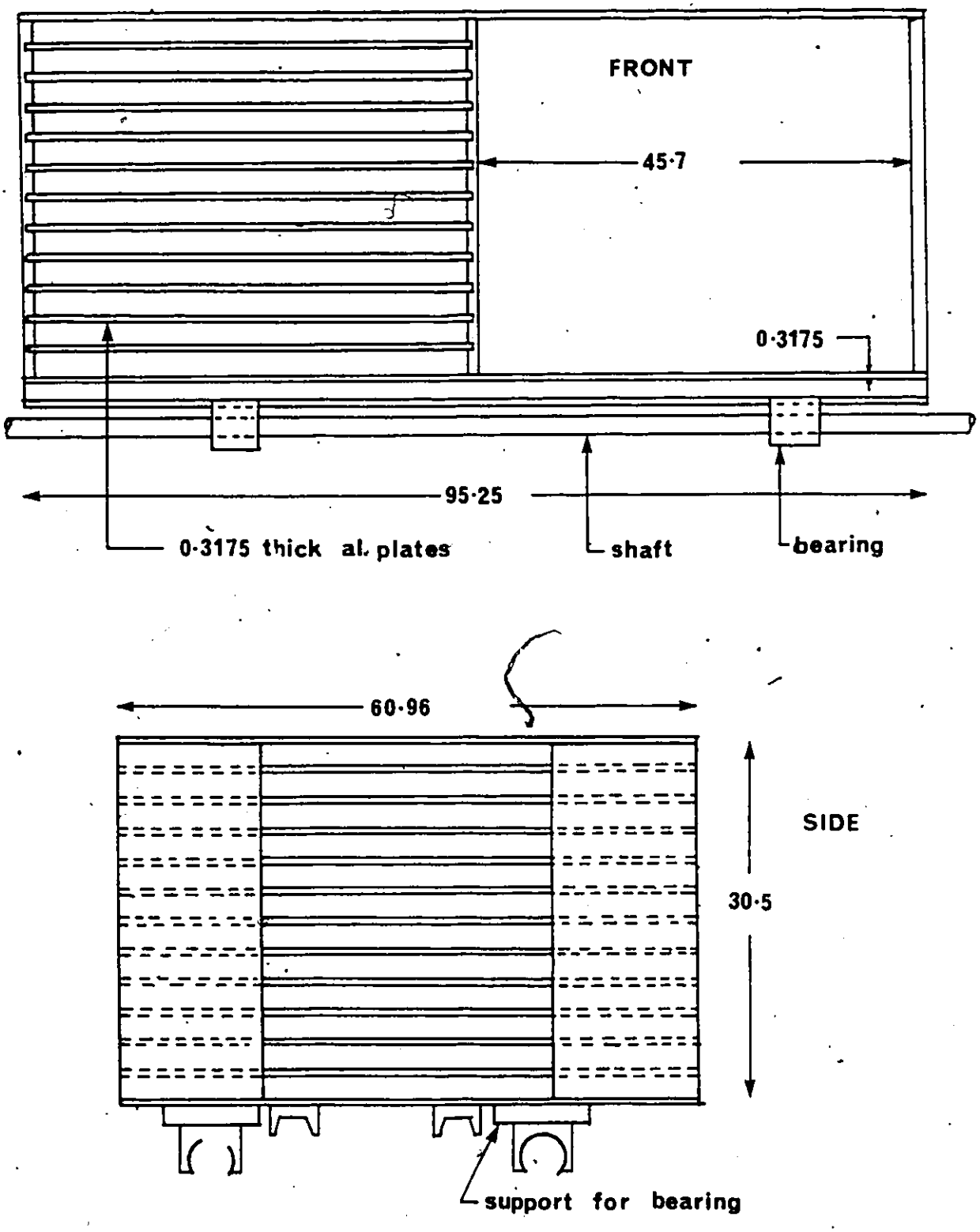

Figure 6. Flow Separator

all dimensions in cm.
scale: 1cm.=6·35cm.

A	B	C	D	U m/s	U_{ref} m/s
0.32	–	–	–	21.2	18.6
0.32*	–	–	–	25.2	18.9
0.32*	0.32*	–	–	22.7	19.0
0.32*	0.32*	0.32	–	19.1	18.7
0.32	–	0.32*	–	20.3	18.8
0.18	–	–	–	22.3	19.0
0.16	–	–	–	20.3	18.8
0.18	0.18	–	–	19.4	18.7
0.16	0.16	–	–	16.9	18.5
0.16	0.18	–	–	18.3	18.6
0.32	0.16	0.18	–	16.4	18.6
0.18	0.18	0.32	–	17.2	18.6

A	B	C	D	U m/s	U_{ref} m/s
0.18	0.18	0.16	–	16.6	18.6
0.18	0.16	0.16	–	15.7	18.5
0.08	0.13	–	–	16.4	18.6
0.08	0.08	–	–	14.2	18.5
0.18	0.18	0.16	0.16	14.8	18.4
0.18	0.16	0.16	0.13	14.2	18.5
0.18	0.16	0.16	0.08	13.6	18.4
0.08	0.08	0.08	–	12.2	18.4
0.08	0.08	0.08	0.08	11.2	18.3
0.06,0.08	0.08	0.13	–	9.8	18.3
0.06,0.08	0.08	0.13	0.06,0.08	8.7	18.3
0.06,0.08	0.06,0.08	0.06,0.08	0.06,0.08	7.8	18.2

Mesh size (cm) : 0.32* 0.32 0.18 0.16 0.13 0.08 0.06

Solidity : 0.25 0.35 0.44 0.46 0.48 0.57 0.64

TABLE 1. Resultant velocities of various screen combinations.

CHANNEL #	A	B	C	D
1				
2				
3	0.32*	0.32++		
4	0.32*	0.32*		
5	0.32			
6	0.08			
7	0.18	0.08		
8	0.16	0.08	0.18	0.32
9	0.08	0.08	0.08	0.16
10	0.06	0.06	0.06	0.06,, 0.08
11	F0.13		0.06	0.06
12	F0.08			0.16

0.32++ - alternate horizontal and vertical strands removed from 0.32*

F - one strip of cotton fabric filter |Farr 30/30|

(a)

A	B	C	D
0.25+		0.25+	
	0.25	0.13	0.25
0.13	0.25	0.06	
	0.06		0.06
0.06	0.06	0.13	0.00
	0.06	0.06	-
0.04	0.04	-	-
0.04	0.04	0.06	
0.04	0.06	0.04	0.04
0.04	0.04	0.03	0.04

0.25+ - every fourth vertical strand removed.

(b)

A	B	C	D
-	0.64	0.13	0.13
-	0.64	0.08	0.13
0.13	0.13	0.13	-
0.08	0.13	-	0.13
0.13	0.08	0.08	-
0.13	0.13	0.13	0.13
0.08	0.08	0.08	0.08
0.08	0.08	0.08	0.13
0.06	0.13	0.13	0.06
0.06	0.06	0.08	0.08

(c)

Table 2. Screen combinations for a uniform shear profile; (a) present study (b) Harris et al. & Tavoularis - Corrsin (c) Champagne et al. Numbers represent mesh sizes in cm.

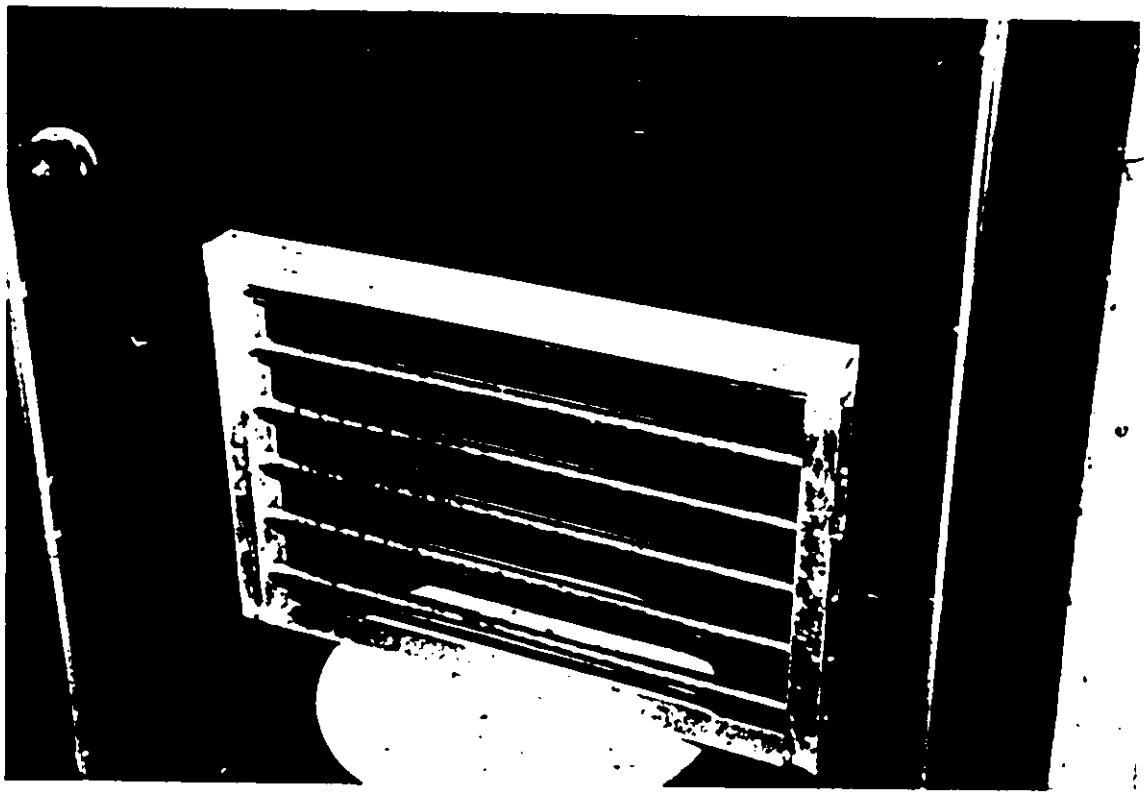

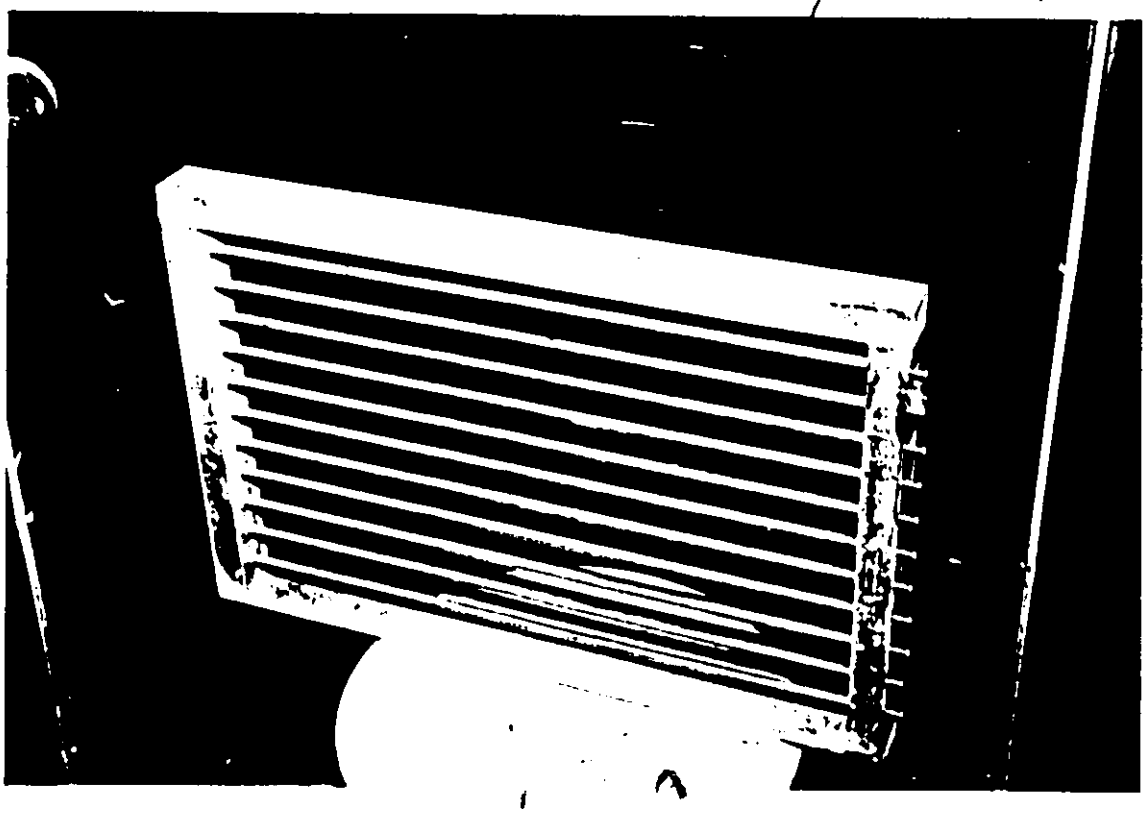

Figure 7. Photographs of the two grids used in the present study. (a) M5.08 cm grid (b) M2.54 cm grid

Chapter IV

INSTRUMENTATION AND MEASUREMENT PROCEDURES

4.1 A BRIEF REVIEW OF TURBULENCE MEASURING TECHNIQUES

The following discussion highlights the main techniques which have been developed for turbulent flow measurement.

4.1.1 Flow Visualization

These techniques make the fluid flow visible thus providing an insight to the physical development and structure of the flow. The most common flow visualization techniques are the following

4.1.1.1 Addition of foreign particles

Flow elements are marked with the addition of foreign particles such as, smoke, dyes or gas bubbles. Significant differences between particle and surrounding fluid velocity might occur for relatively large particles or for particles with density substantially different from that of the fluid.

4.1.1.2 Density difference methods

These methods are used in compressible flow and utilize the fact that the refractive index is a function of the density of the flowing medium. The shadowgraph method, the Schlieren technique and interferometry are based on this principle. A description of flow visualization techniques can be found in the book by Merzkirch (1974).

4.1.2 Measurement of Turbulent Velocity

4.1.2.1 Hot-wire anemometry

The roots of hot wire anemometry probably originate with the work of Oberbeck (1895) and the experiments of Shakespear (1902), the latter being reported by L.V.King (1915). It was King (1914-1916) who established a relation for the response of heated wires. This technique is a powerful method for measuring fluctuating velocity as well as temperature, density and concentration fluctuations (see Marton 1981).

The hot wire sensors consist of thin metallic wires, usually tungsten, platinum and their alloys, mounted onto thin parallel prongs. The wire is then heated by an electric current; when placed in a flow, the flow velocity 'U' normal to the wire can be related to the heat loss from the wire by the semi-empirical modified King's law

$$\frac{\dot{Q}}{T_w - T_f} = A + BU^n$$

where $\dot{Q} = I^2 R_w = VI$ is the rate of heat transfer, V is the voltage across the wire, R_w is the resistance of the wire, I is the current, T_w is the absolute temperature of the wire, T_f is the absolute temperature of the surrounding fluid, and A, B, n, are empirical constants.

Hot-film sensors have a response similar to that of hot wires. They consist of a thin platinum film deposited on a quartz support, usually in the shape of a cylinder, wedge or cone. The film is insulated with a thin quartz coating and, thus, can be operated in electrically conductive fluids.

Two modes of operation are used for wire heating

(a) Constant current mode

(b) Constant temperature mode

Constant temperature mode is normally used because it results in a better frequency response, a lower chance of wire burn-out and allows direct temperature corrections. Constant current mode is used whenever signal to noise ratio is extremely low.

Hot wires have been used in single or multiple-sensor configurations such as X-wire probes, derivative probes, and vorticity probes. Detailed discussion on hot wire anemometry has been documented in a number of books and articles e.g. those by Corrsin (1963), Comte-Bellot (1976), Reynolds (1974) and Perry (1982).

4.1.2.2 Laser Doppler velocimetry

A laser-Doppler velocimeter is an instrumentation system that measures velocity through the Doppler frequency shift of laser beam light scattered by moving particles. The Doppler frequency shift exhibits a linear relationship with the velocity of the moving particle. This technique does not place any restrictions on the composition of the flow fluid and it does not disturb the flow. For a review, see books by Durst (1981) and Reithmuller (1977).

4.2 PRESSURE INSTRUMENTATION

The pressure transducer (MKS Baratron, type 220B) used in the present experiments had a 1333.22 Pa differential pressure range, corresponding to a 10 volt D.C. output. Its operation was based on the change of capacitance caused by deflection of a taut metal diaphragm proportional to the difference of pressure applied on its two sides. The transducer was calibrated versus a MERIAM manometer (Figure 8) which could read a minimum pressure difference of 2.49 Pa., using a Pitot-static tube as a sensor. The calibration curve has shown in Figure 10.

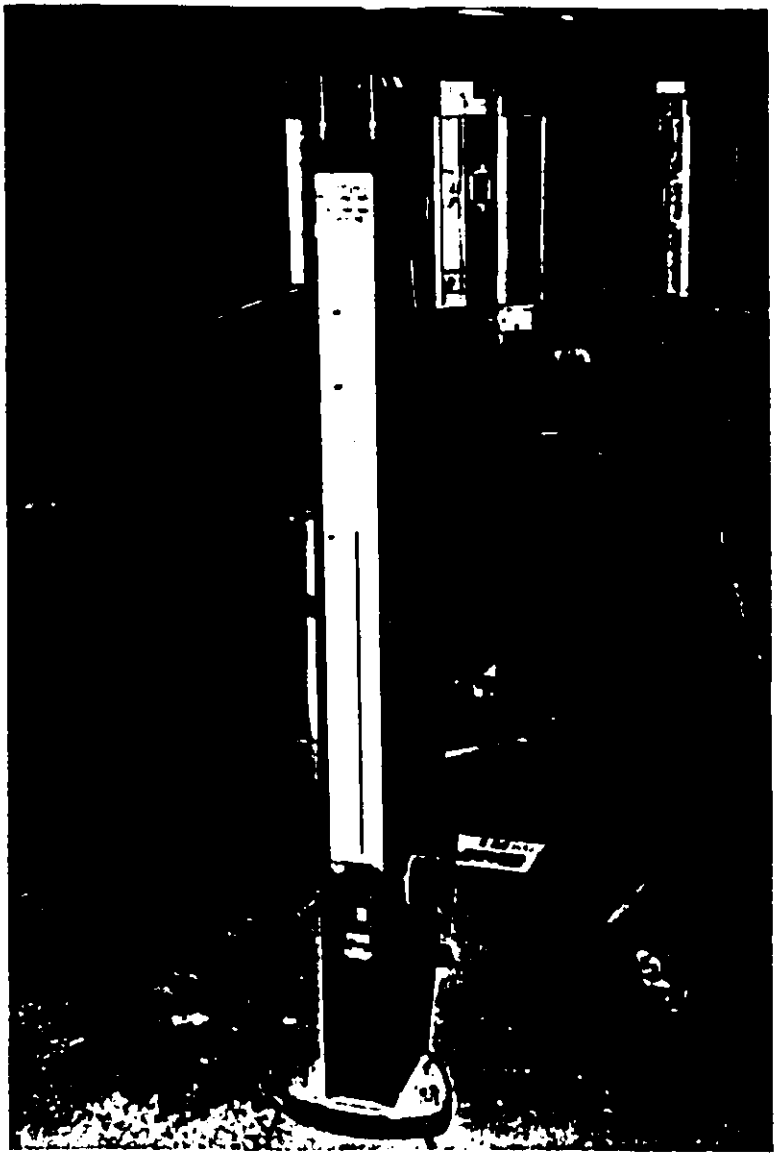

Figure 8. Photograph of the MERIAM manometer used to calibrate the pressure transducer.

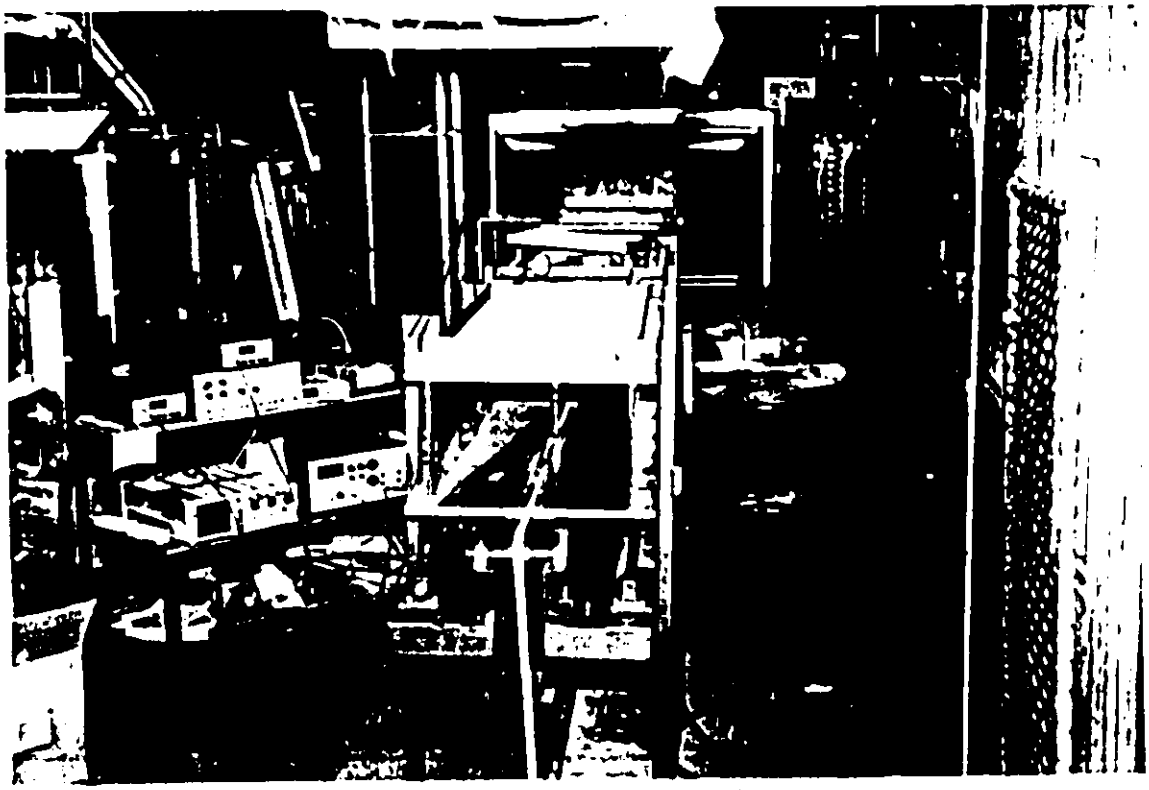

Figure 9. Photographs show two views of the wind tunnel and the instruments.

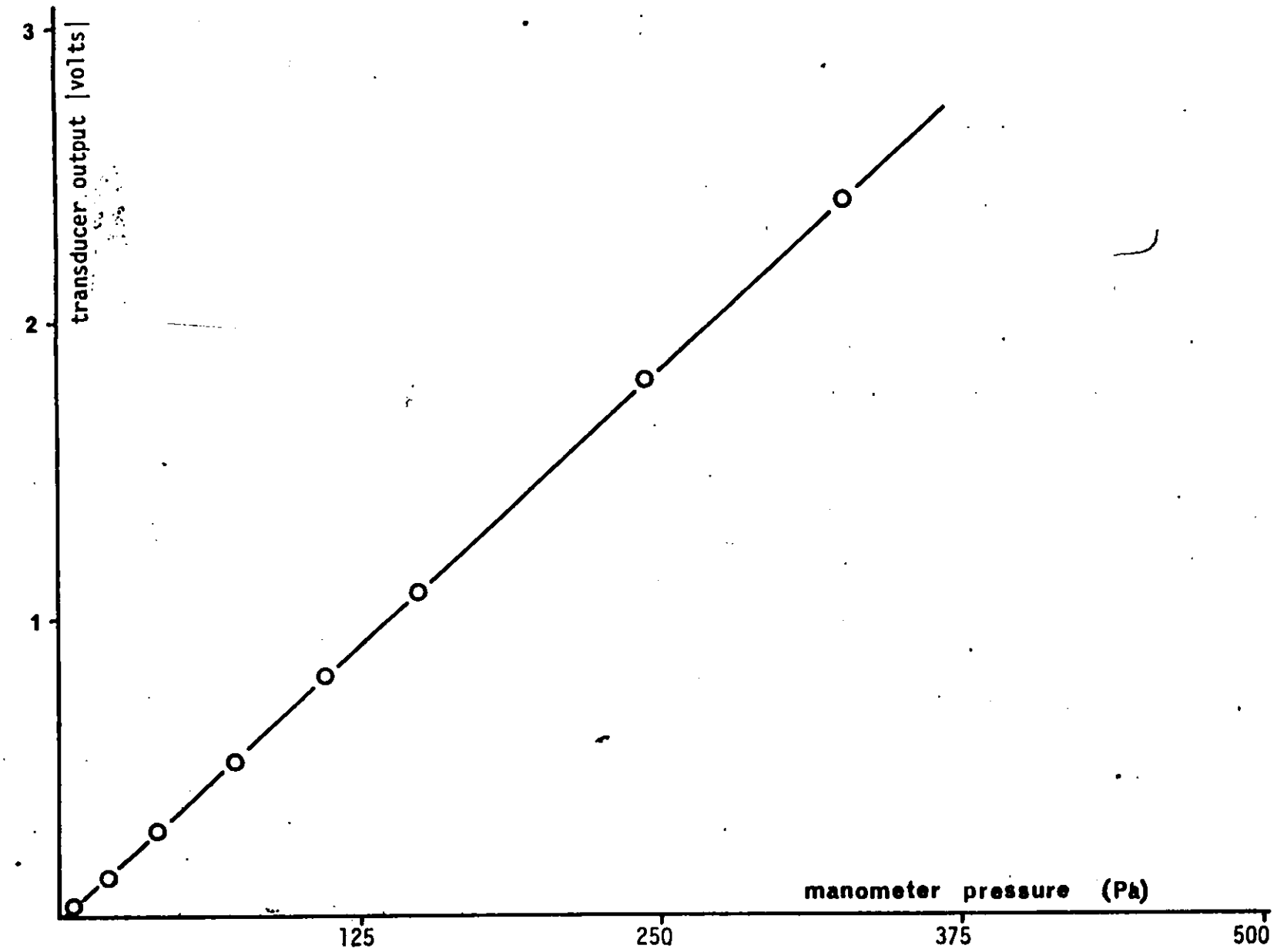

Figure 10. Calibration curve of the pressure transducer vs the liquid manometer reading.

4.3 HOT-WIRE INSTRUMENTATION

Hot-wire anemometry was used extensively throughout the present study. The streamwise component of turbulent velocity was measured by a single wire whereas a cross-wire probe was used to measure the transverse components and the shear stress. Commercial (DISA, model 55P11) as well as home made probes have been available for this study. The procedures for manufacturing home-made probes are described in Appendix A.

A TSI 1051 2D Monitor and Power Supply was used to power two TSI 1050 constant temperature anemometer modules. The 3 1/2 digit panel meter of the monitor had a range of 0 - 20 volts with an accuracy of ±0.05% of F.S. reading ±1 digit. The anemometer was used in the constant temperature mode; constant current mode was also available for temperature measurements. The anemometer outputs were linearized with two TSI 1052 linearizers by approximating the calibration curve with a fourth degree polynomial of the form

$$U = A_0 + A_1E + A_2E^2 + A_3E^3 + A_4E^4 \qquad (4.1)$$

where U is the flow velocity and E is the output voltage. The coefficients were determined as suggested by the TSI manual. The linearizer was equipped with an amplitude control switch that could attenuate the output by a factor of 10.

4.4 HOT-WIRE CALIBRATION

The anemometer output voltage was calibrated versus the flow velocity measured by a Pitot tube in a smooth flow in the wind tunnel. The wire was placed near the entrance to the test section and the velocity at the end of the contraction was used as a reference.

Initially the resistance of the unheated wire was determined and the operating resistance was set using an overheat ratio of 1.7. The wire frequency response was optimized using the standard square wave test under typical flow conditions. The linearizer was set up by determining and setting the coefficients of the fourth order polynomial, equation (4.1). A typical calibration curve of the linearized output is shown in Figure 11.

Each of the cross wires was individually calibrated as described earlier. The linearizer settings were selected such that the slopes of their linearized curves matched. Thus, the streamwise and transverse velocity fluctuations could be obtained by direct addition and subtraction of the two wire signals (for details, see Appendix B), assuming that both wires formed 45 angles with the flow direction. Pilot measurements of the turbulent intensity ratio and the shear stress correlation coefficient in grid turbulence and in uniformly sheared flow using the present probes were close to the ones reported in the literature. Typical li-

nearized cross wire calibration curves are shown in Figure 12.

4.5 ANALOG DATA PROCESSING

Two TSI 1076 rms voltmeters were used to analyse the fluctuating signals each providing the average, mean squared and true root mean square value of the input signal. Each voltmeter had six ranges between 1 mv rms to 100 v rms full scale, with an accuracy of 1% of F.S. within a frequency range of 0.5 hz to 100 khz and 10% of F.S. within the range 100 khz to 500 khz. The integrating time could be adjusted to values of 0.1, 1.0, 10.0 or 100.0 seconds. Two D.C. ranges 10 v and 100 v, were available with an accuracy + 0.05% of full scale.

The signals from the cross wire were analysed by a DISA type 55D70 correlator to supply the mean square value of each signal and the sum and the difference of the two signals. The gain function for each signal was adjusted to unity.

A Tektronix model 5113 dual beam storage oscilloscope was used to observe the anemometer output signals. The oscilloscope was equipped with two differential amplifiers (Tektronix 5A22N) with gains ranging from 0.1 to 50000 and built in high pass and low pass filters with a 3db drop off per octave. The amplified, conditioned signals were available

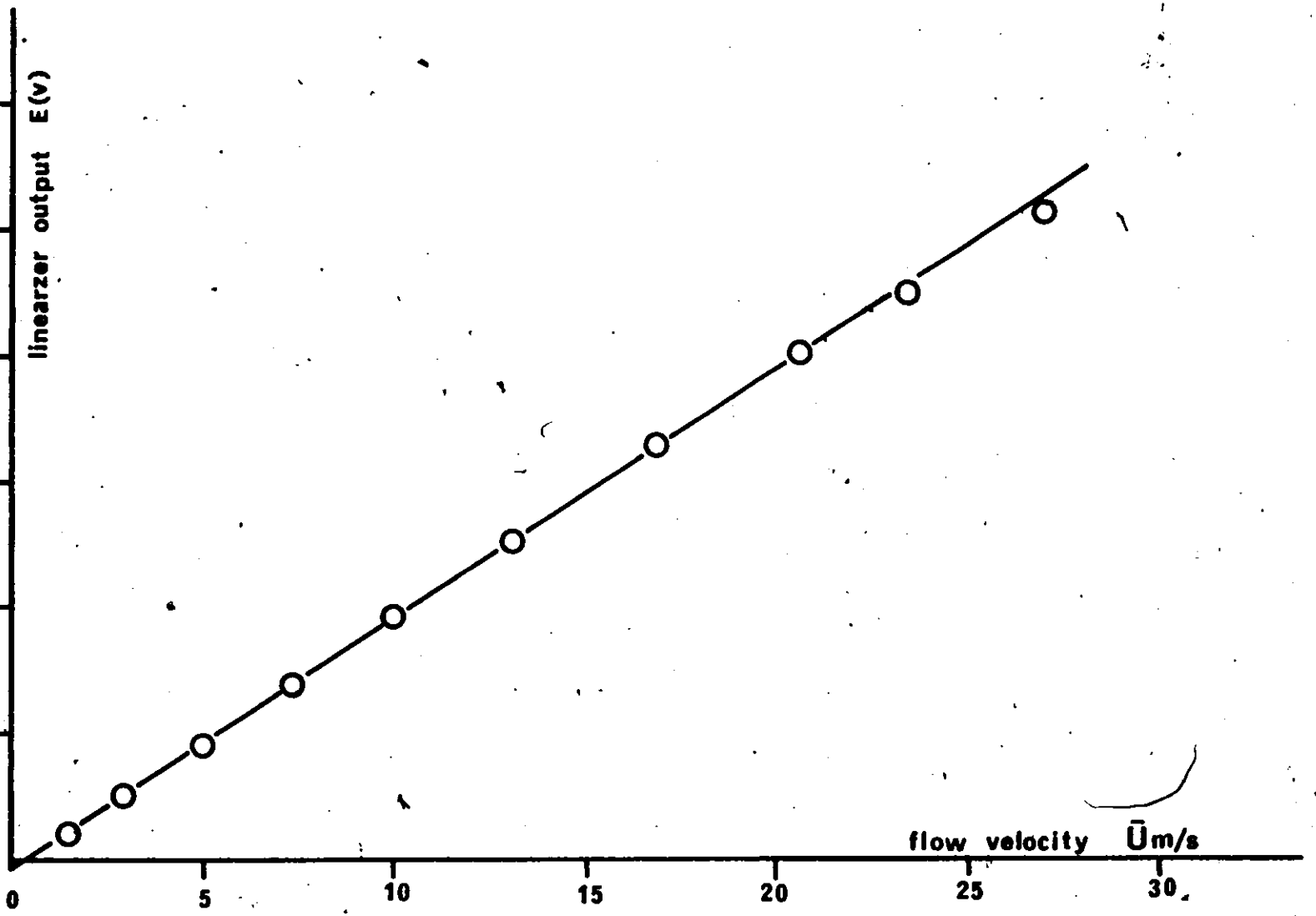

Figure 11. Typical linearized calibration curve for a single hot wire probe.

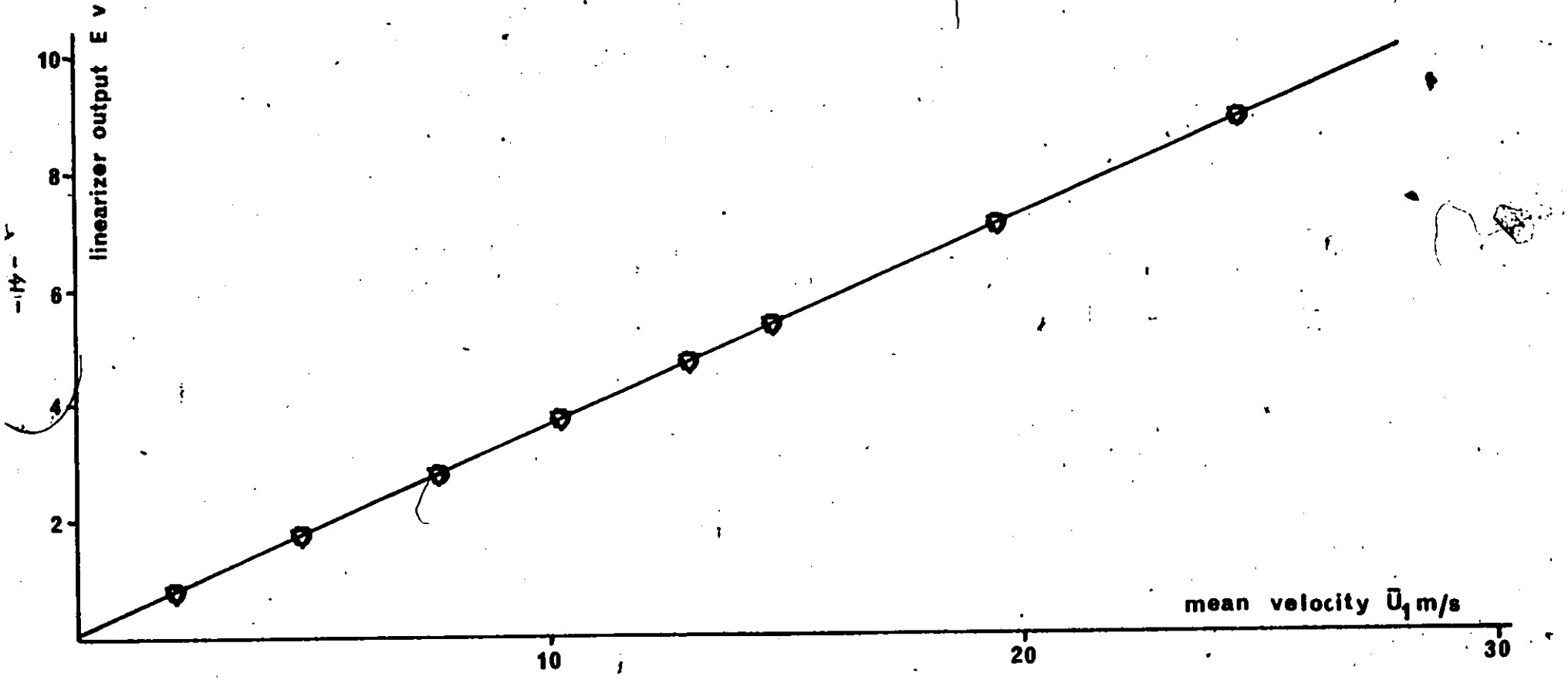

Figure 12. Typical linearized calibration curve for a cross wire.

at the rear panel of the oscilloscope. Results of the calibration of the amplifier are shown in table 3. The time base of the oscilloscope (Tektronix 5B10N) covered the range 1 us/div to 5 s/div and had 21 steps in a 1-2-5 sequence.

4.6 DIGITAL DATA ACQUISITION AND PROCESSING

Signal discretization and processing was done using a LSI 11/23 micro-computer with a 64K byte memory and equipped with an ADAC model 1601GPT programmable 16 bit general purpose timer and a 12 bit analog to digital converter (ADAC model 1012) with a 16 channel multiplexer.

The input voltage range of the analog to digital converter was programmable and usually set between -1.0 and +1.0 volt. Signals outside this range had to be attenuated or offset while low level signals had to be amplified in order to utilize the full capacity of the system. The digital output ranged between 0 and 4096 which ensured a digitizing accuracy of about 0.5 mV.

The linear relationship between input and output values is given by

$$X = 2048\ Y \qquad \text{for } 0 < X < 1$$

$$\text{and} \quad X = (Y - 4096)/2048 \qquad \text{for } -1 < X < 0$$

where X is the input in volts and Y is the digital output.

amplifier setting V/div	gain
5	0·1
2	0·25
1	0·5
0·5	1
0·2	2·5
0·1	5
50×10^{-3}	10
20×10^{-3}	25
10×10^{-3}	50

amplifier setting V/div	gain
5×10^{-3}	100
2×10^{-3}	250
1×10^{-3}	500
$0{\cdot}5 \times 10^{-3}$	1000
$0{\cdot}2 \times 10^{-3}$	2500
$0{\cdot}1 \times 10^{-3}$	5000
50×10^{-6}	10000
20×10^{-6}	25000
10×10^{-6}	50000

Table 3. Calibration of amplifer gain.

The minimum conversion time was 40 us with direct memory access which introduced a delay between consecutive samples, thus producing appreciable errors in cross wire measurements. As a remedy one of the signals was delayed by passing through a home-made analog delay line. The delay circuit shown in Figure 13, featured D.C or A.C. coupling and was isolated from the input and the output signals by two voltage followers. Its frequency response, as shown in Figure 14, was good to about 5 KHz (-3db point). Figure 15 shows that the correlation factor between two consecutive A/D converter channels, one with direct signal input and the other with the same input delayed, had negligible decrease for input frequencies below 10 KHz. However, the input signal amplitude had to be kept below 0.3 V to avoid non-linear distortion by the delay circuit.

Other peripheral units were RX02 diskettes, Winchester drive, LA50 printer and a VT100 CRT display monitor. Sampling was accomplished using assembly language software and all computations were performed in FORTRAN language.

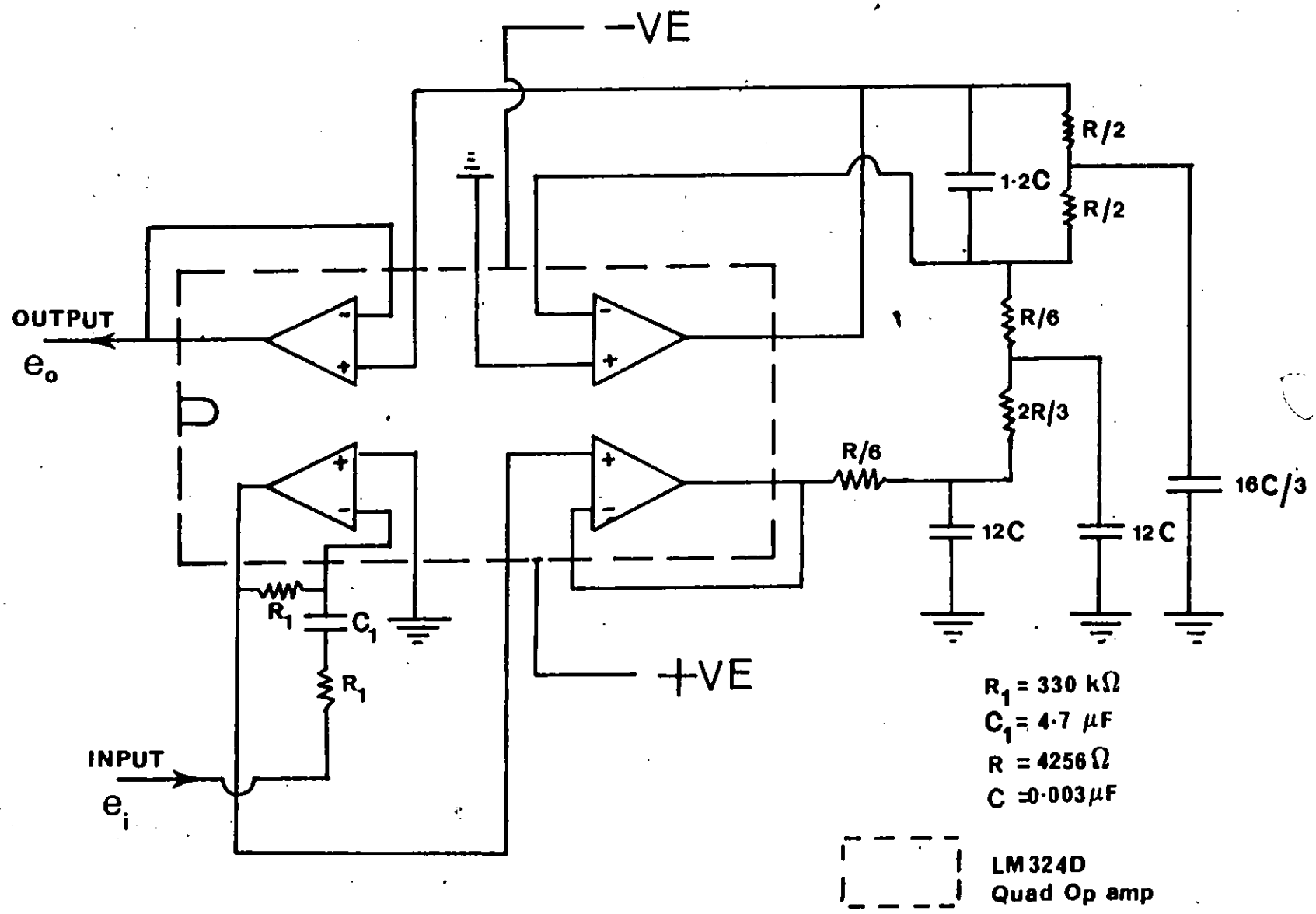

Figure 13. Circuit diagram for the analog time delay line.

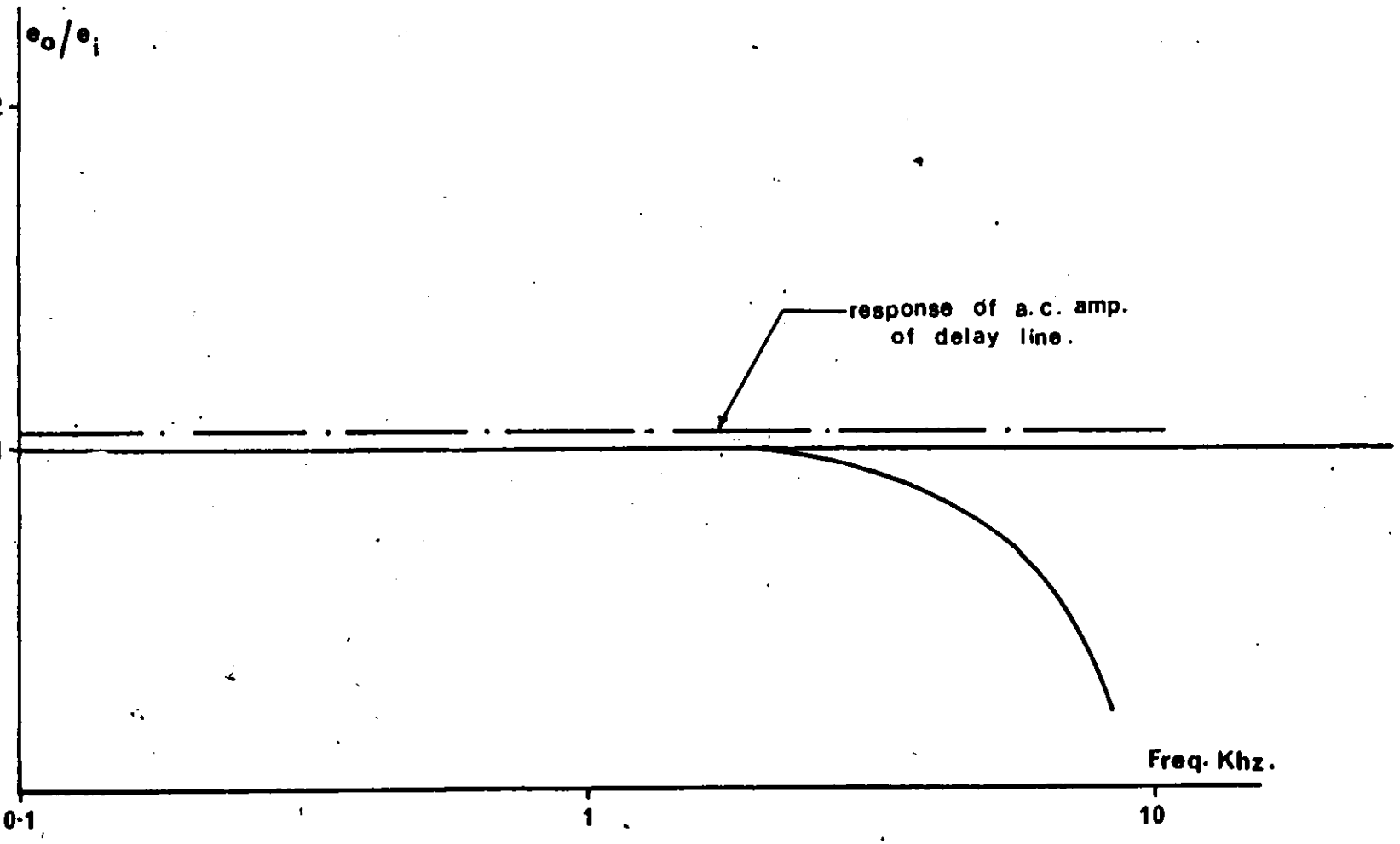

Figure 14. Frequency response of the analog time delay line.

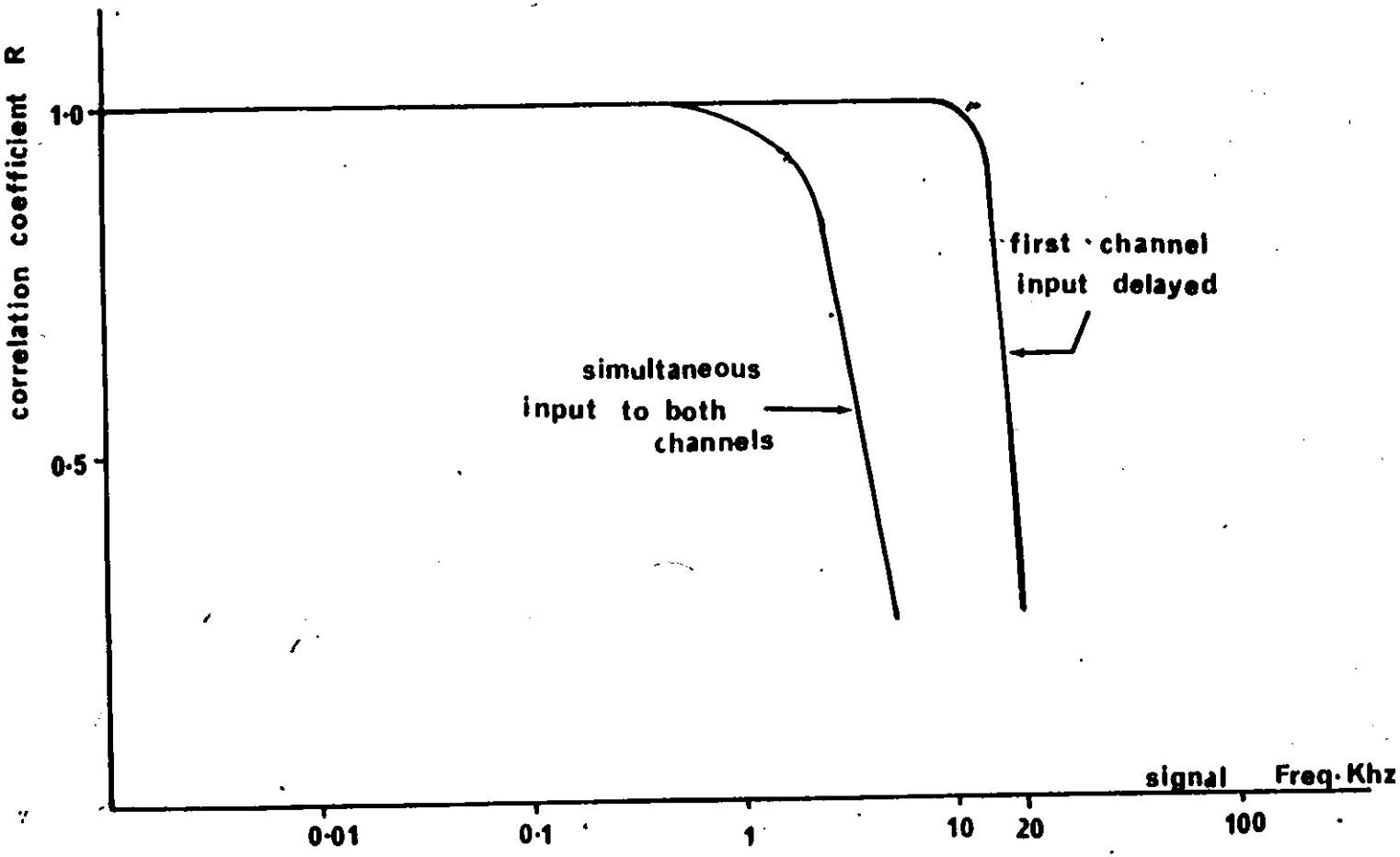

Figure 15. Correlation coefficient between two consecutive digital channels.

Chapter V

MEASUREMENTS

5.1 FREE STREAM MEASUREMENTS

A number of test measurements were made in the empty test section in order to test the wind tunnel performance and to adjust the moveable walls of the test section for boundary layer blockage compensation, such that the centreline streamwise mean velocity remained constant.

Measurements at reference speeds of 10 m/s, 17 m/s and 23 m/s, shown in Figure 16, demonstrate the near constancy of the centreline mean velocity except in the initial part of the test section that had fixed walls and where, in the low speed range, the mean speed was 0-2% lower than its asymptotic reference value.

Typical transverse profiles of the centerplane mean velocity, shown in Figure 17, confirm that the mean velocity profile was uniform away from the walls in both the vertical and the spanwise direction.

Figures 18 and 19 show that the free stream turbulent intensity remained below 0.4% for all examined speeds and measuring positions. Such levels are comparable to or better

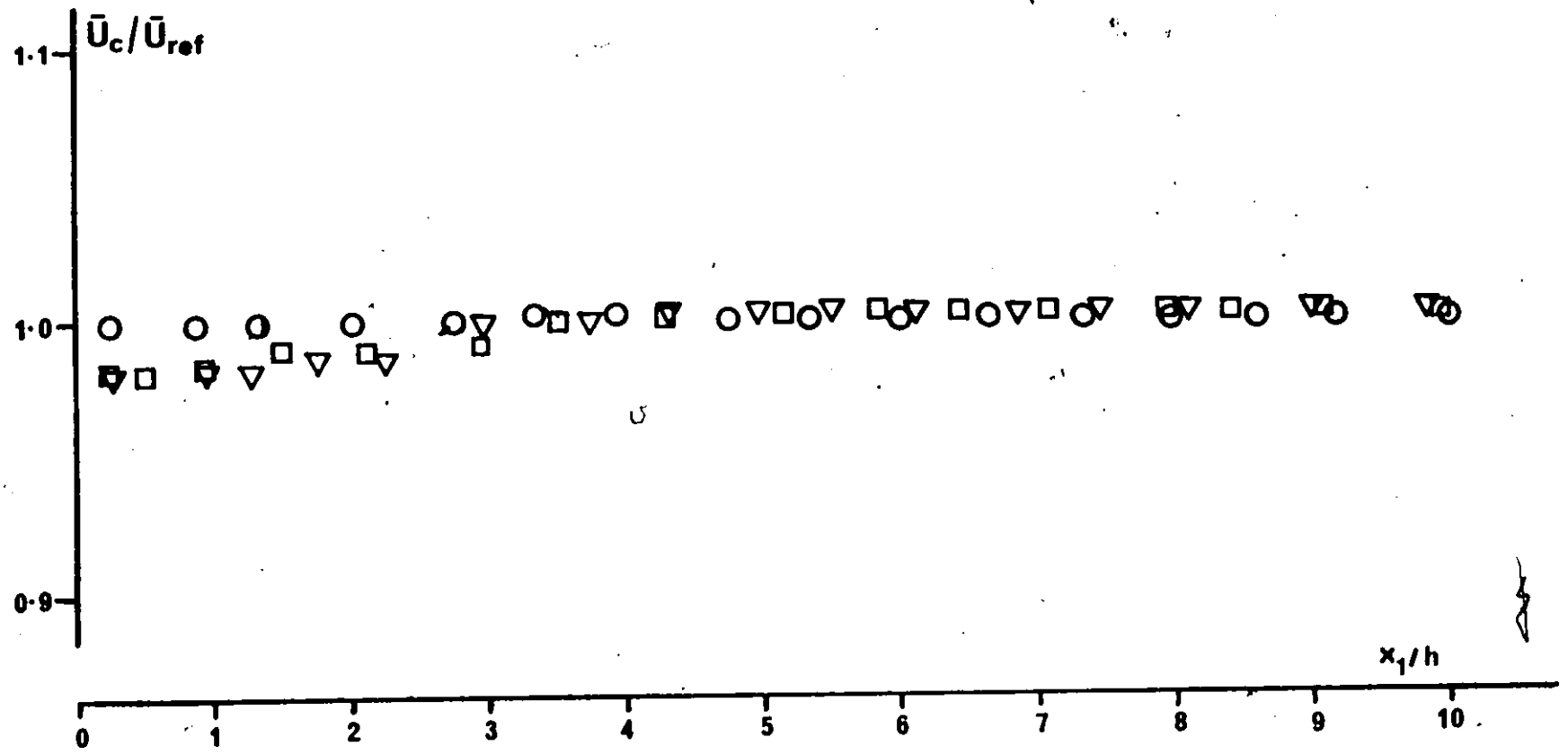

Figure 16. Downstream development of the centreline free stream mean velocity; □ Üref=10m/s, ▽ Üref=17m/s, ○ Üref=23m/s.

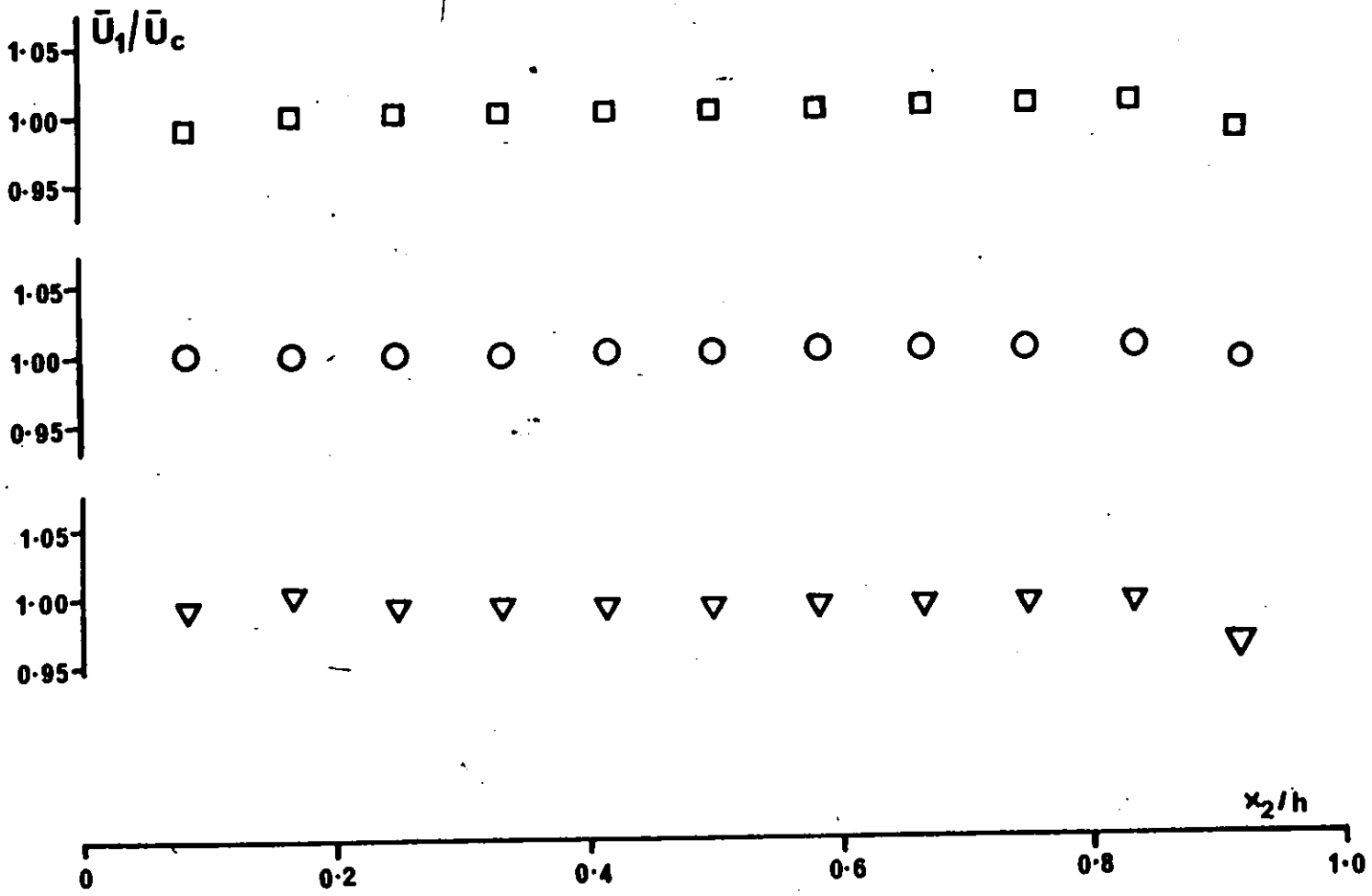

Figure 17. Transverse free stream mean velocity profiles;

▽ $x_3/h=-0.451$ ○ $x_3/h=0.0$, □ $x_3/h=+0.451$

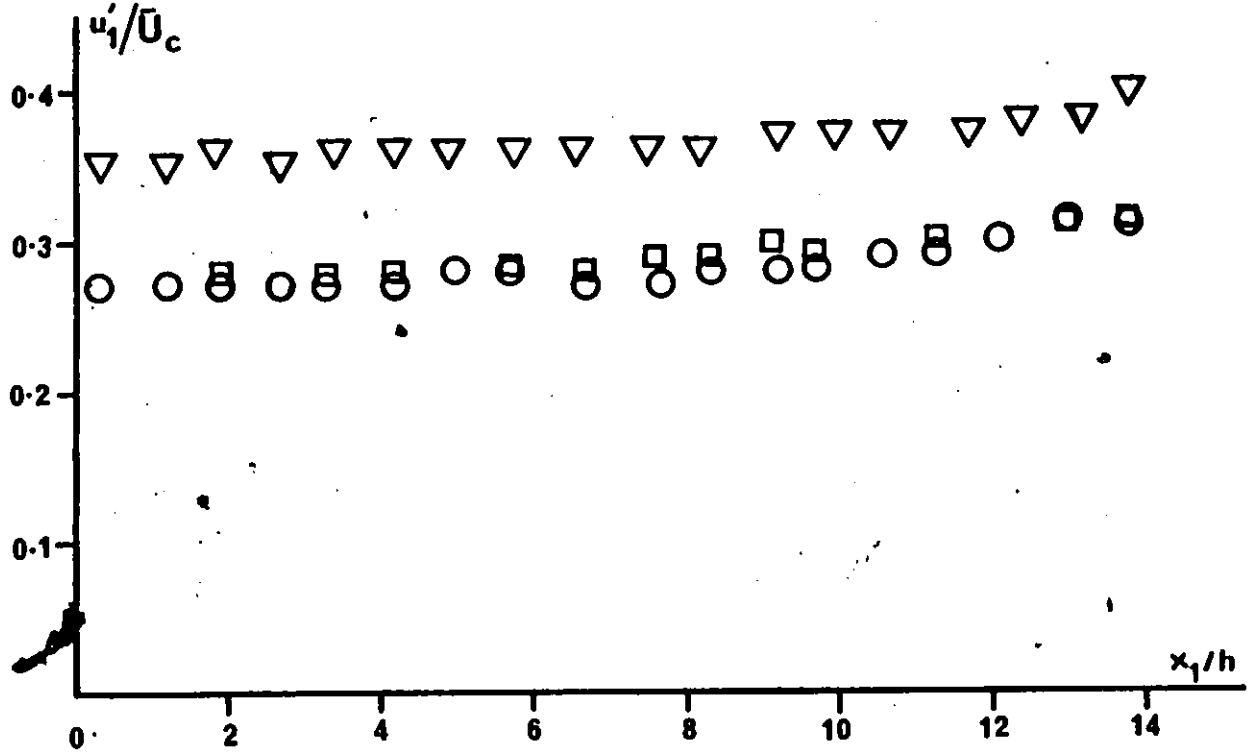

Figure 18. Downstream distribution of free stream rms turbulent velocities; ▽ $\bar{U}c$=10m/s, ○ $\bar{U}c$=15m/s, □ $\bar{U}c$=20m/s.

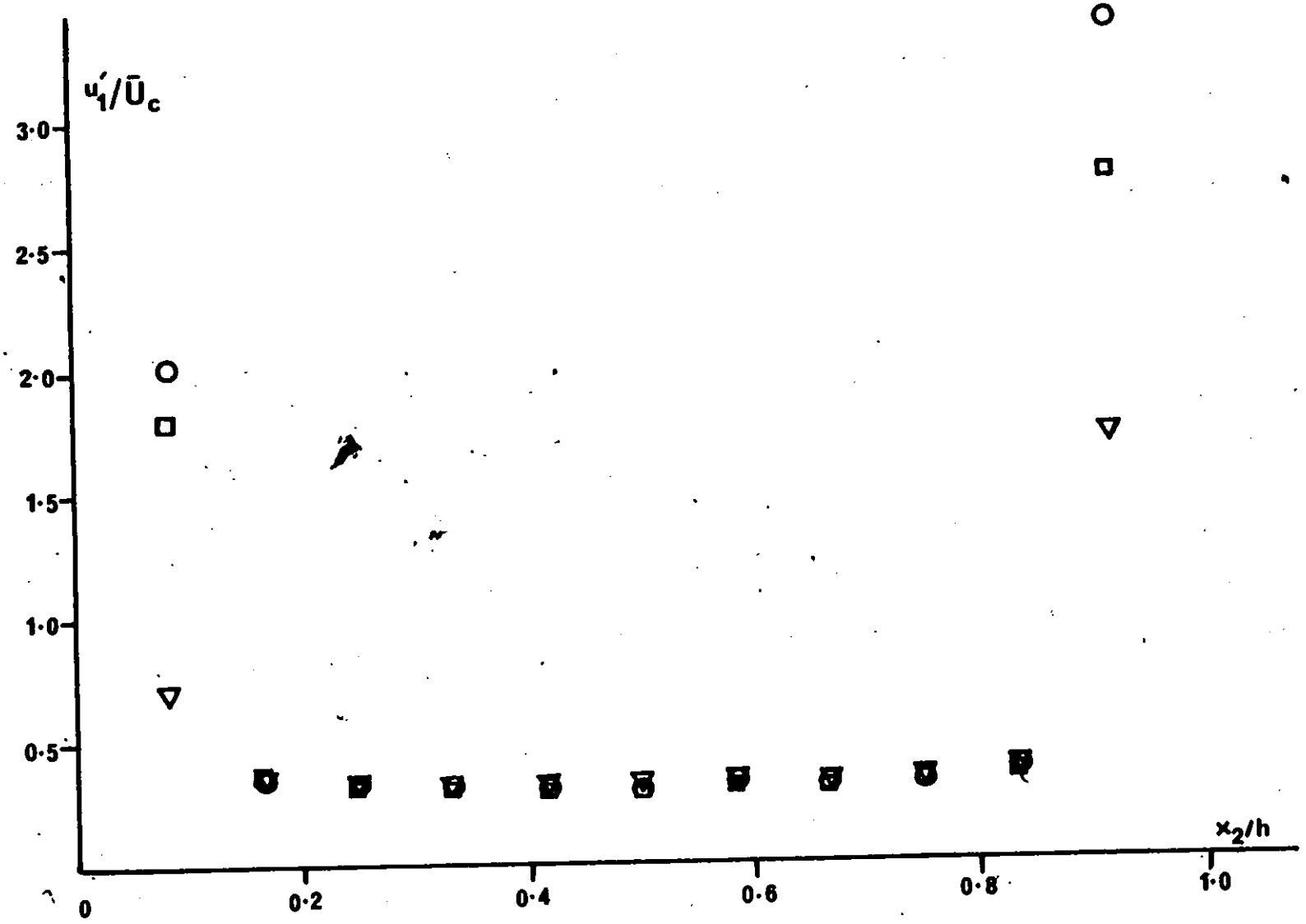

Figure 19. Transverse distribution of free stream rms turbulent velocities; flow conditions and symbols as in Figure 18.

than those encountered in wind tunnels used for most earlier turbulent flow investigations.

In conclusion the flow facility was found capable of generating a stable uniform mean free stream with an acceptably low free stream turbulence level.

5.2 MEAN SHEAR MEASUREMENTS

These measurements were taken with the shear generator and with none, one or two grids inserted in the flow. Figures 20, 21 and 22, show the mean velocity profiles in the vertical centreplane of the tunnel ($X/h = 0$) and for three centreline speeds, $U = 6.0$, 9.0 and 13.0 m/s, at four downstream locations, $X/h = 2.0$, 7.5, 10.0 and 13.0, with only the shear generator inserted in the flow. The slope of the velocity profiles was constant in all cases and was preserved downstream. In all cases boundary effects were negligible in the tunnel core, i.e. for $0.2 < X/h < 0.8$. The values of the mean shear attained for centreline mean velocities 6.0, 9.0 and 13.0 m/s were respectively 43.5, 60.0 and 84.0 s-1, corresponding to shear parameters $(h/U)dU/dX$ equal to 2.0, 2.0 and 2.2.

Introduction of a specific grid into the flow was found to reduce the magnitude of the incoming mean shear by a constant factor which was nearly independent of the grid position (Figure 23) and which was 1.9 for the M1.27 cm grid, 2.2 for the M2.54 cm grid (Figure 25) and 3.0 for the

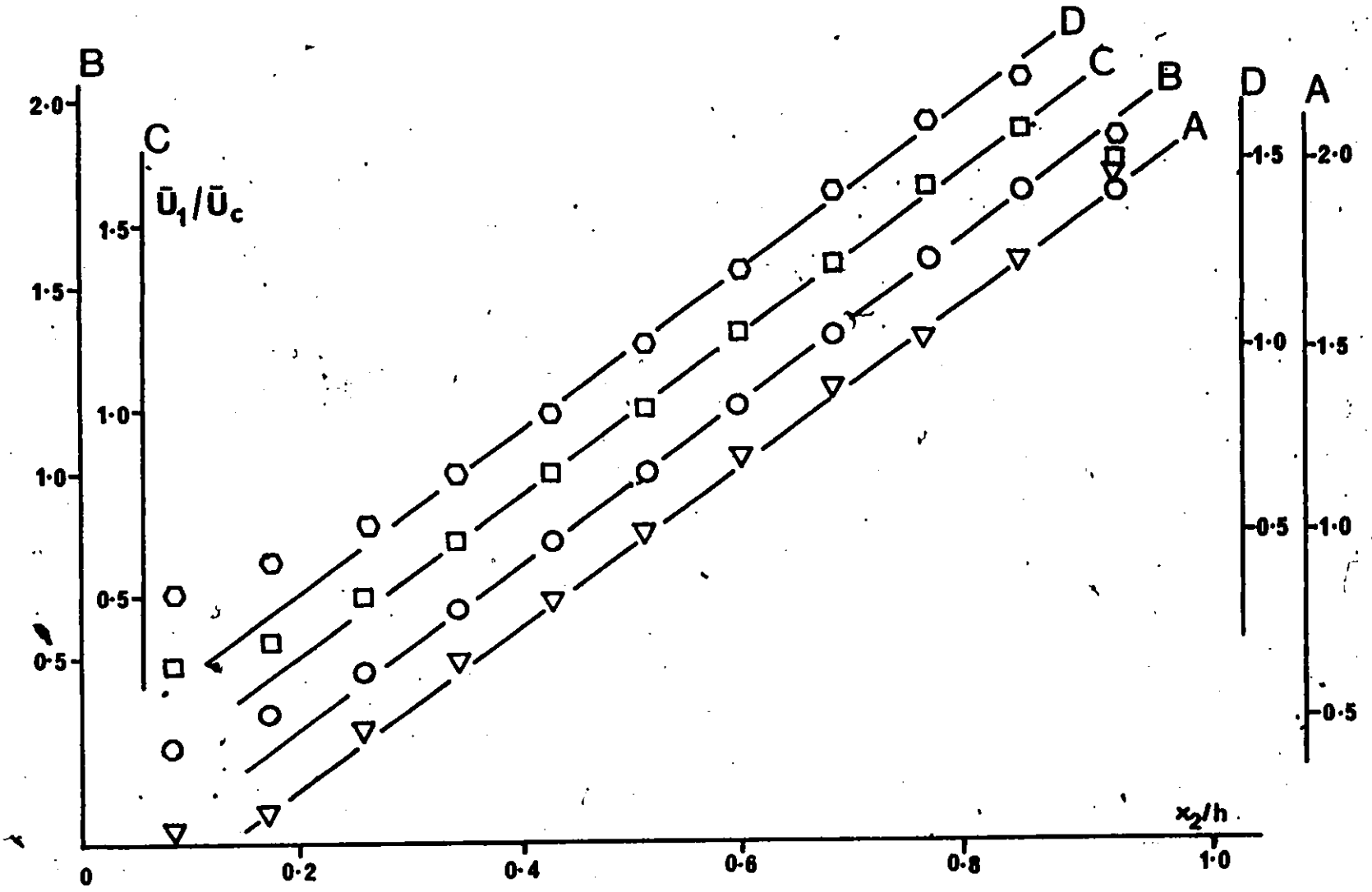

Figure 20. Transverse mean velocity shear profiles, $\bar{U}c$=6m/s, $d\bar{U}_1/dx_2$ =43.5s-1
▽ x_1/h=2.0, ○ x_1/h=7.5, □ x_1/h=10.0, ○ x_1/h=13.0

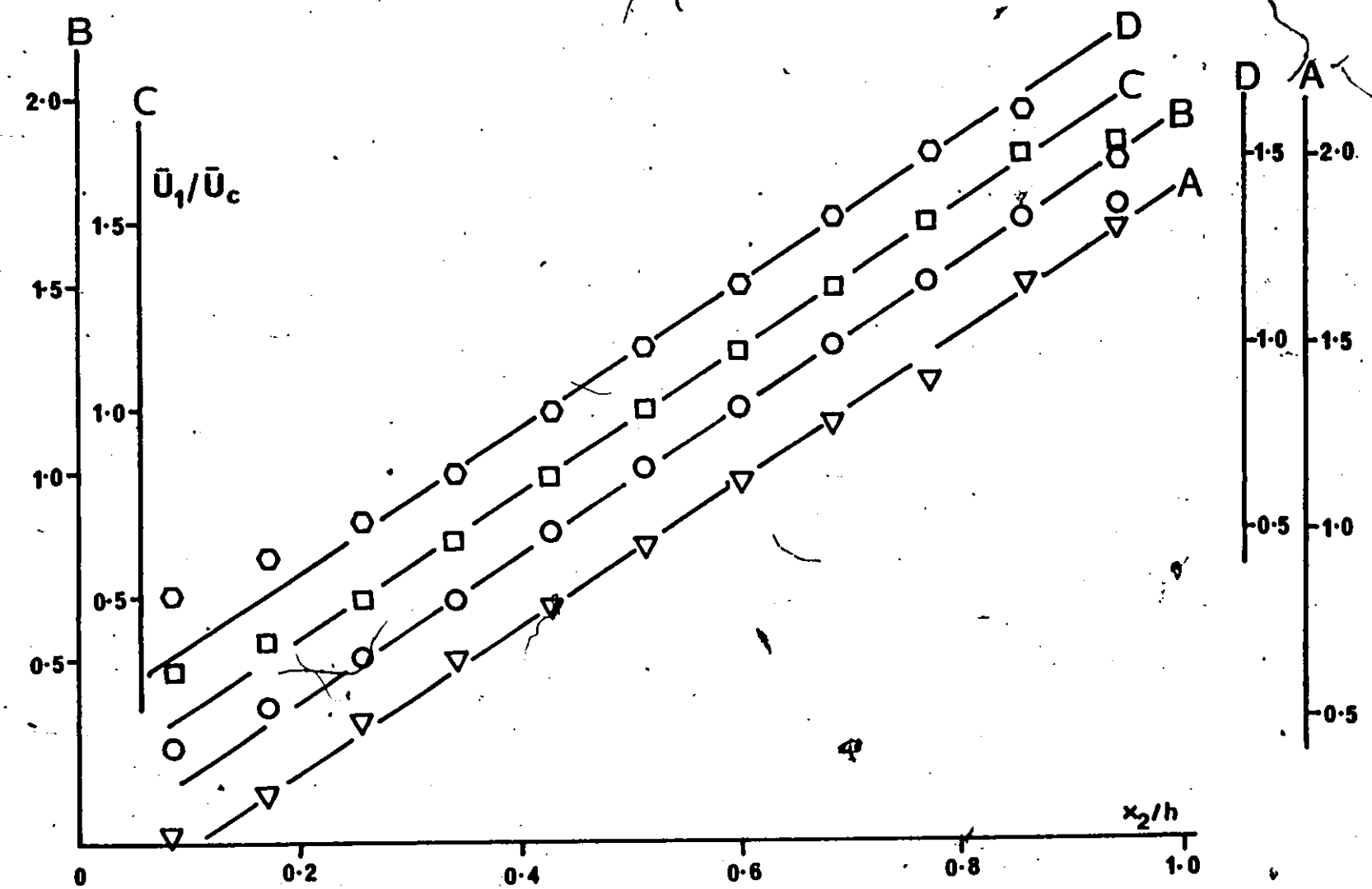

Figure 21. Transverse mean velocity shear profiles, $\bar{U}c$=9m/s, $d\bar{U}_1/dx_2$ = 60s-1 symbols as in Figure 20.

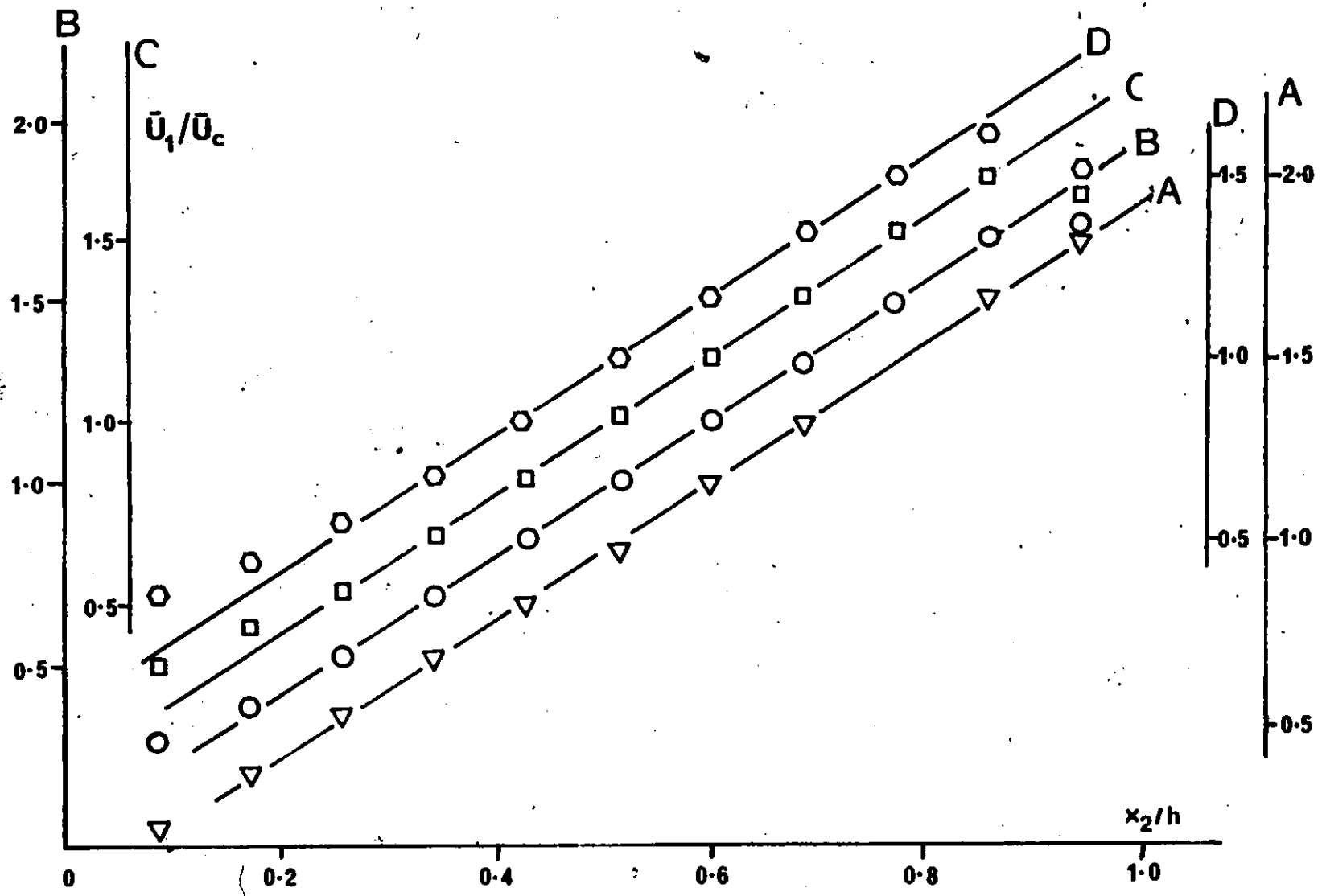

Figure 22. Transverse mean velocity shear profiles, $\bar{U}c$=13m/s, $d\bar{U}_1/dx_2$=84s-1 symbols as in Figure 20.

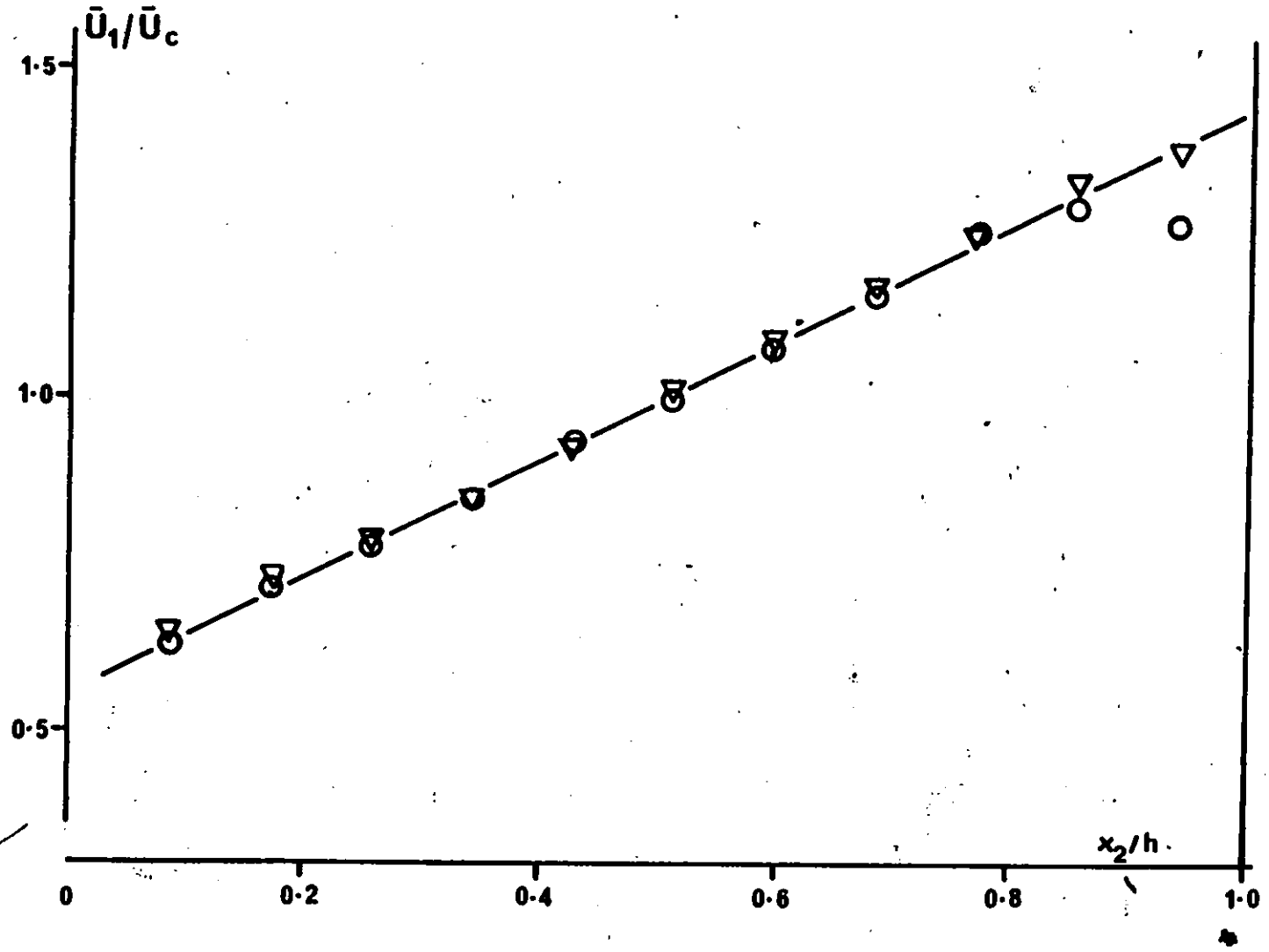

Figure 23. Transverse mean velocity profile downstream of M2.54 cm grid placed at $x_1/h=12.0$; $\bar{U}c=13m/s$; grid position: ▽ $x_1/h=1.04$, ○ $x_1/h=4.5$

M5.08 cm grid (Figure 26). Thus, a variety of mean shear values could be generated for different combinations of flow obstructions and flow speeds as shown in Table 4.

5.3 DEGREE OF TRANSVERSE HOMOGENEITY OF TURBULENT VELOCITY

Although the flow was designed to produce transversely homogeneous velocity fluctuation statistics, measurable inhomogeneities were observed, for example in the transverse profile of the rms streamwise velocity. The largest degree of inhomogeneity appeared in the shear flow without grids (Figures 27, 28 and 29), which also had the largest shear values. As expected, introduction of the grids reduced the transverse inhomogeneity of the flow; the effect was less pronounced for the M1.27 cm grid (Figure 30) and the M2.54 cm grid (Figure 31) than for the M5.08 cm grid (Figure 32). This reduction of inhomogeneity was also noticed when combinations of grids were used (Figure 30). Grids and screens have been used extensively in earlier investigations for the purpose of reducing mean velocity inhomogeneities and turbulence levels. The overall pattern of inhomogeneities did not appear systematic and was probably due to local mean shear non- uniformities, imperfections of the apparatus and remaining effects of initial conditions. The inhomogeneity levels were comparable to those in earlier investigations for similar values of the mean shear and are

Inserted grid(s)		centreline speed	shear reduction factor	shear
Rod spacing cm	location x_1/h	$\bar{U}_c$ m/s		$(d\bar{U}_1/dx_2)$ s^{-1}
–	–	6	–	43.5
–	–	9	–	60
–	–	13	–	84
M2.54	4.5	6	2.30	18.9
M2.54	4.5	9	2.17	27.7
M2.54	4.5	13	2.17	38.8
M5.08	1.04	6	3.06	14.2
M5.08	1.04	9	2.90	20.8
M5.08	1.04	13	2.90	29.3
M2.54	1.04	13	2.17	38.8
M1.27	4.5	9	1.90	31.2
M5.08 M2.54	1.04 4.5	13	6.00	14
M2.54 M5.08	1.04 4.5	13	6.05	13.8
M5.08 M2.54	1.04 4.5	6	6.83	6.37
M5.08 M2.54 M1.27	1.04 2.08 4.5	13	9.9	8.48

TABLE 4.

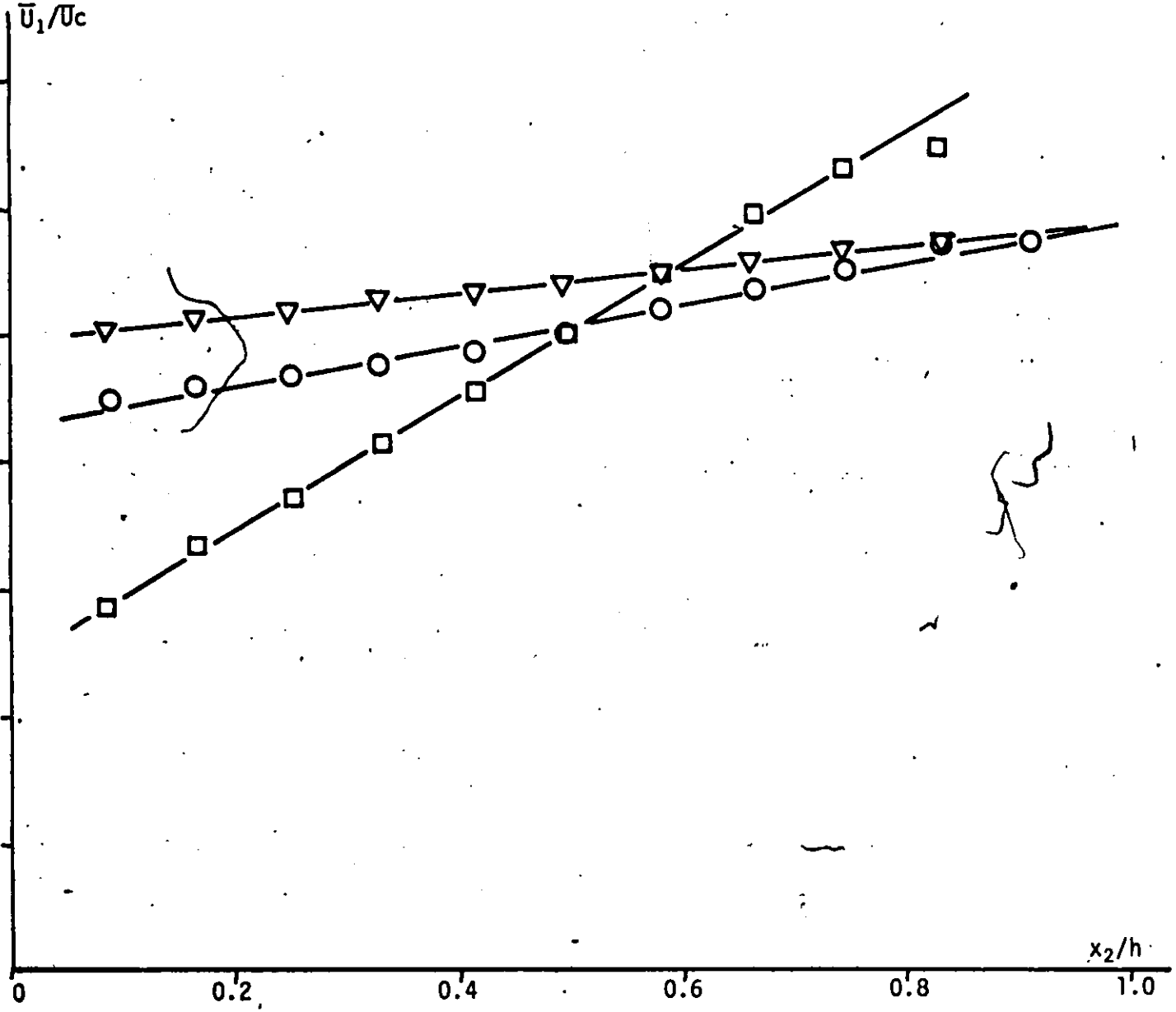

Figure 24:

Transverse mean shear profiles. Symbols as in Figure 30.

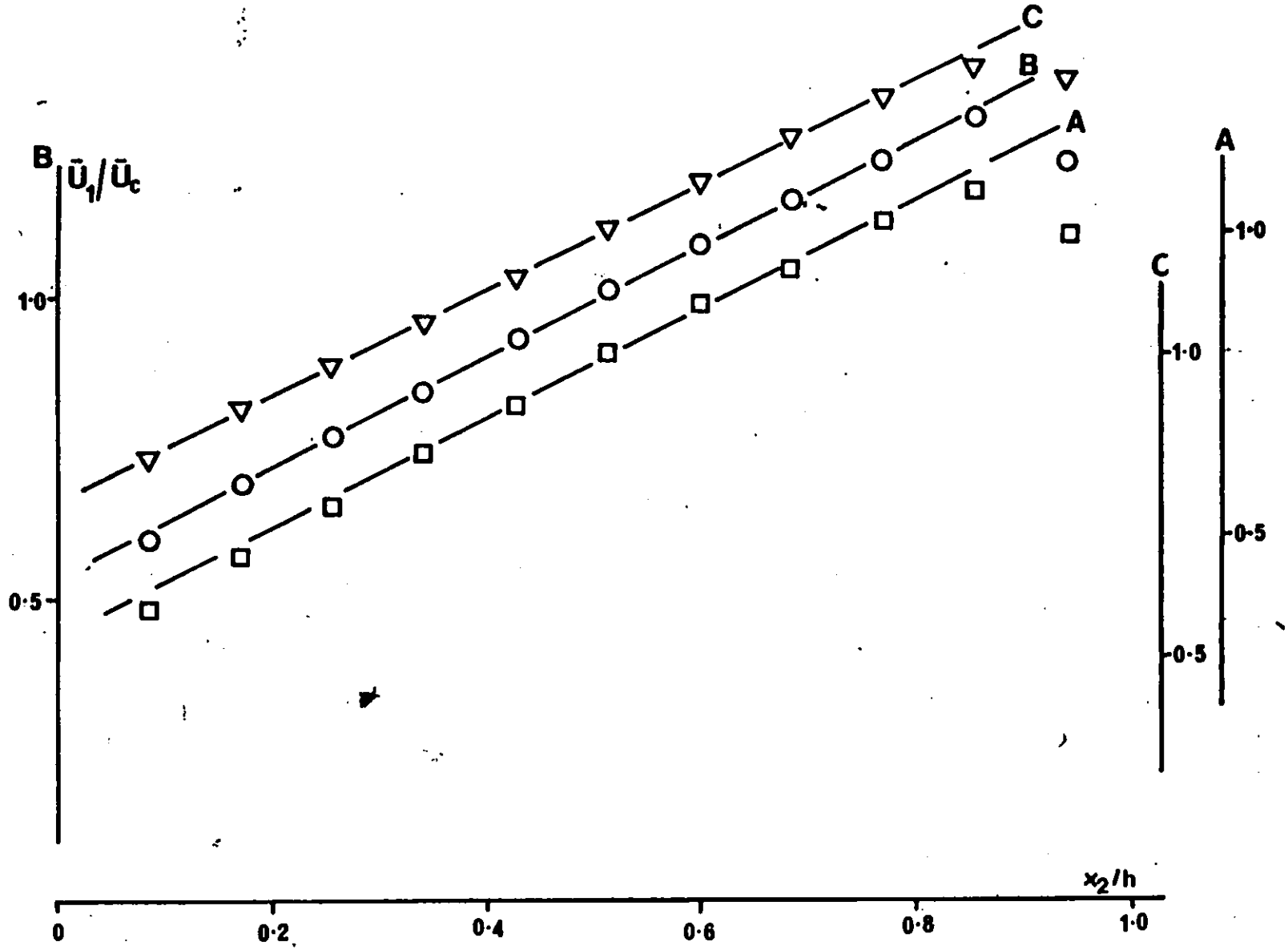

Figure 25. Transverse mean velocity profiles downstream of M2.54 cm grid placed at $x_1/h=4.5$; □ $\bar{U}c=6m/s$, ○ $\bar{U}c=9m/s$, ▽ $\bar{U}c=13m/s$.

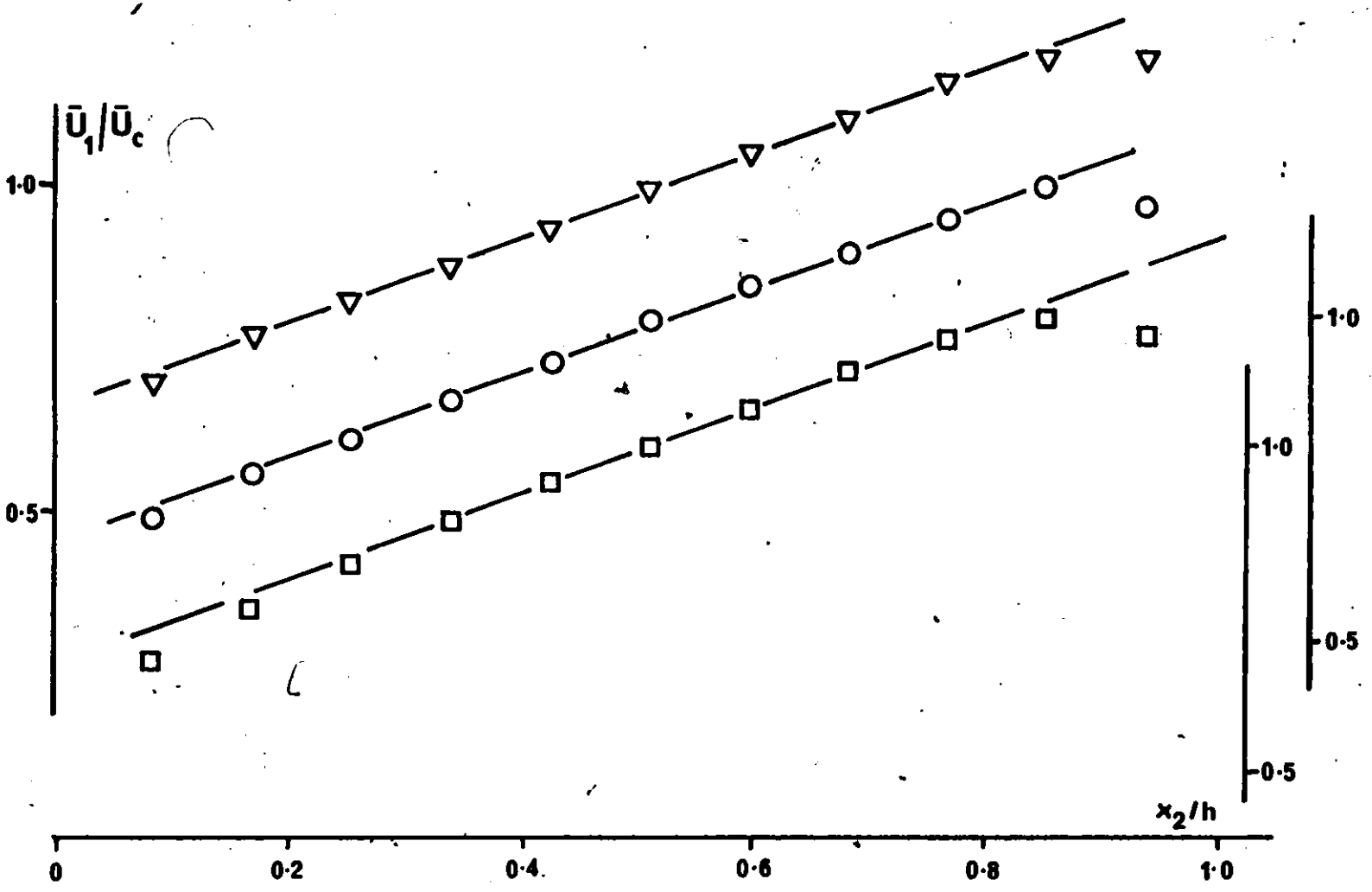

Figure 2 . Transverse mean velocity profiles downstream of M5.08 cm grid placed at x_1/h=1.04; symbols as in Figure 24.

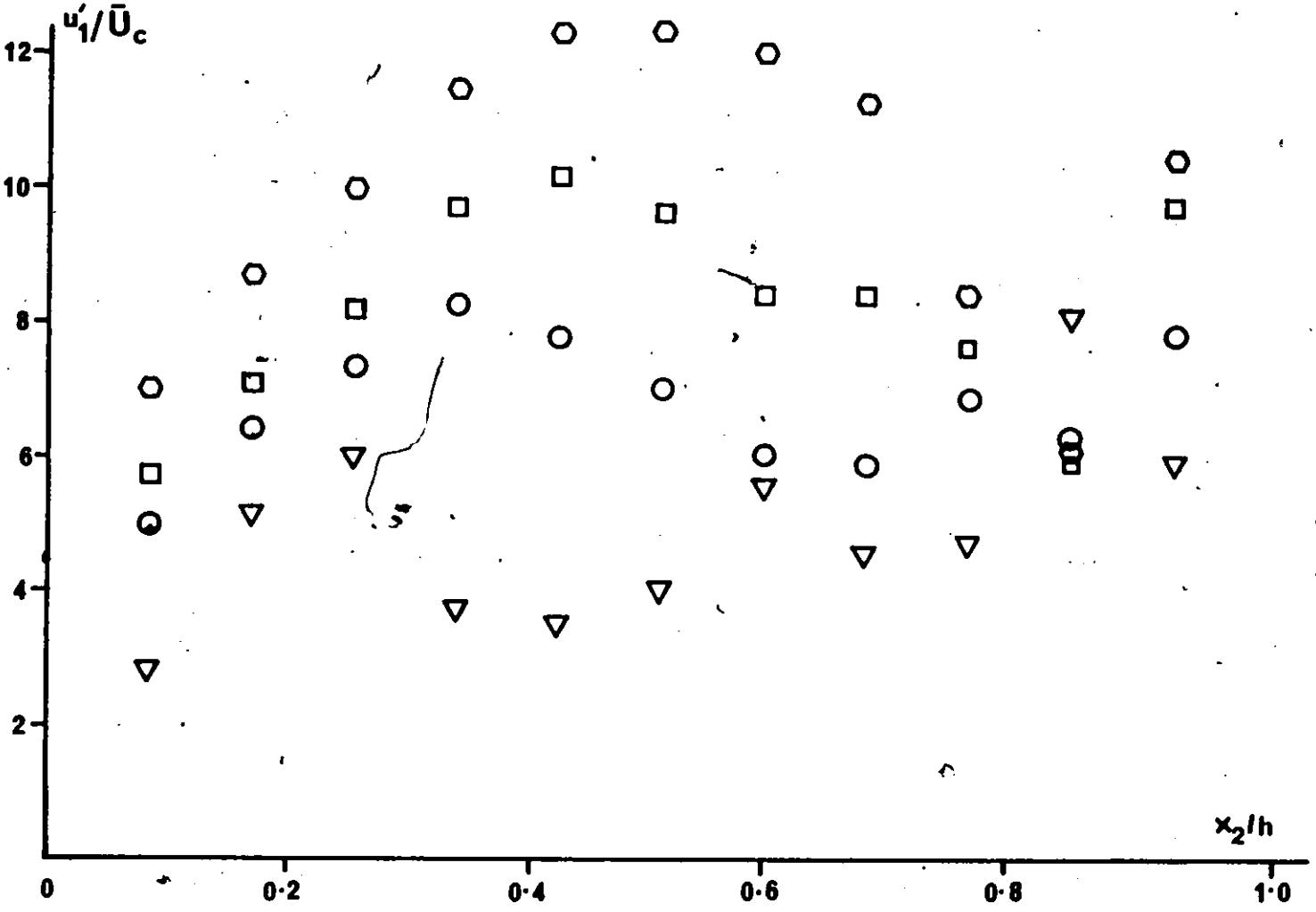

Figure 27. Transverse distribution of rms turbulent velocities; $\bar{U}c$=6m/s symbols as in Figure 20.

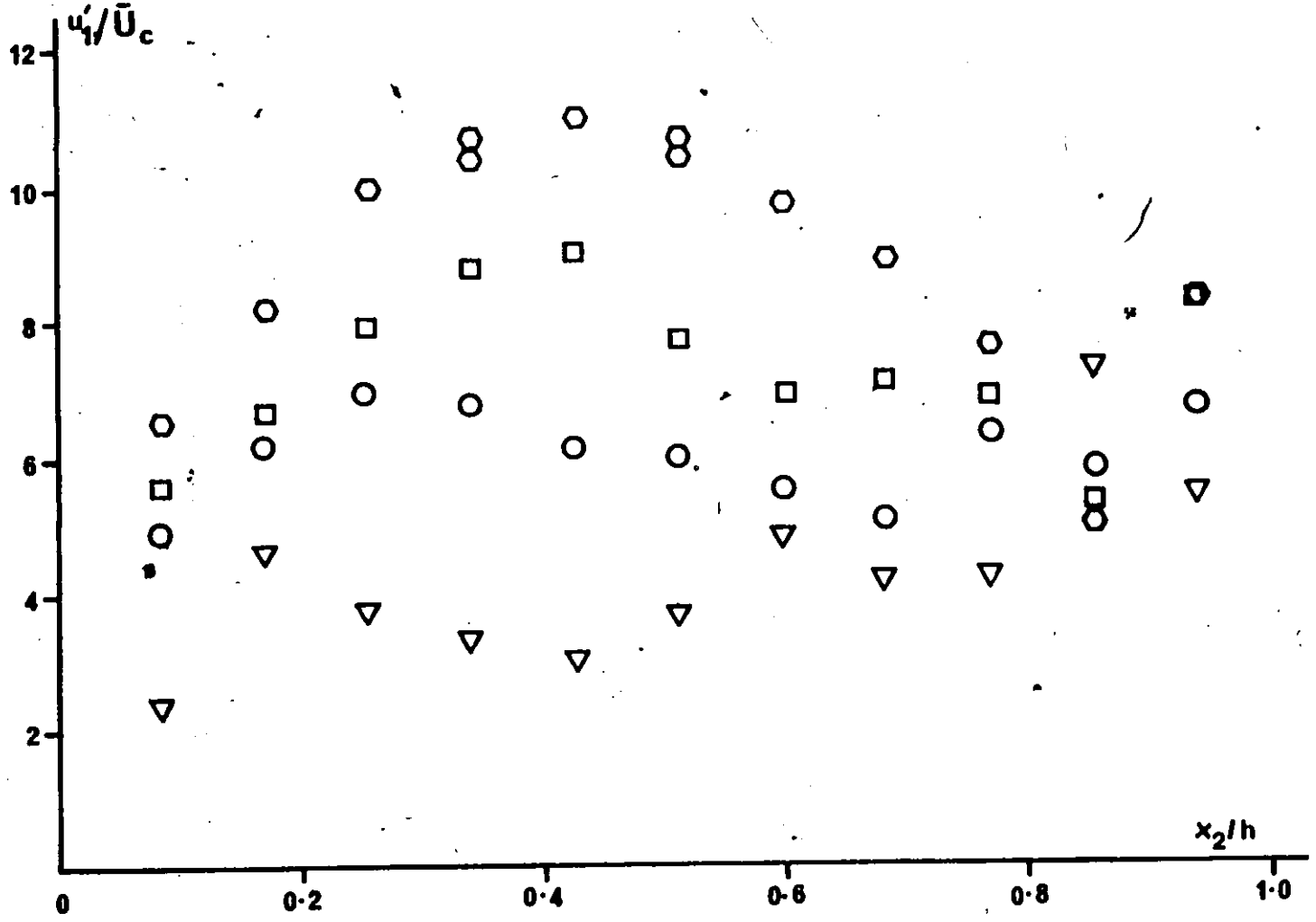

Figure 28. Transverse distribution of rms turbulent velocities; $\bar{U}c$=9m/s symbols as shown in Figure 20.

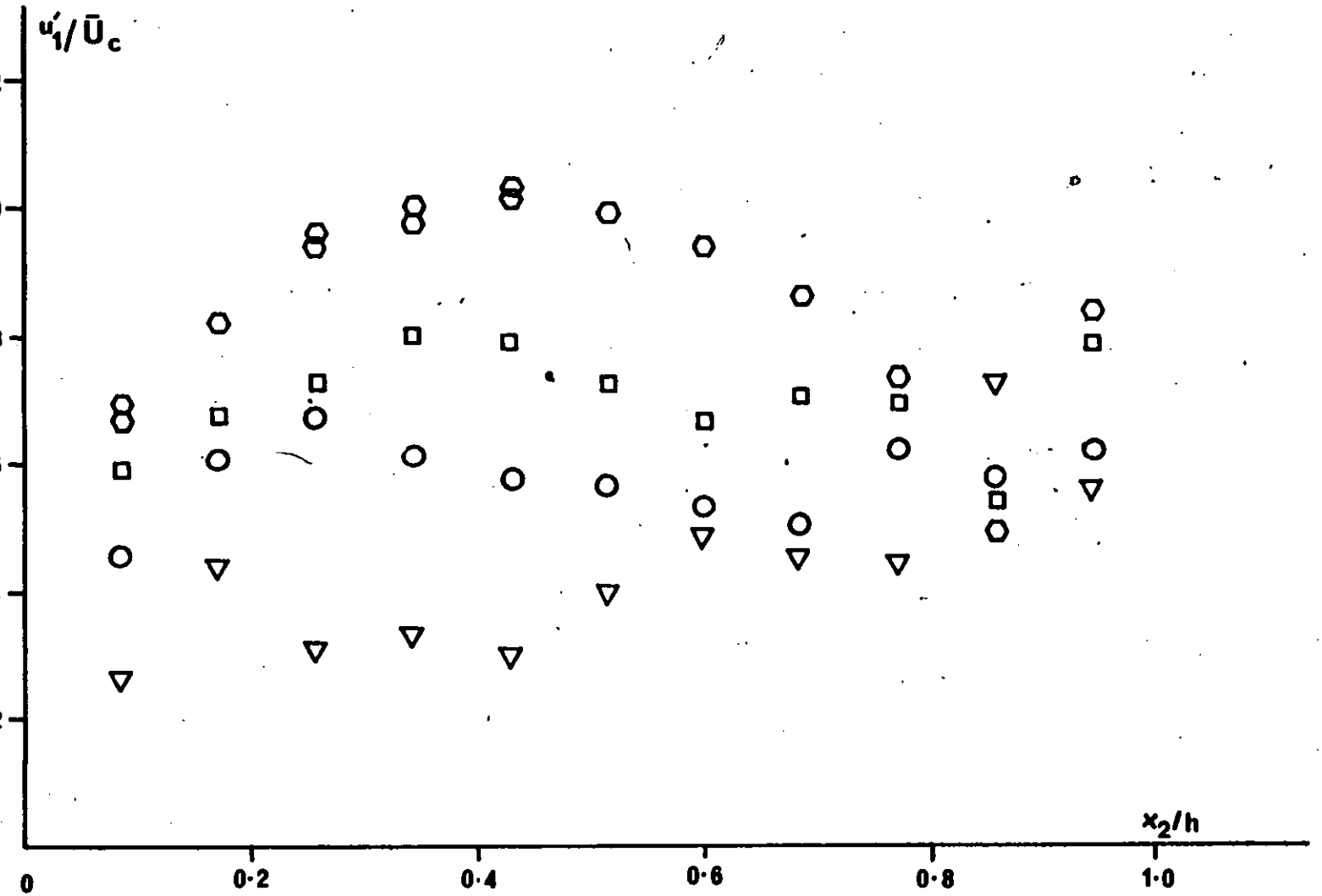

Figure 29. Transverse distribution of rms turbulent velocities; $\bar{U}c$=13m/s symbols as in Figure 20.

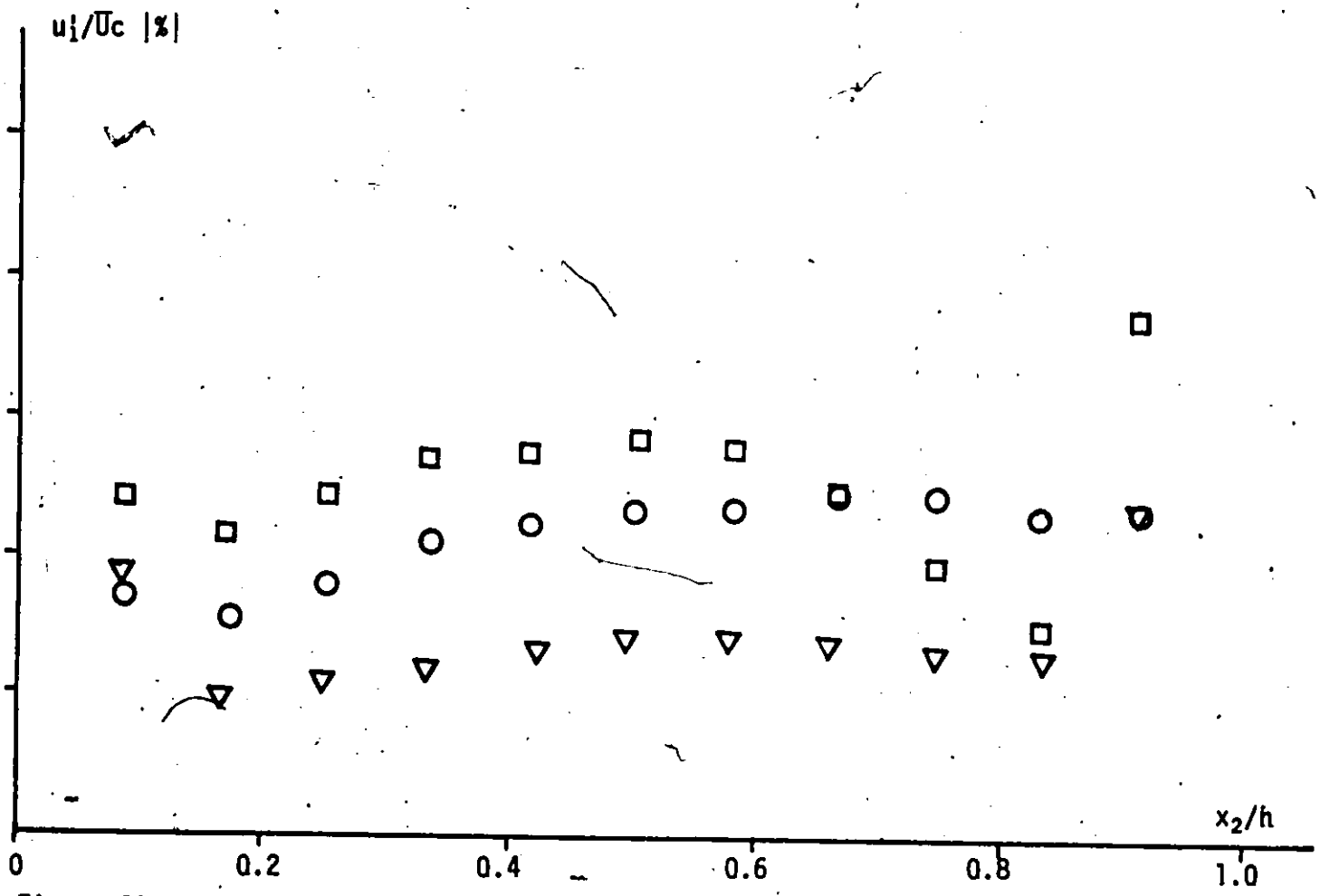

Figure 30:

Transverse distribution of rms turbulent velocities: □ m1.27, $\bar{U}c$ = 9 m/s, profile at x_1/h = 10; ○ m5.08 & m2.54 at x_1/h = 1.04 & 4.5 respectively $\bar{U}c$ = 13 m/s, profile at x_1/h = 12; ▽ m5.08, m2.57 & m1.27 at x_1/h = 1.04, 2.08 & 4.5 respectively, $\bar{U}c$ = 13 m/s, profile at x_1/h = 12.

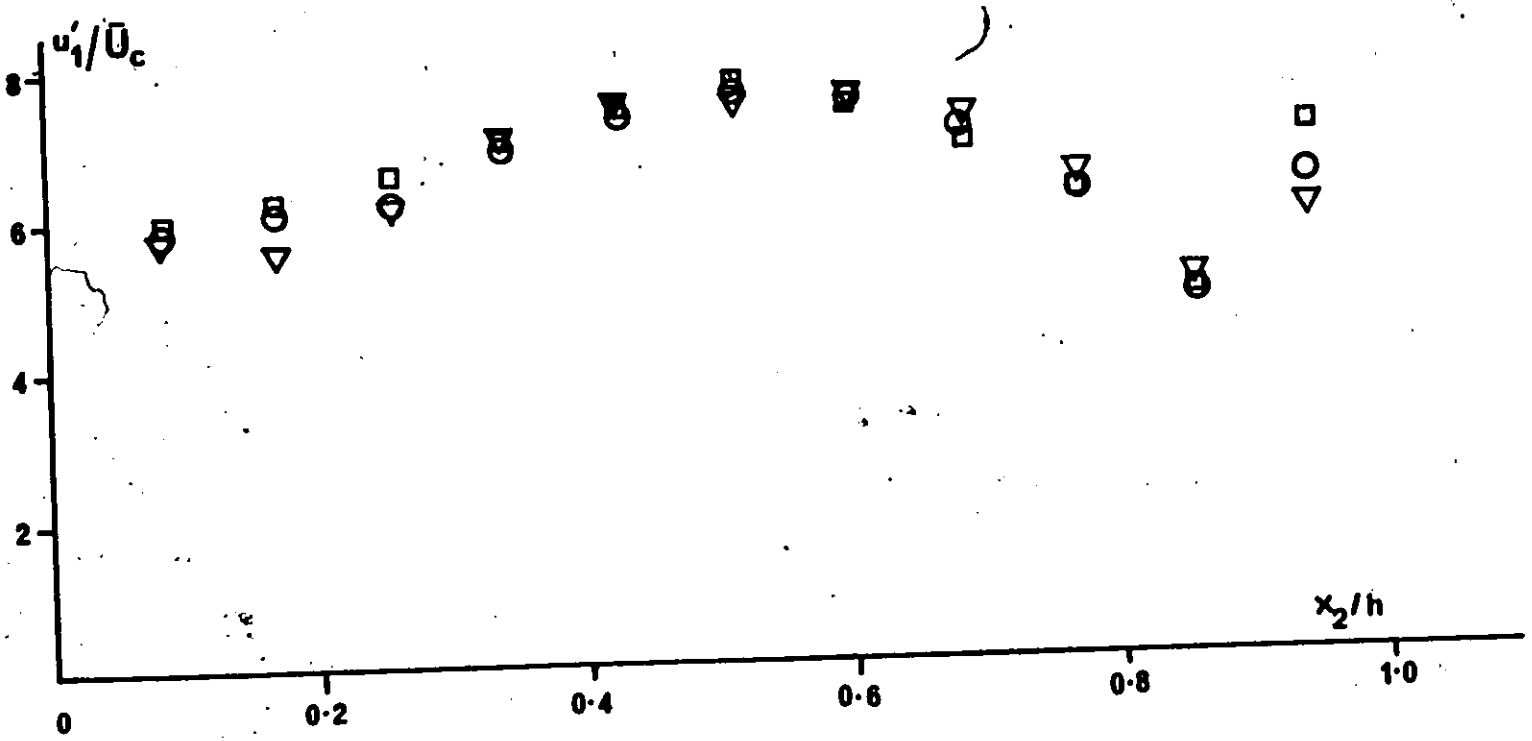

Figure 31. Transverse distribution of rms turbulent velocities downstream of M2.54 cm grid; □ $\bar{U}c$=6m/s, ○ $\bar{U}c$=9m/s, ▽ $\bar{U}c$=13m/s.

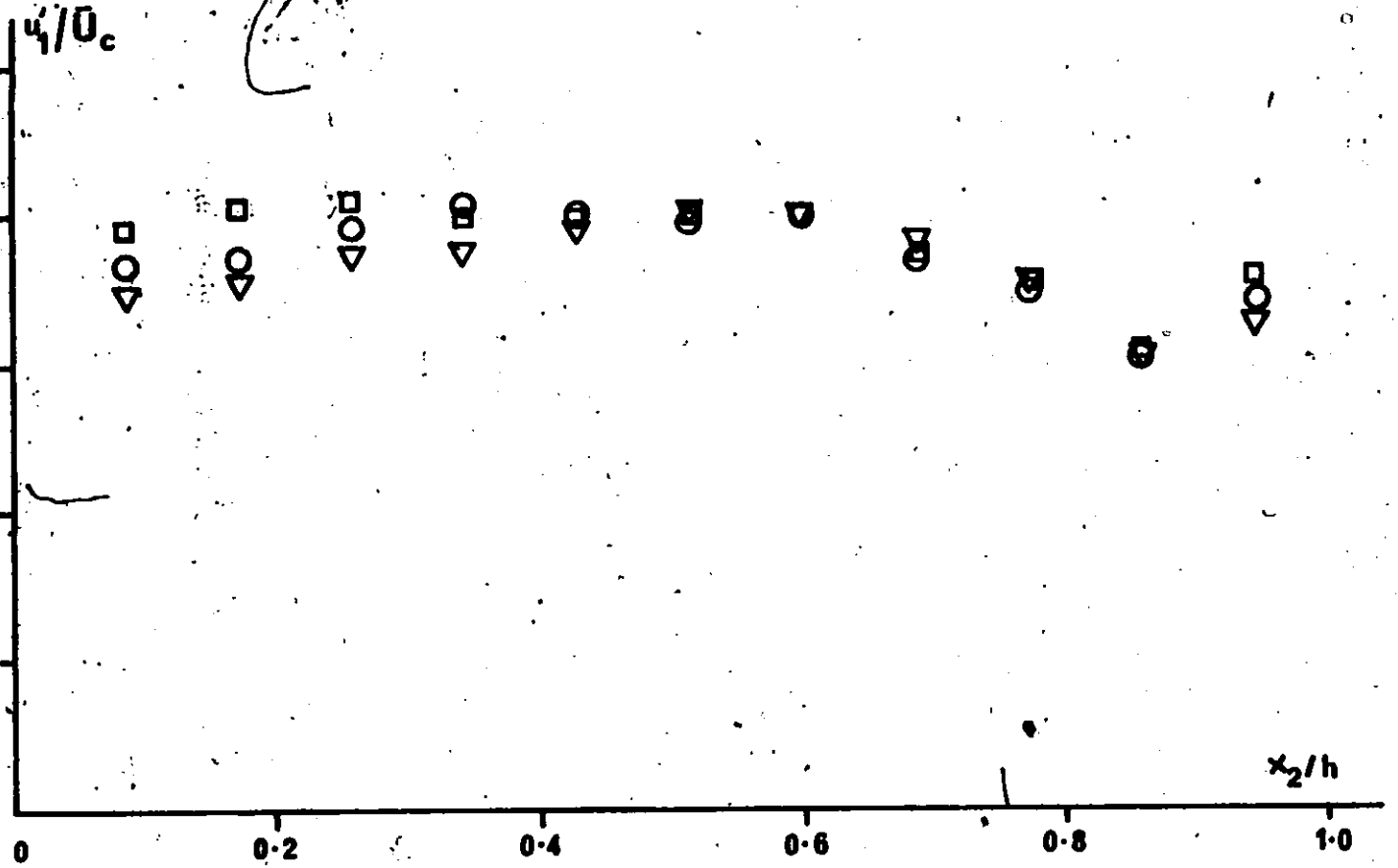

Figure 32. Transverse distribution of rms turbulent velocities downstream of M5.08 cm grid; symbols as in Figure 31.

sufficiently low for the purpose of the present investigation.

5.4 DOWNSTREAM DEVELOPMENT OF REYNOLDS STRESSES AND THE TURBULENT K.E.

Following the analysis of Chapter 2, the components of the Reynolds stress tensor $\overline{u_i u_j}$ and the turbulent kinetic energy q^2 were plotted versus the downstream distance on semi-logarithmic co-ordinates in order to reveal possible exponential laws. Indeed, in all cases, the data was compatible with such laws.

In the cases of the shear generator alone (Figures 33, 34 and 35), and with the M1.27 (Figure 36) and M2.54 cm grid (Figures 37, 38 and 39) inserted individually, exponential growth with the same exponent for all Reynolds stresses was observed in the asymptotic state. However, in the case of the M5.08 cm grid (Figures 40, 41 and 42) and for the two-grid combinations (Figure 36) the Reynolds stresses attained asymptotically constant values.

The presence of a grid initially increased the turbulence level but the grid effect decayed downstream and, sufficiently far behind the grid, mean shear was presumably the only source of turbulence production. Another observation was that in all cases away from flow obstructions, the Reynolds stresses were ordered as $\overline{u_1^2} > \overline{u_3^2} > \overline{u_2^2} > -\overline{u_1 u_2}$, as was also the case in earlier investigations.

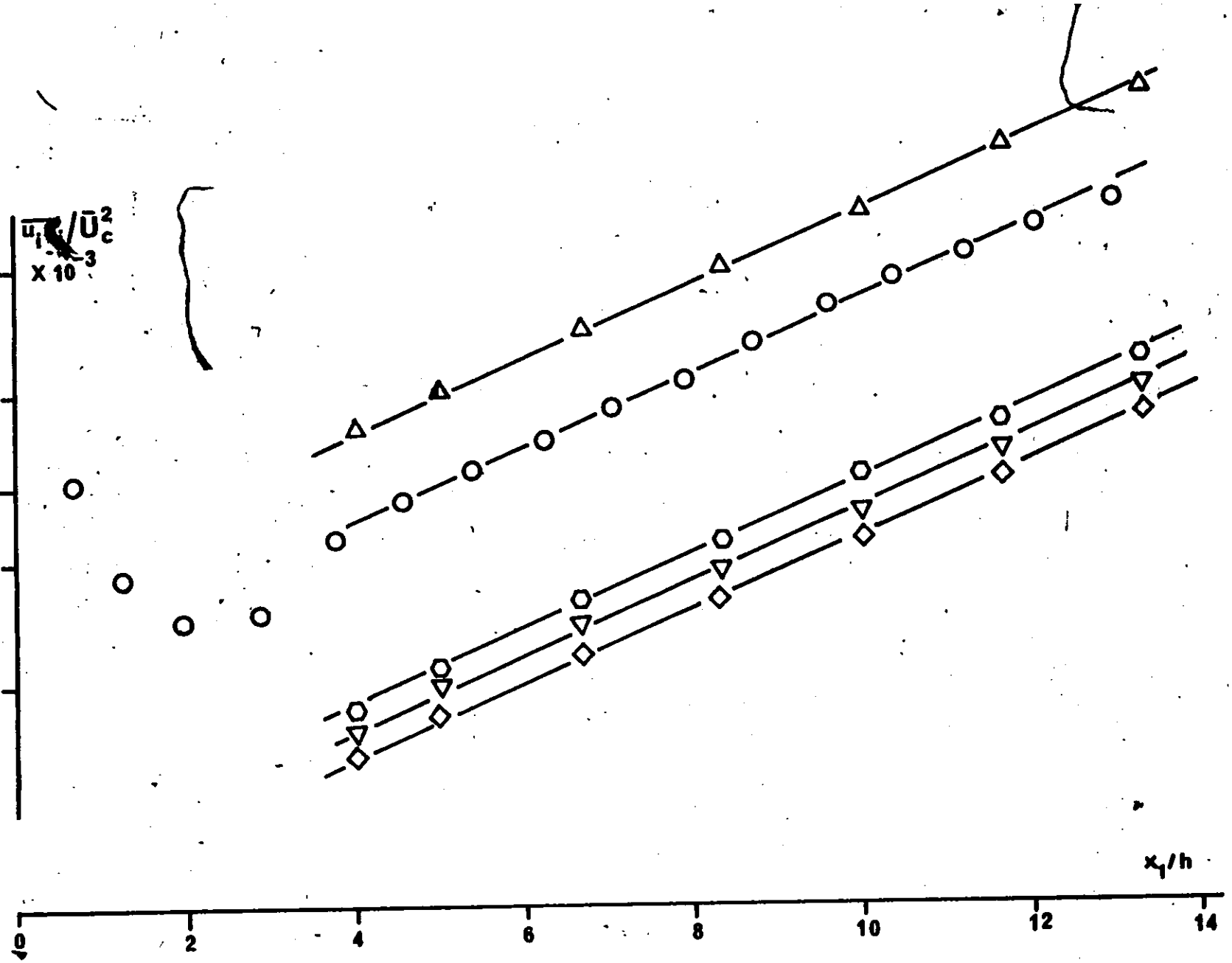

Figure 3. Downstream development of Reynolds stresses; $\bar{U}c$=6m/s; ◇ i=1, j=2; ▽ i=j=2; ○ i=j=3; ○ i=j=1; △ i=j.

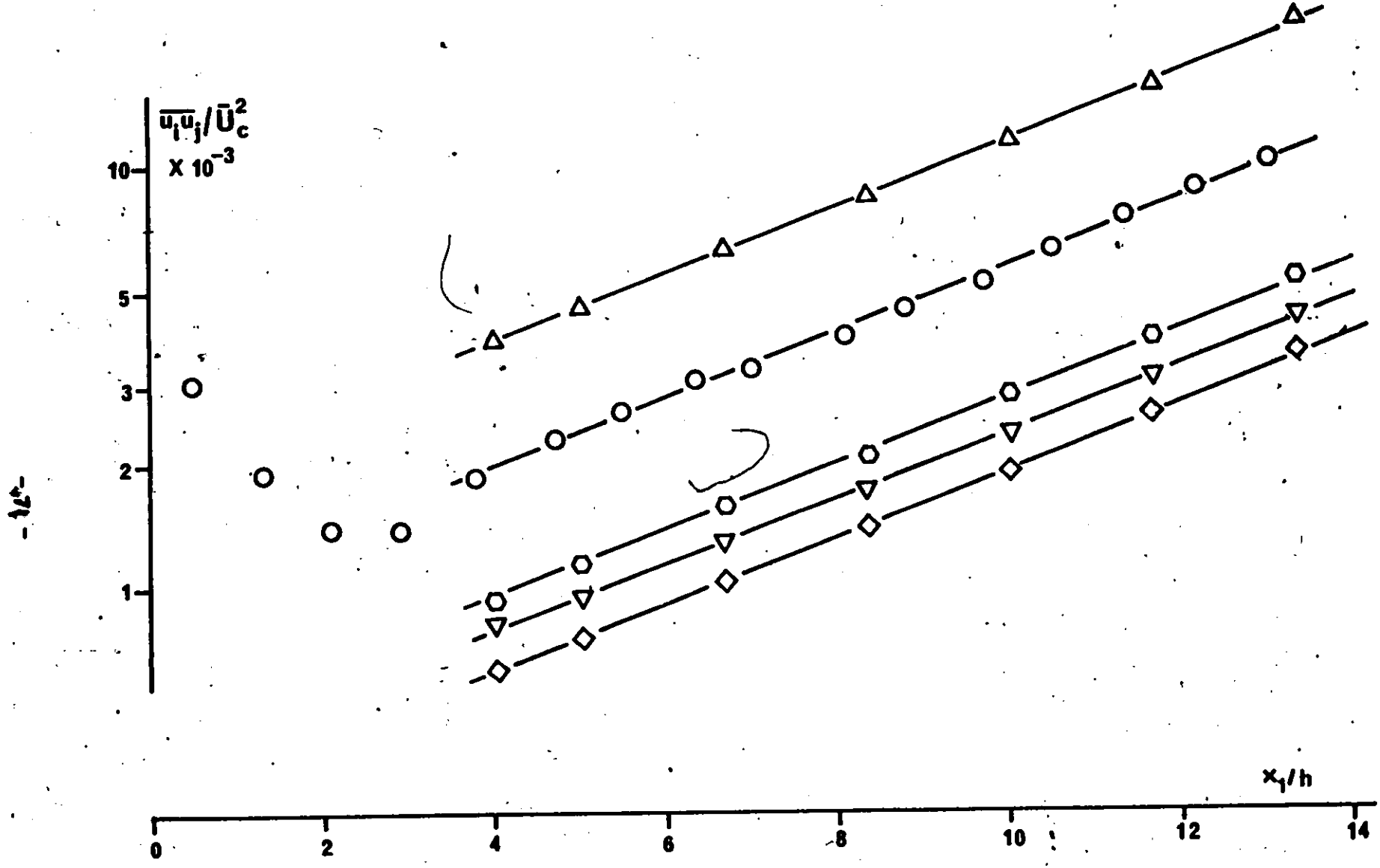

Figure 34. Downstream development of Reynolds stresses; $\bar{U}c$=9m/s; symbols as in Figure 33.

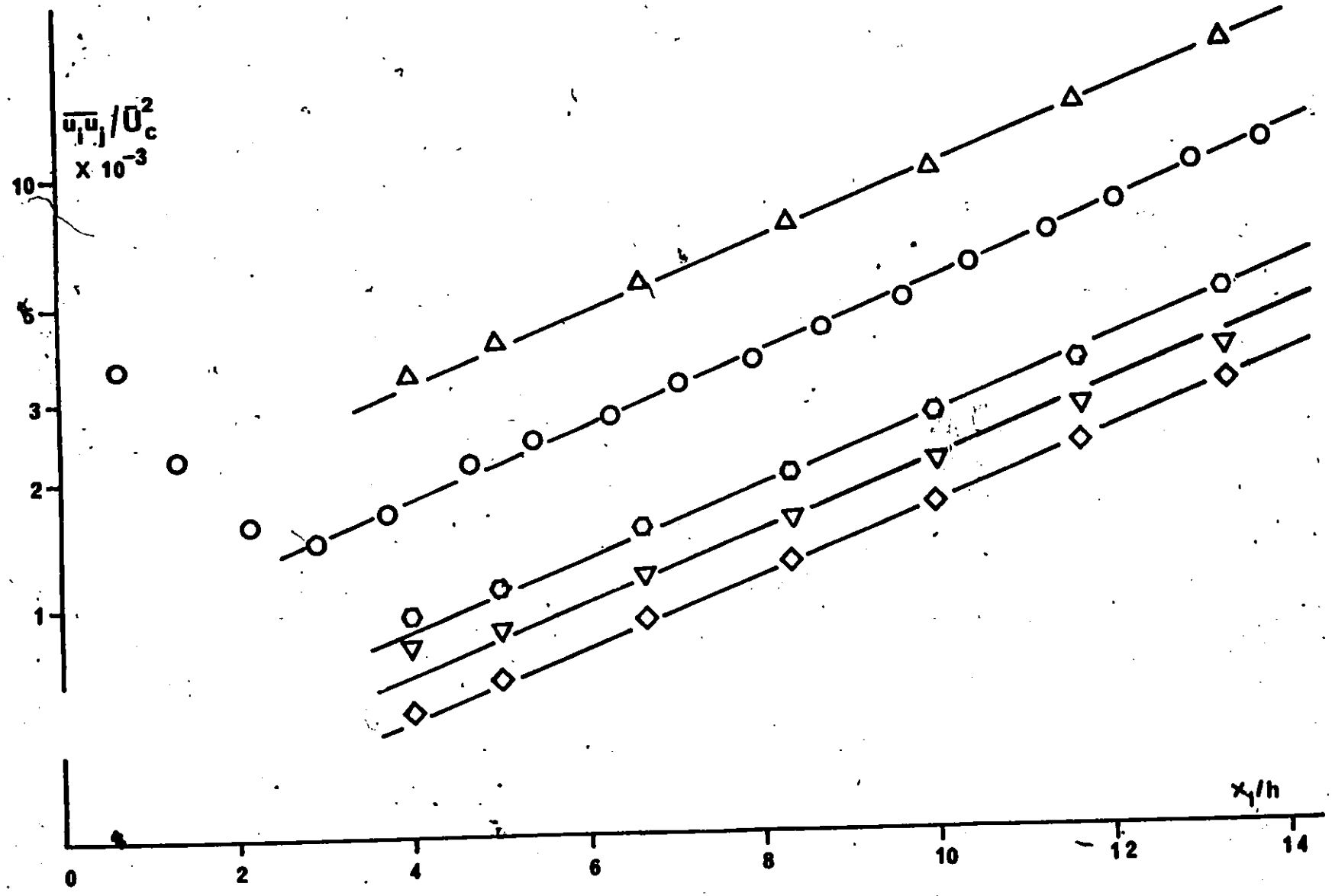

Figure 35. Downstream development of Reynolds stresses; U_c=13 m/s; symbols as in Figure 33.

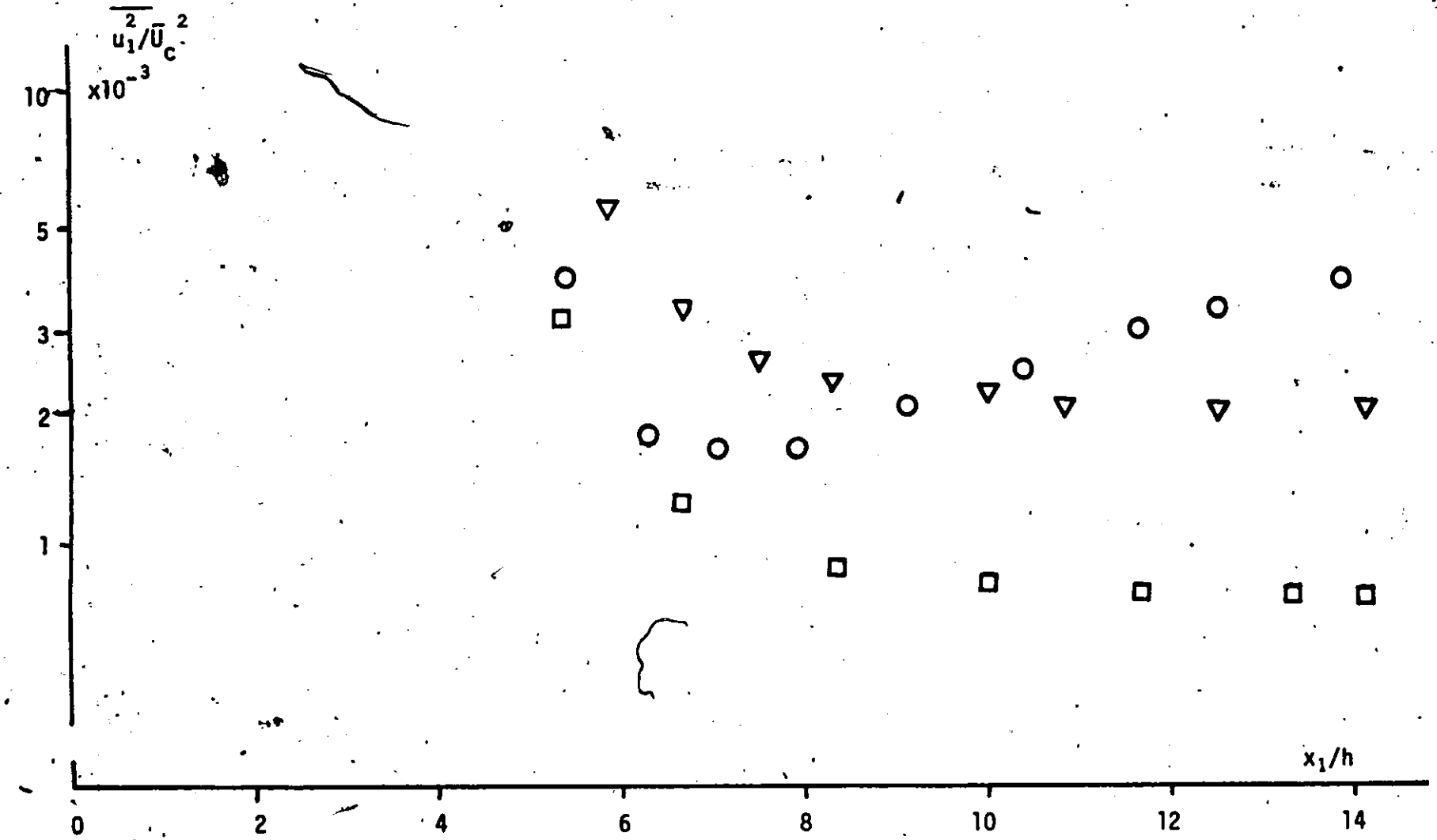

Figure 36:

Downstream development of Reynolds stress.
O m1.27 cm grid at $x_1/h = 4.5$, $\bar{U}c = 9$ m/s, ▽ m5.08 cm and m2.54 cm grids at $x_1/h = 1.04$ and 4.5 respectively, $\bar{U}c = 13$ m/s; □ m5.08 cm m2.54 cm, m1.27 cm grids at $h_1/h = 1.04$, 2.08 and 4.5 respectively, $\bar{U}c = 13$ m/s.

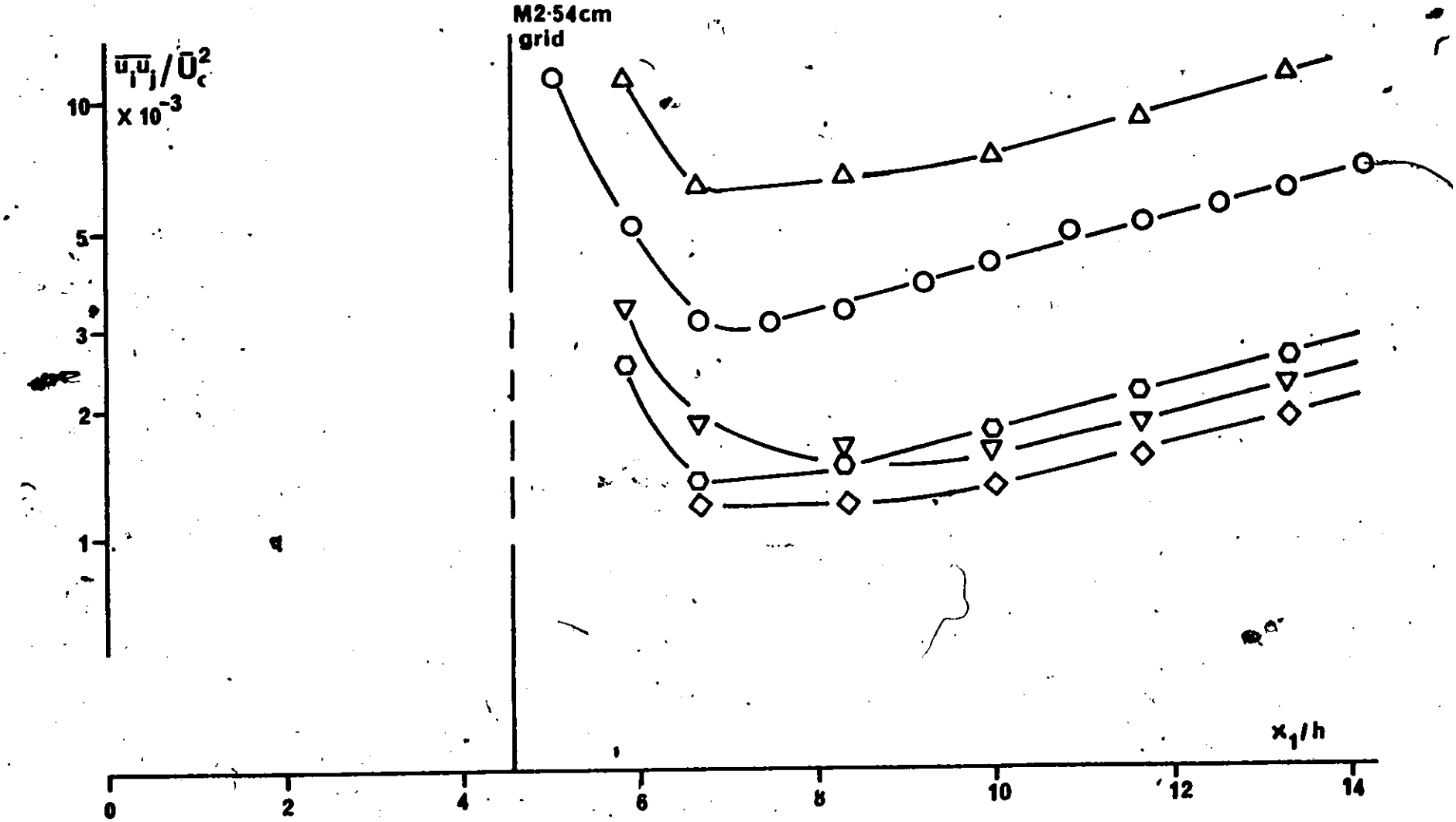

Figure 37: Downstrean development of Reynolds stresses $\bar{U}c$=6m/s, M2.54grid, symbols as in Figure 33.

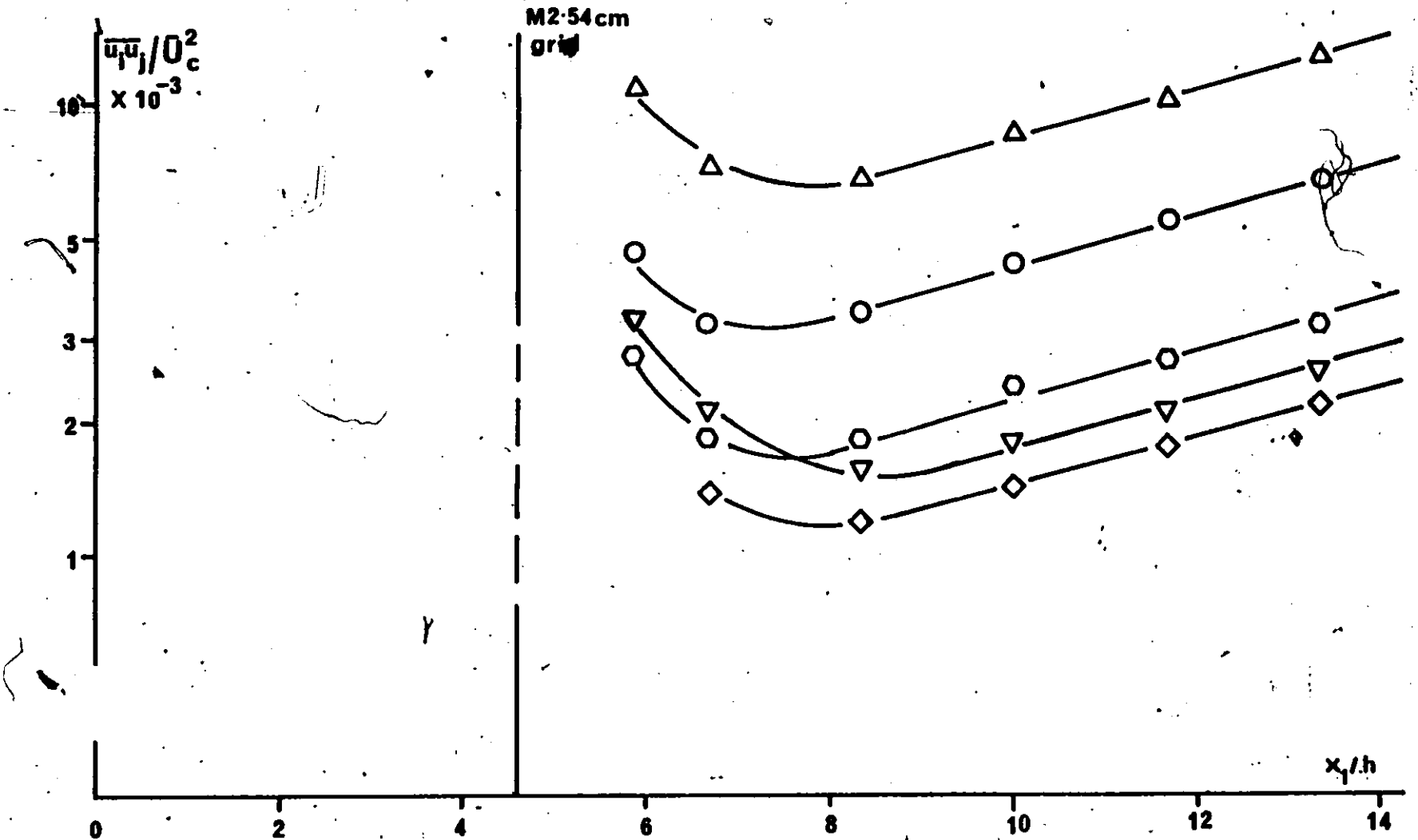

Figure 39: Downstream development of Reynolds stresses $\bar{U}c$=9m/s, M2.54grid; symbols as in Figure 33

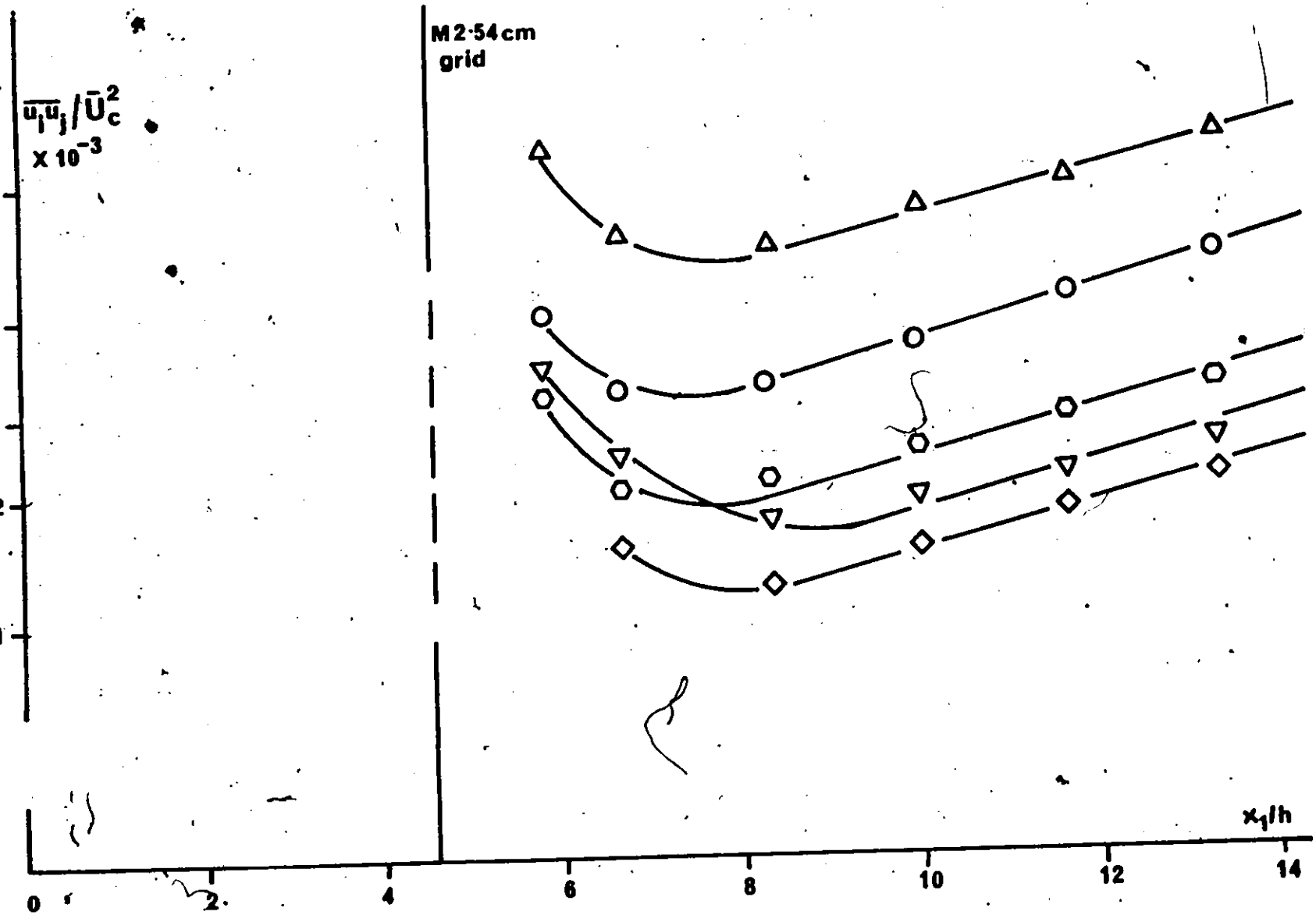

Figure 39: Downstream development of Reynolds stresses $\bar{U}c$=13m/s, M2.54grid, symbols as in Figure 33.

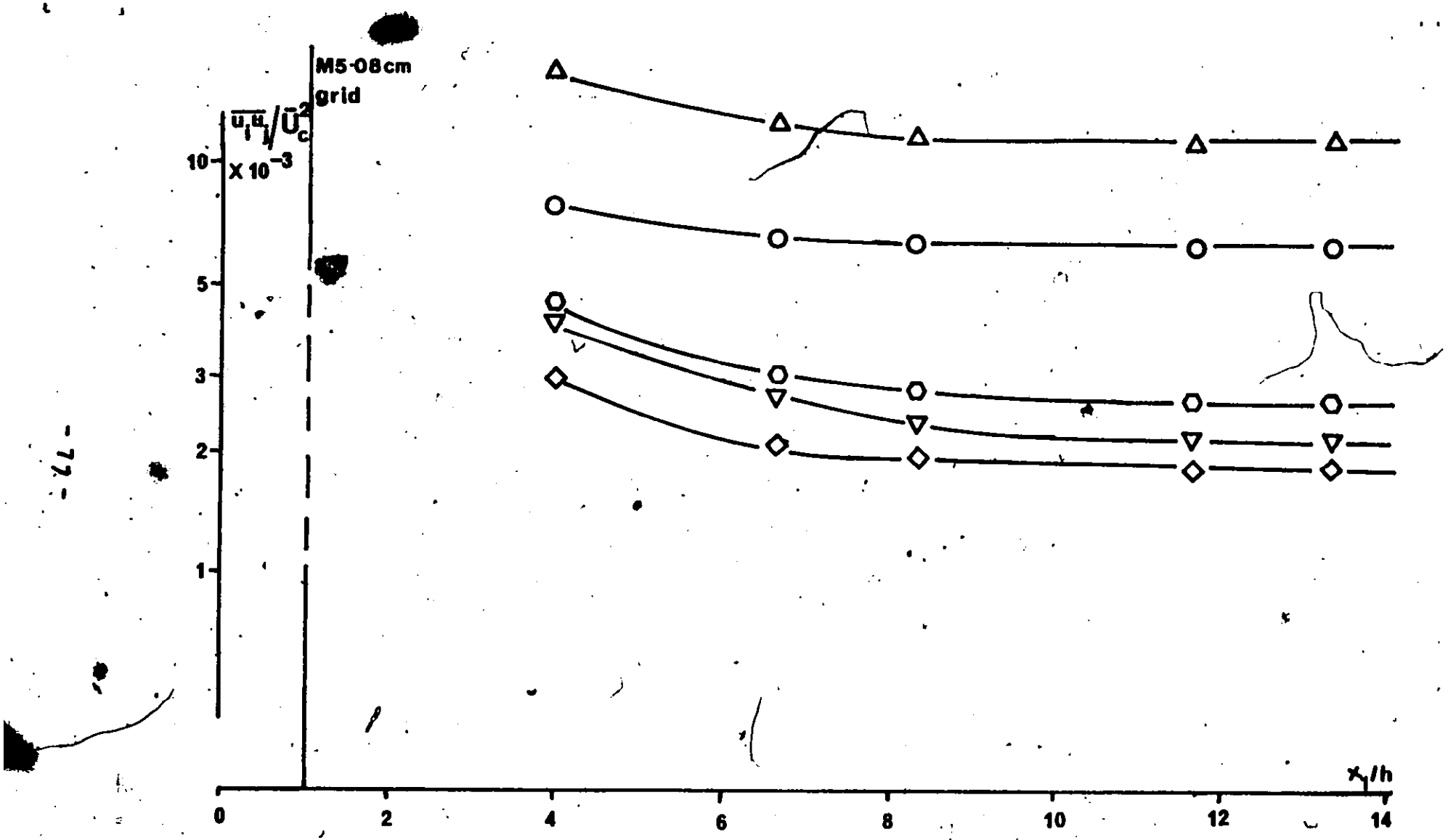

Figure 40: Downstream development of Reynolds stresses $\bar{U}c$=6m/s, M5.08grid; symbols as in Figure 33

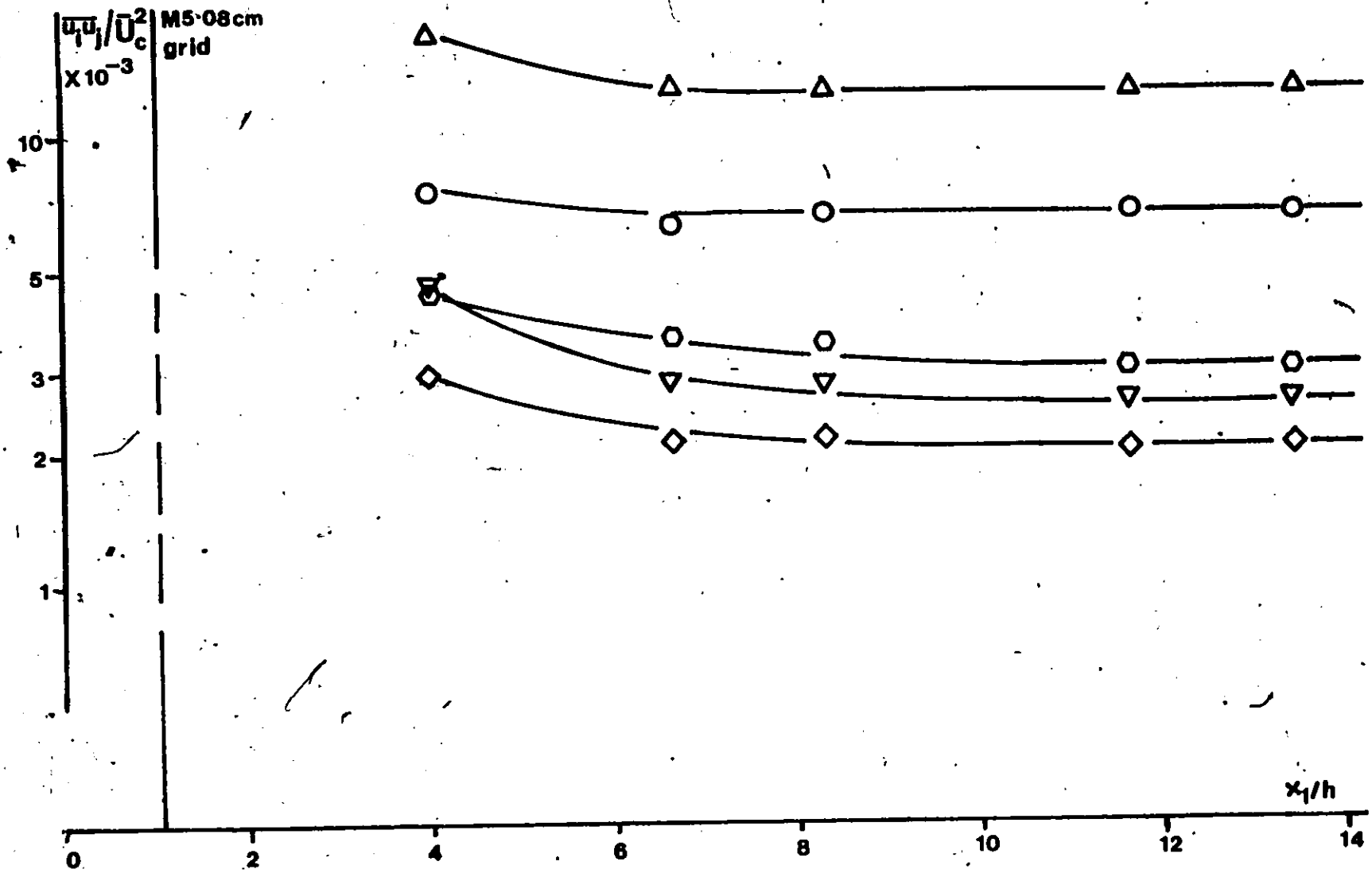

Figure 41: Downstream development of Reynolds stresses
$\bar{U}c$=9m/s.M5.08grid; symbols as in Figure 33

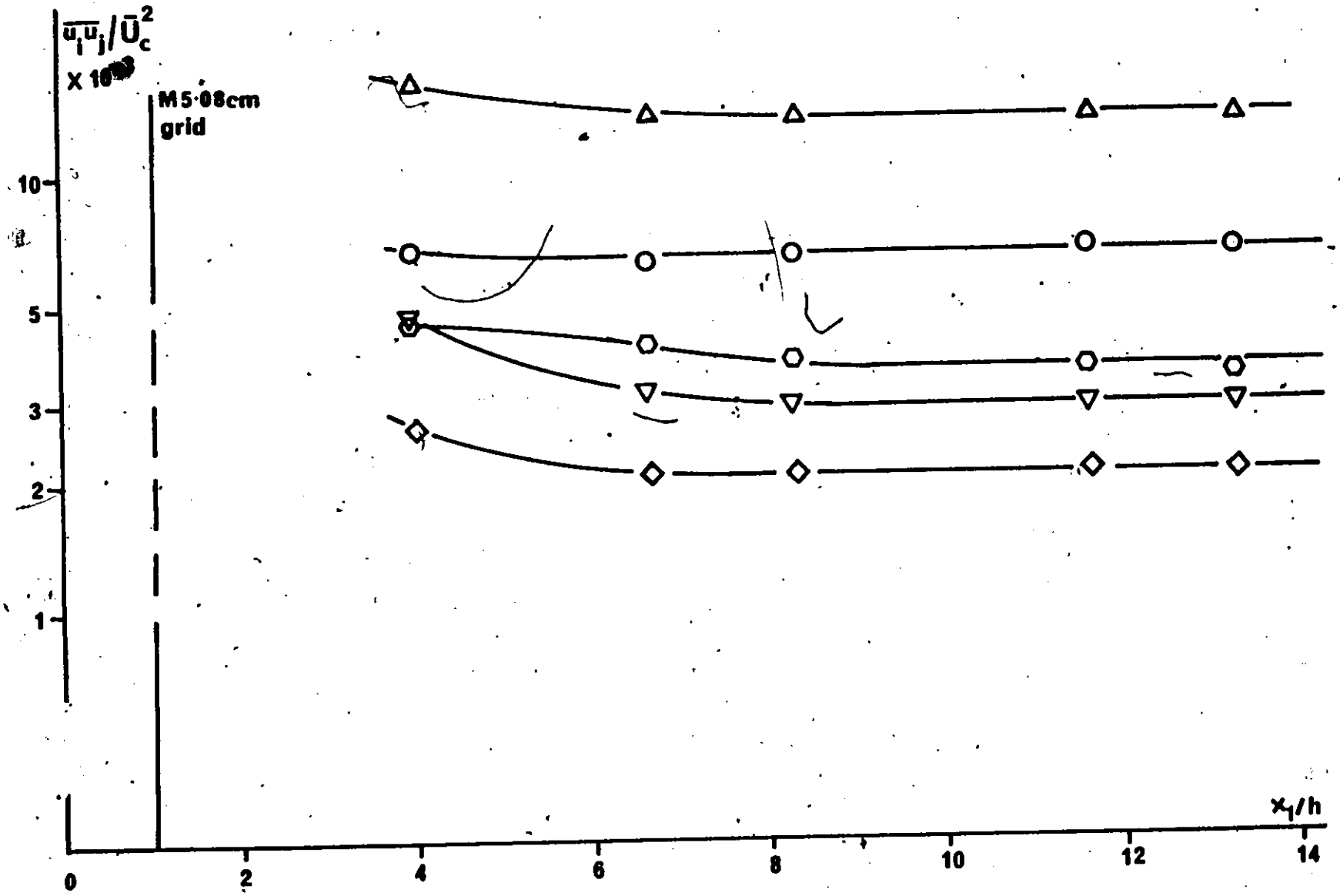

Figure 42: Downstream development of Reynolds stresses
$\bar{U}c$=13m/s, M5.08grid, symbols as in Figure 33

5.5 STREAMWISE VELOCITY INTEGRAL LENGTH SCALES

Integral time scales of the streamwise velocity fluctuations were measured by integrating the corresponding autocorrelation function to its first zero. The product of this time scale and the centreline mean velocity resulted in the required length scale (Taylor's approximation) under the assumption that the turbulent fluctuations were substantially lower than the mean velocity . An examination of the turbulent intensities justifies this assumption. The validity of this assumption in other similar flows has been tested by Champagne et al(1970) and Tavoularis & Corrsin (1980)

An approximately exponential growth was demonstrated by all measurements. For any given shear generating configuration the values and the growth rate of the length scales at each measuring station appeared to be nearly independent of the centreline mean speed and thus, the shear magnitude (Figure 43). Behind the grids the length scales appear to be adjusted to a value proportional to the spacing between the grid rods but still exhibited independence of shear and a nearly exponential growth as shown in Figures 44 and 45. The exponential law coefficients were 0·19 (Figure 43), 0·15 (Figure 44) and 0·18 (Figure 45), substantially different from the corresponding coefficients for the turbulent kinetic energy development, which were $0.32\,m^{-1}$, $0.22\,m^{-1}$ and 0 . The results reported in this thesis are preliminary. Detailed measure-

ments are in progress which would lead to accurate conclusions.

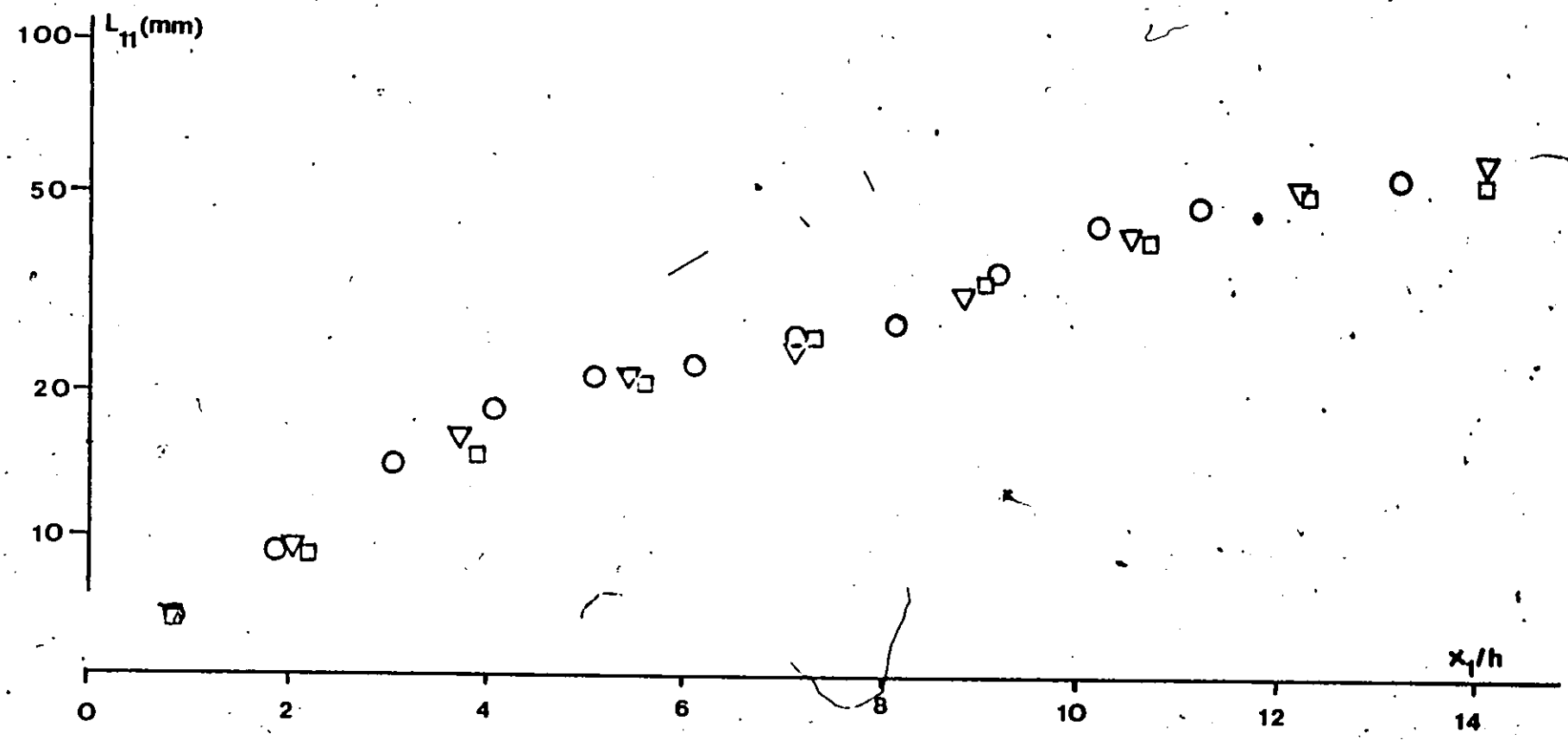

Figure 43. Downstream development of streamwise velocity integral length scales in an unobstructed flow; O $\bar{U}c$=6m/s, ▽ $\bar{U}c$=9m/s, □ $\bar{U}c$=13m/s

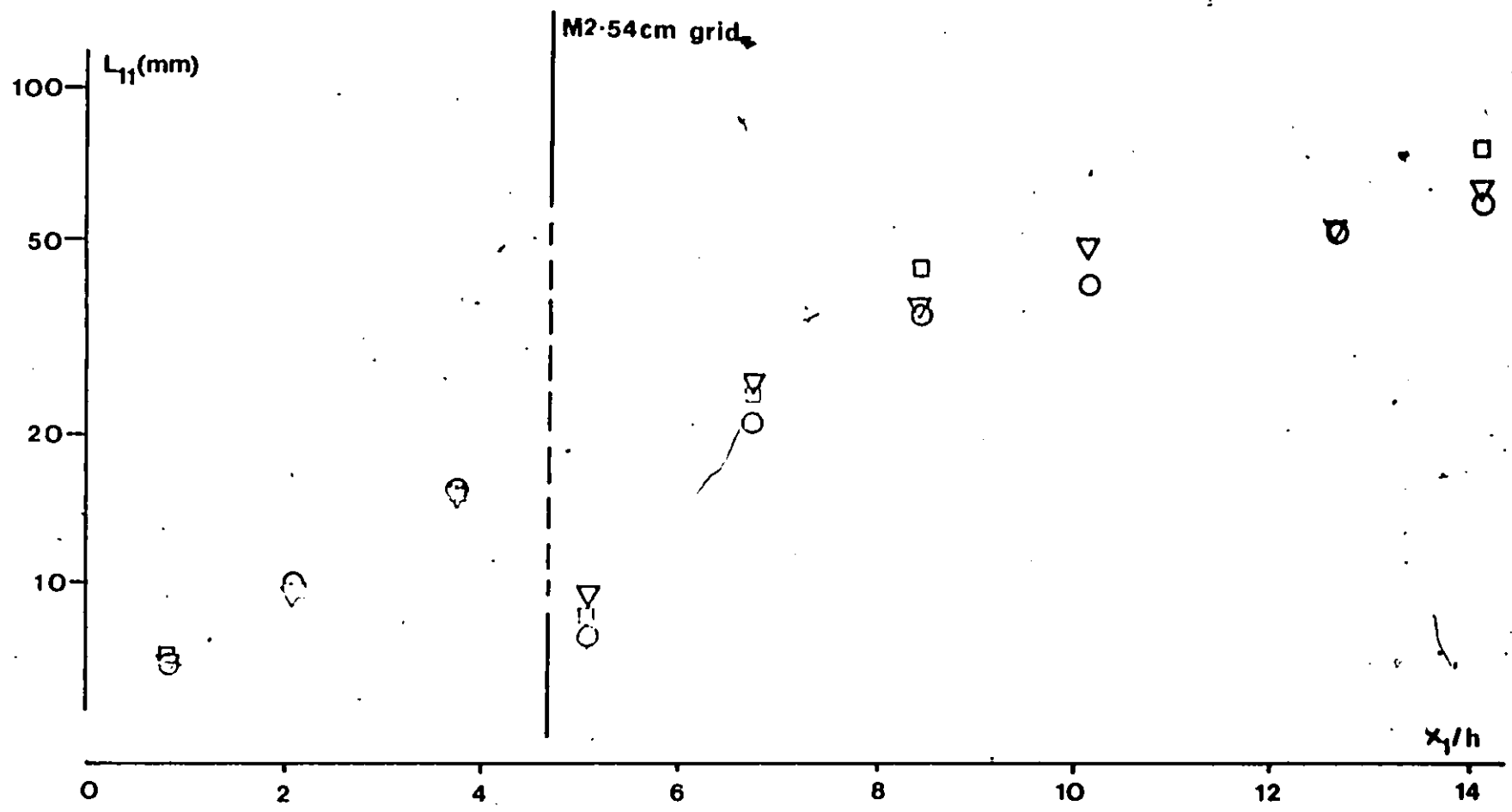

Figure 44. Downstream development of streamwise velocity integral length scales with M2.54 cm grid; symbols as in Figure 43.

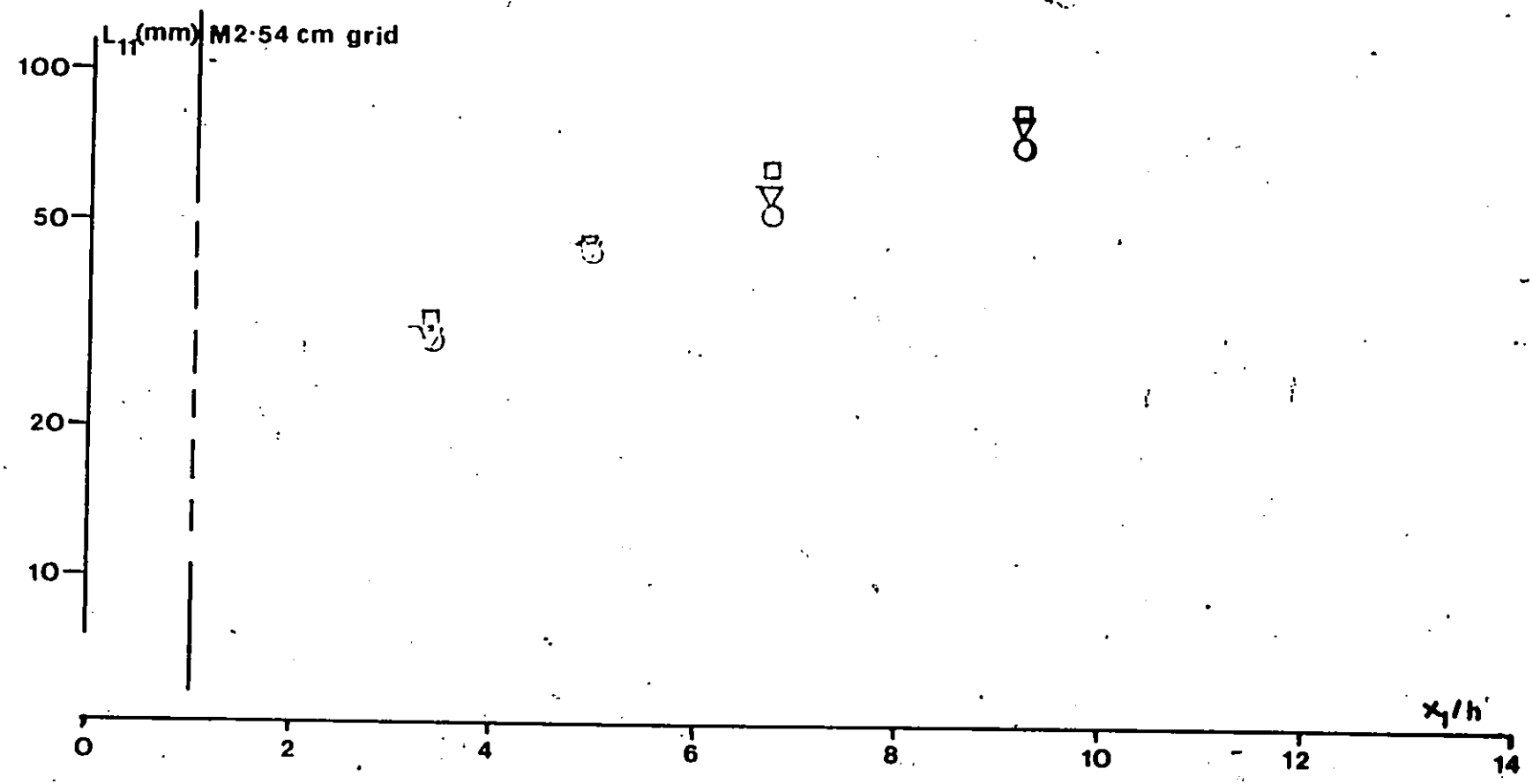

Figure 45. Downstream development of streamwise velocity integral length scales with M5.08 cm grid; symbols as in Figure 43.

Chapter VI

ANALYSIS AND DISCUSSION OF RESULTS

The present and past experiments span sufficiently wide ranges of mean shear, Reynolds number, dimensionless strain and length scales to attempt a quantitative parametrization of possible universal features of uniformly sheared flow.

6.1 EFFECT OF GRIDS ON THE MEAN SHEAR

For a grid placed normal to the stream it has been shown analytically by Elder (1958) that, a linear relationship exists between the upstream and the downstream velocity distribution. The parameters influencing this relation are solidity and the rod spacing. If the solidity were to be constant, the rod spacing alone would be the influential parameter. Hence, for a given grid, the rod spacing being constant, it would be expected that the grid would reduce the upstream velocity profile by a constant value. In the present experimental study the solidity is kept constant and insertion of a grid reduced the incoming shear by a roughly constant value depending on the rod spacing.

6.2 DIMENSIONLESS PARAMETRIZATION

Various parameters have been used in the past (e.g. Townsend 1976) to characterize the self-similar asymptotic development of a turbulent flow by which proper dimensionless ratios attain universal profiles when plotted versus co-ordinates normalized with the local scales. In the present case of uniformly sheared flow, transverse homogeneity precludes the use of the transverse co-ordinate as a parameter, so that transverse profiles of all dimensionless ratios must be roughly uniform and the streamwise distance remains as the only independent co-ordinate.

A criterion for the degree of self similarity is the downstream constancy of the dimensionless Reynolds stresses K_{ij}, introduced in Chapter 2. Figures 46 and 47 present K_{ij} for the experiments of Rose, Champagne et al Mulhearn & Luxton and Tavoularis & Corrsin and Figures 48 to 56 for the present experiments. In all cases, there exists an appreciable region near the end of the test section where all measured components of K_{ij} appear constant and are ordered as

$$K_{11} > K_{33} > K_{22} > -K_{12}$$

Evidently, uniform shear organizes the flow structure in this fashion and will inadverently produce a self-similar structure given sufficient time to act on the flow. These facts are supported by the tendency of all flows to return to the above structure even after strong deviation produced

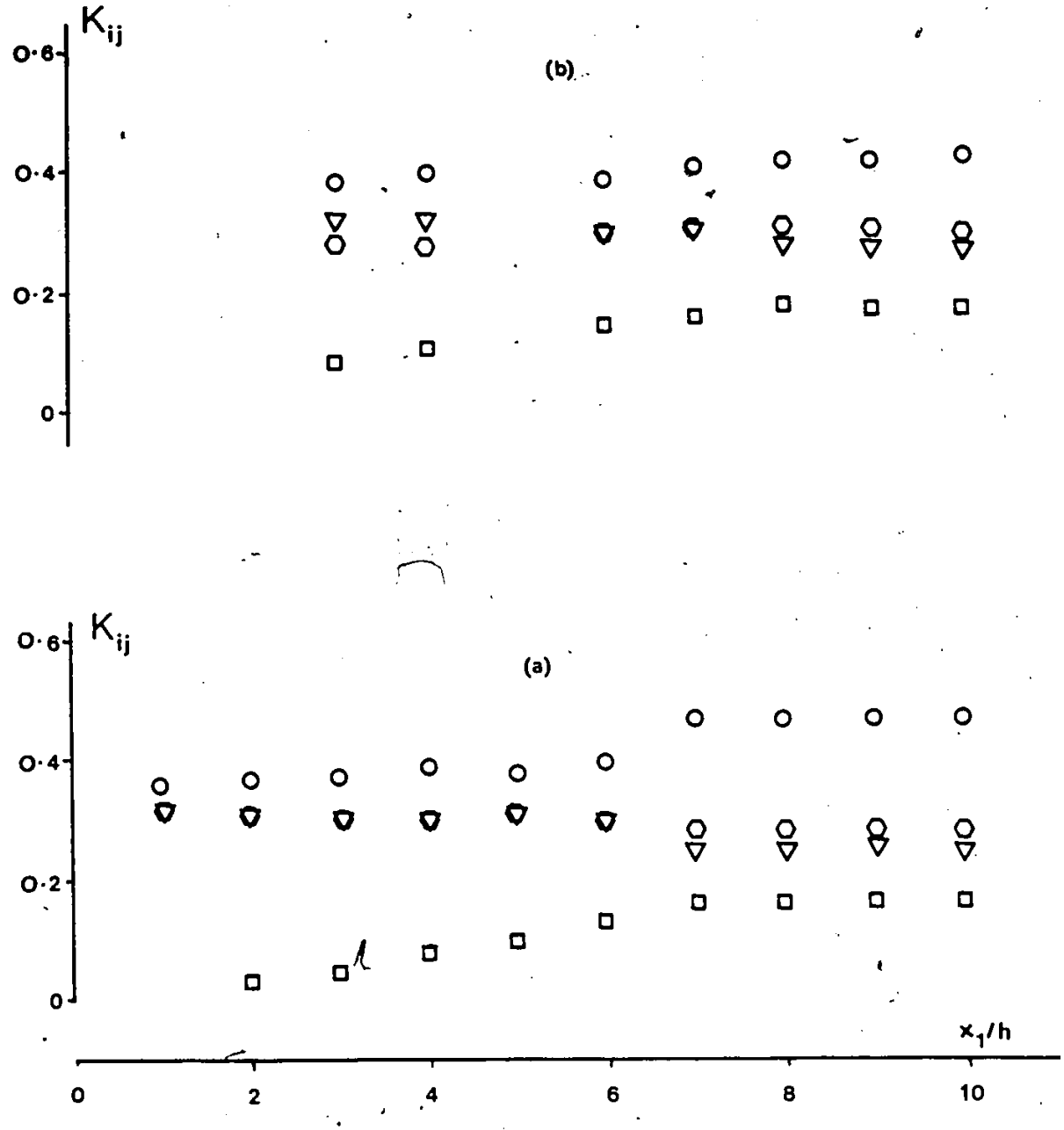

Figure 46. Asymptotic development of dimensionless Reynolds stresses; (a) Rose (b) Champagne et al

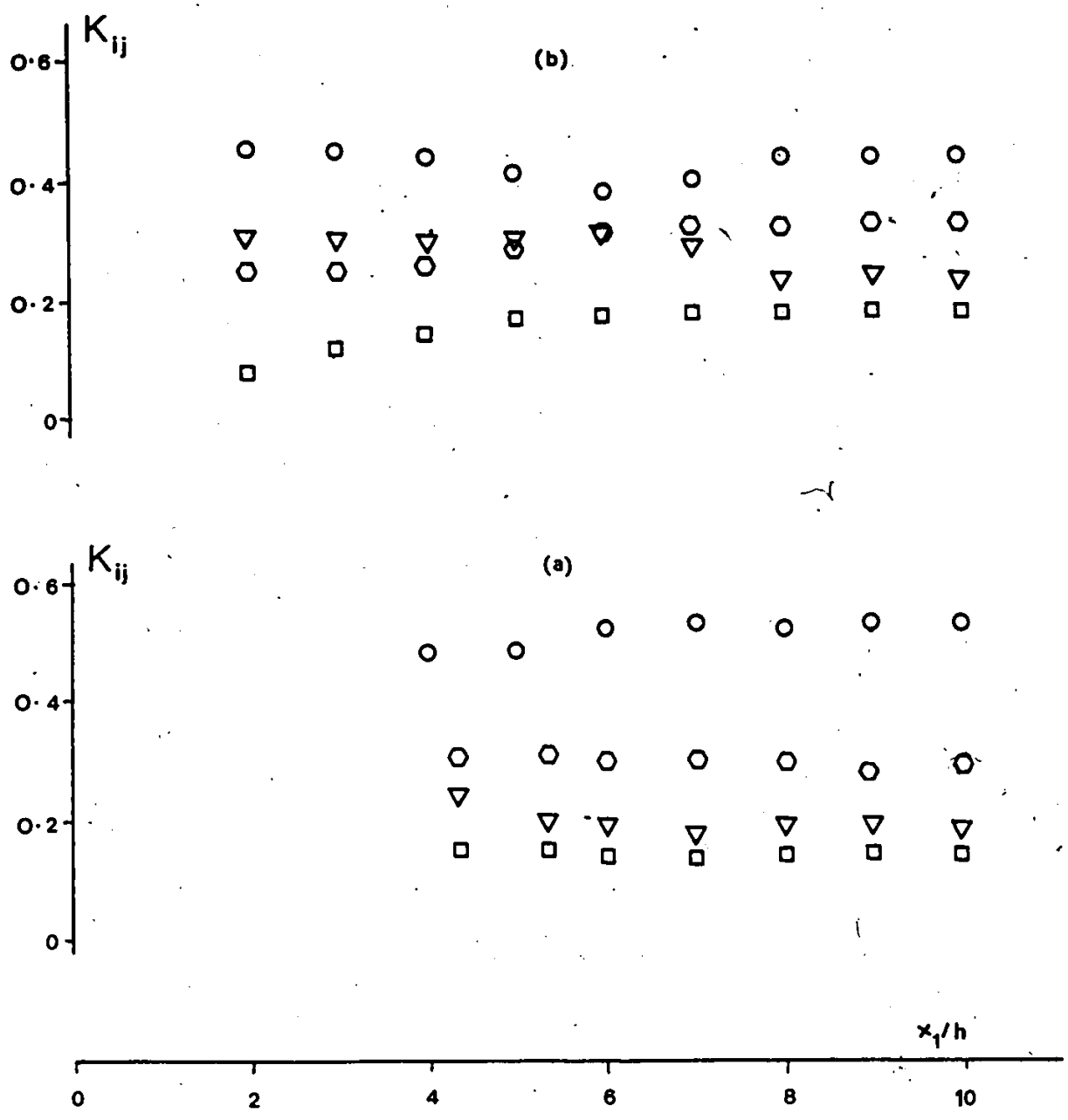

Figure 47. Asymptotic development of dimensionless Reynolds stresses; (a) Tavoularis & Corrsin (b) Mulhearn & Luxton

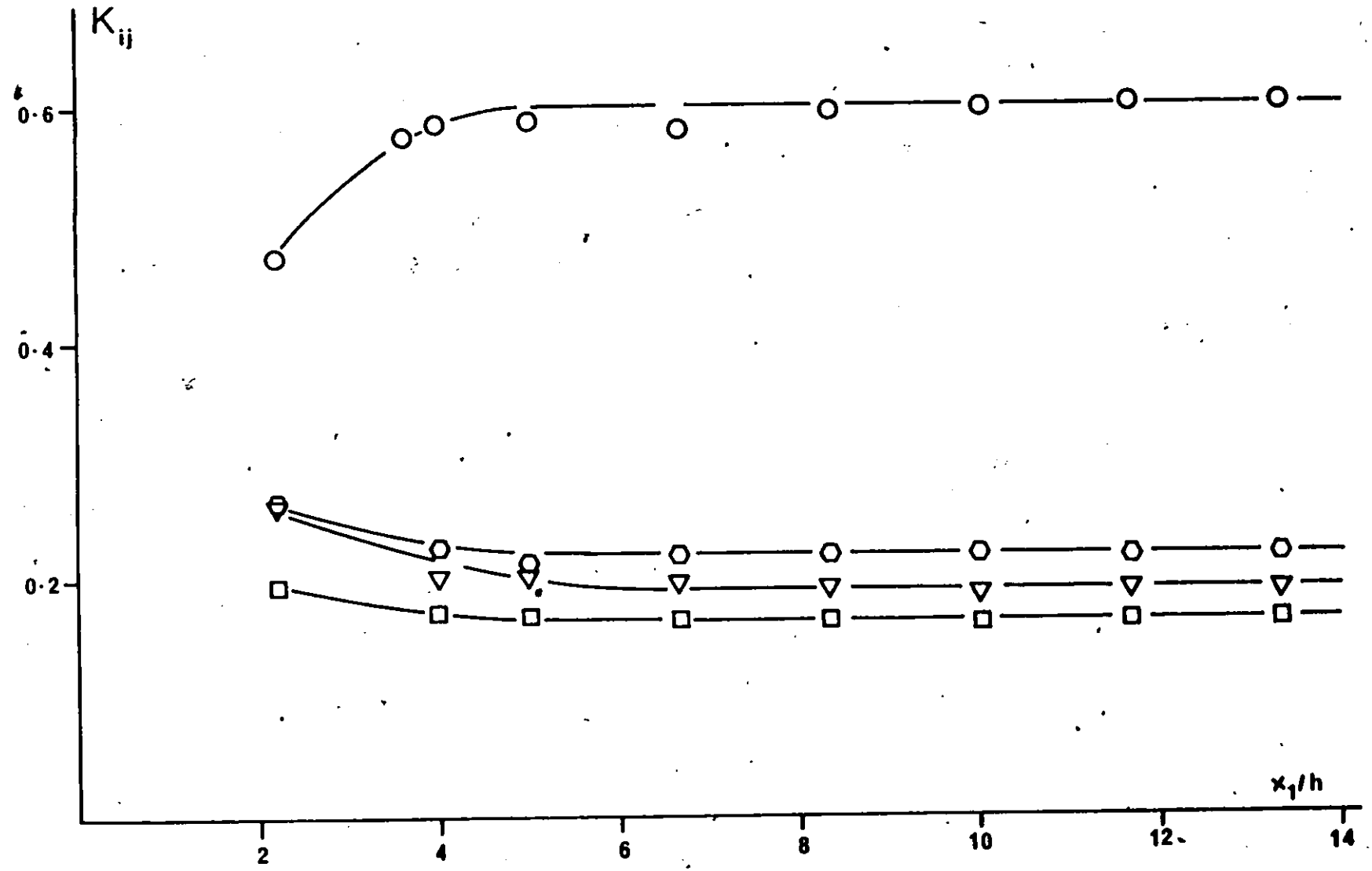

Figure 48. Asymptotic development of dimensionless Reynolds stresses; $\bar{U}c=6m/s$; ○ K_{11}, ▽ K_{22}, ○ K_{33}, □ K_{12}.

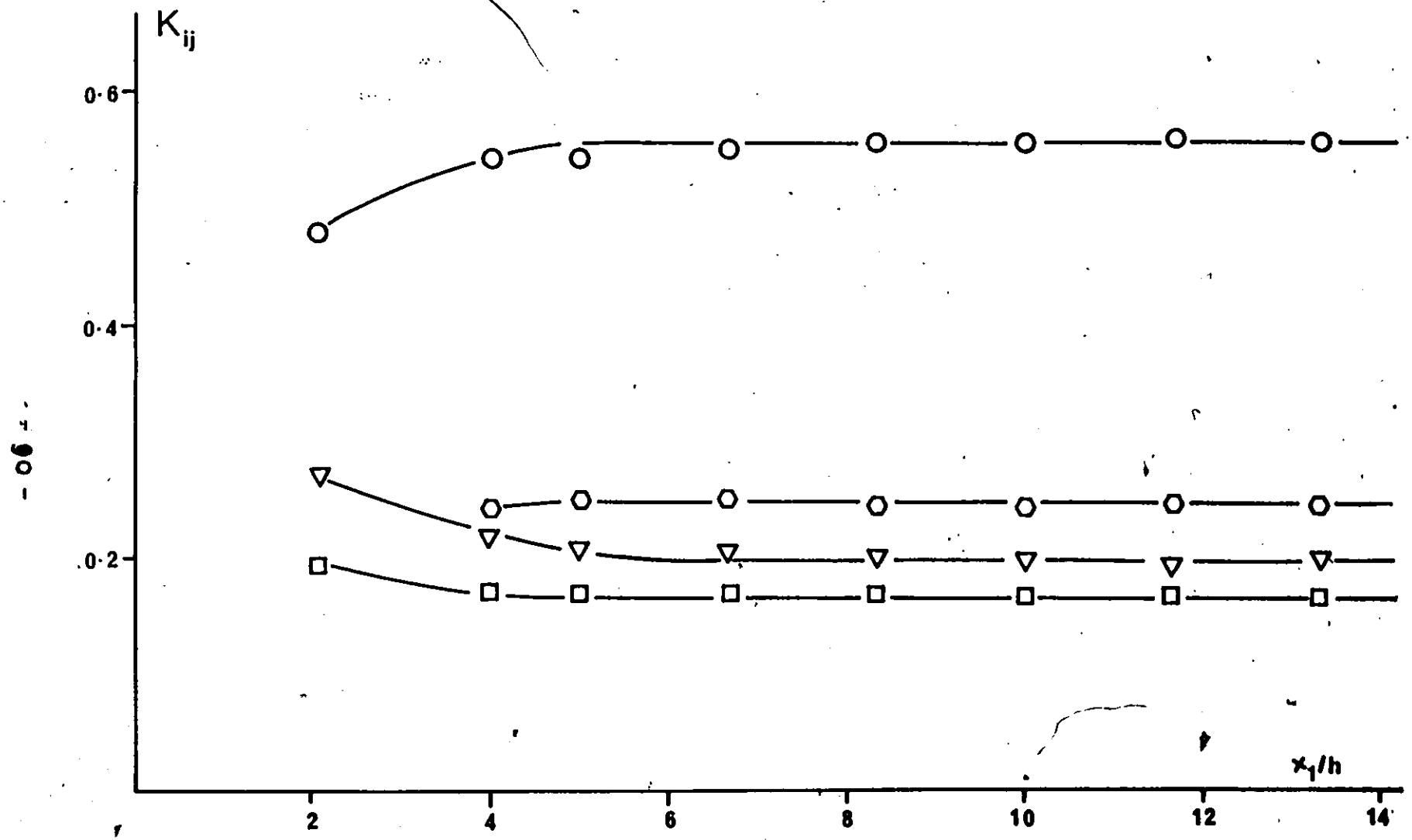

Figure 49. Asymptotic development of dimensionless Reynolds stresses; $\bar{U}c$=9m/s; symbols as in Figure 48.

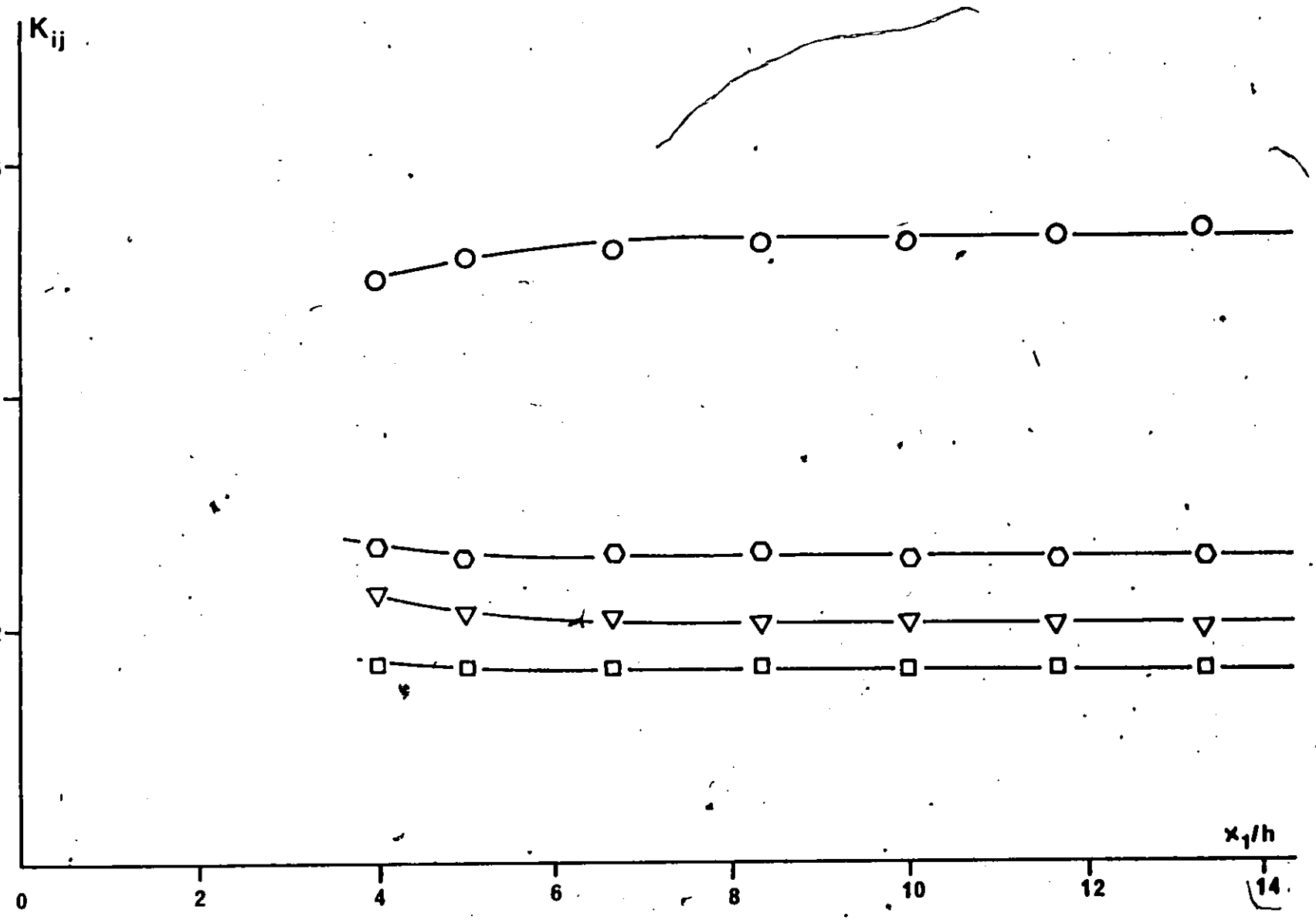

Figure 50. Asymptotic development of dimensionless Reynolds Stresses; Üc=13m/s; symbols as in Figure 48.

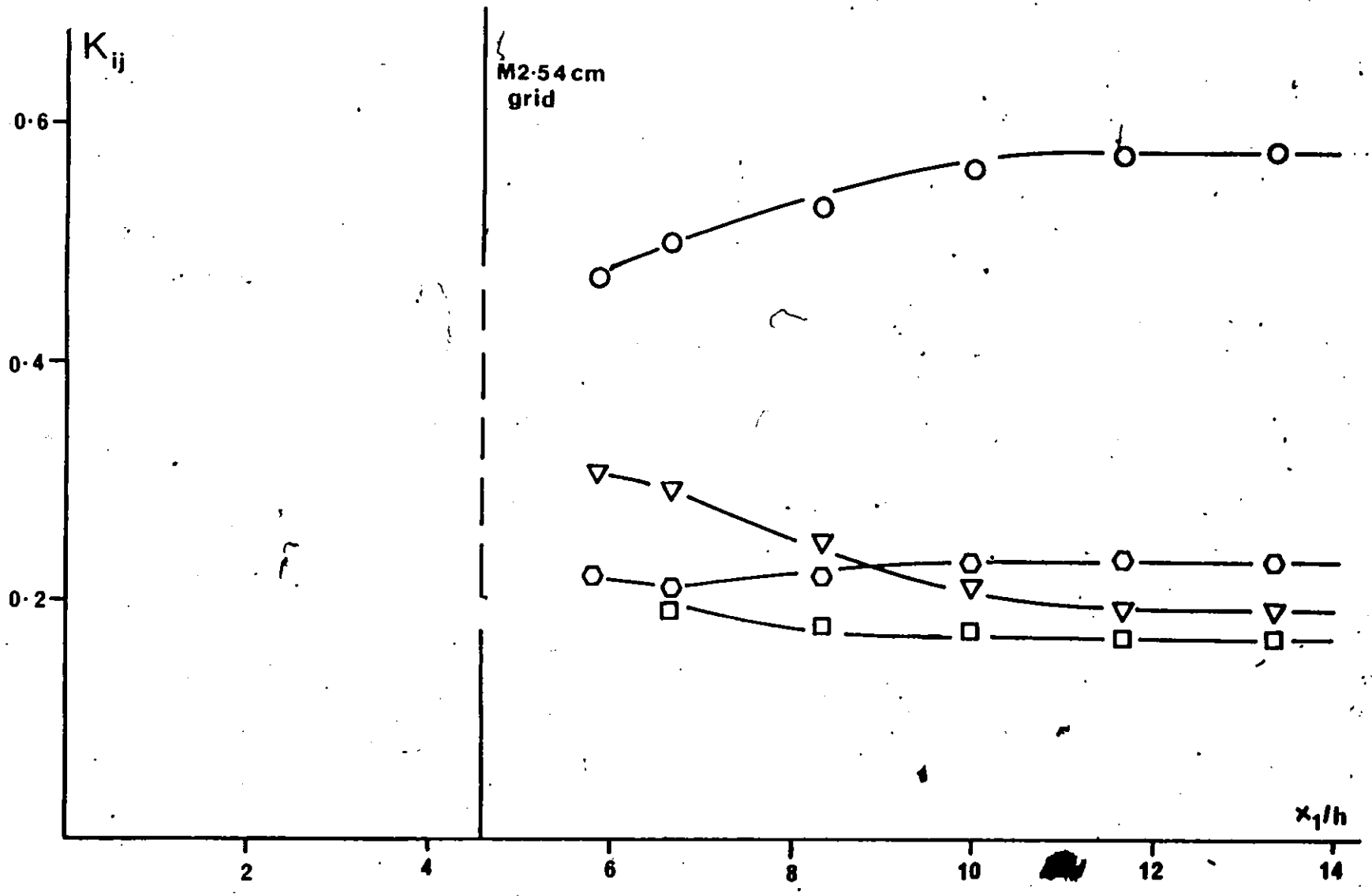

Figure 51. Asymptotic develpoment of dimensionless Reynolds stresses; $\bar{U}c$=6m/s; with M2.54 cm grid; symbols as in Figure 48.

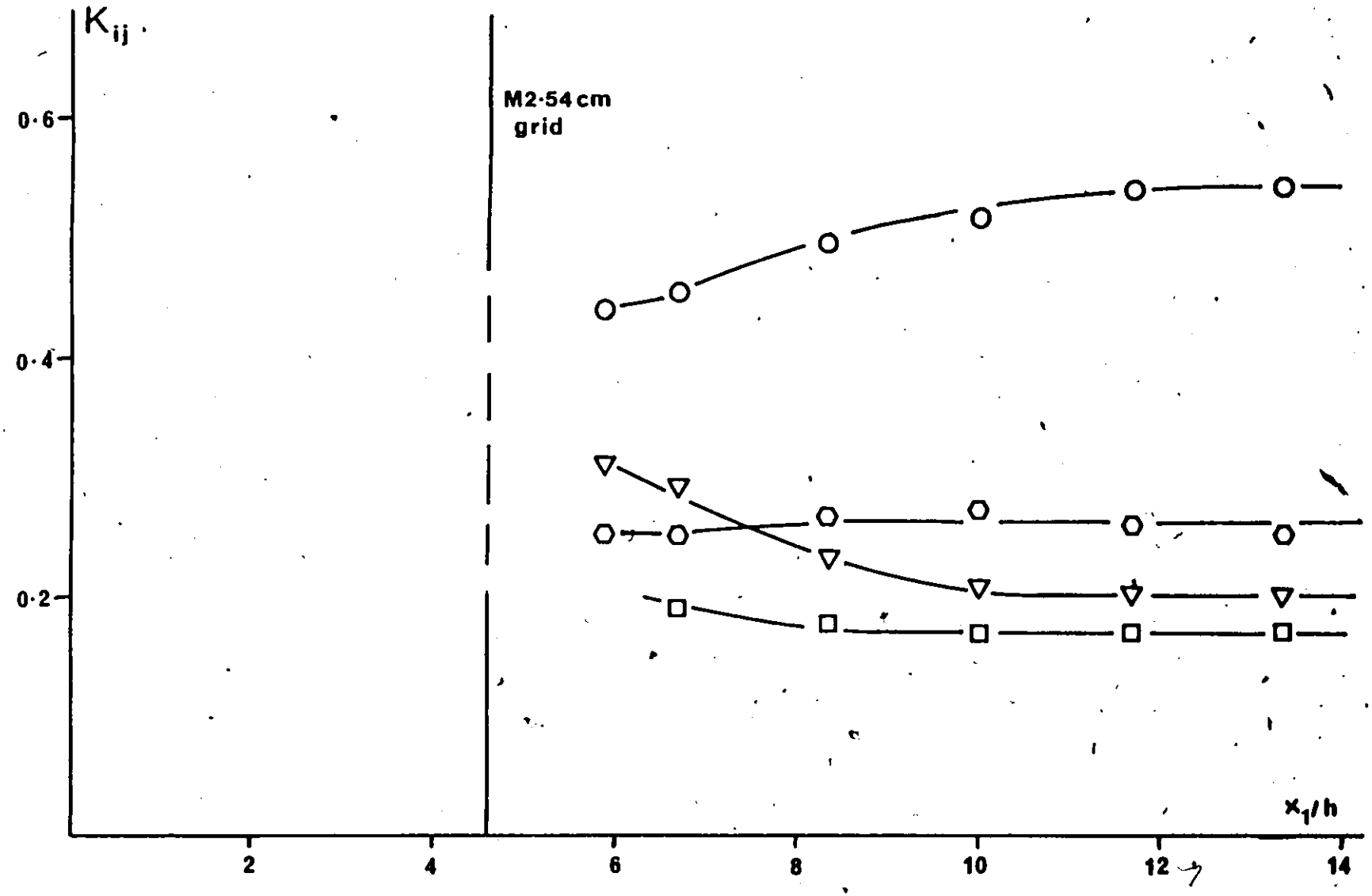

Figure 52. Asymptotic development of dimensionless Reynolds stresses; $\bar{U}c$=9m/s; with M2.54 cm grid; symbols as in Figure 4 .

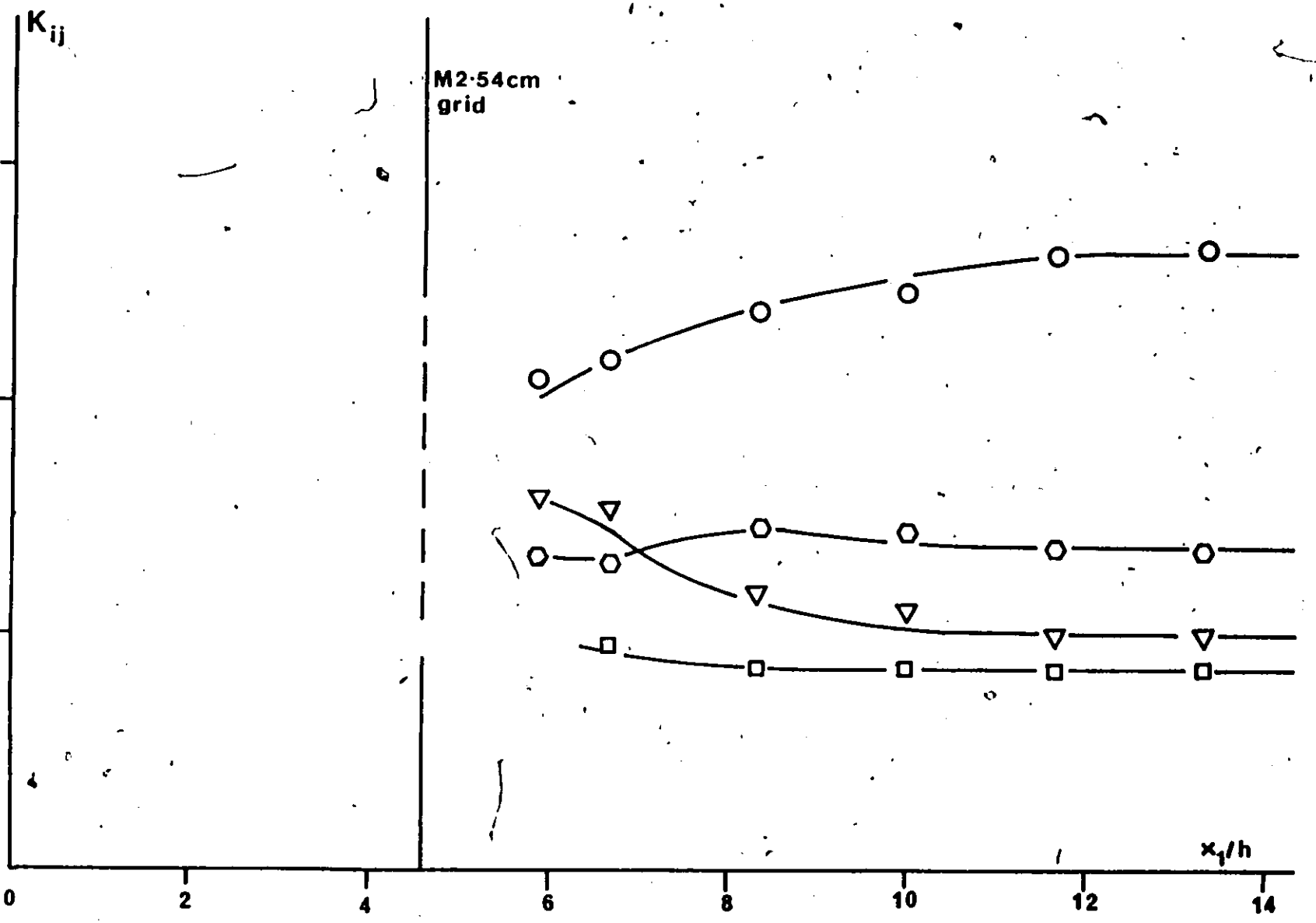

Figure 53. Asymptotic development of dimensionless Reynolds stresses; $\bar{U}c$=13m/s; with M2.54 cm grid; symbols as in Figure 48.

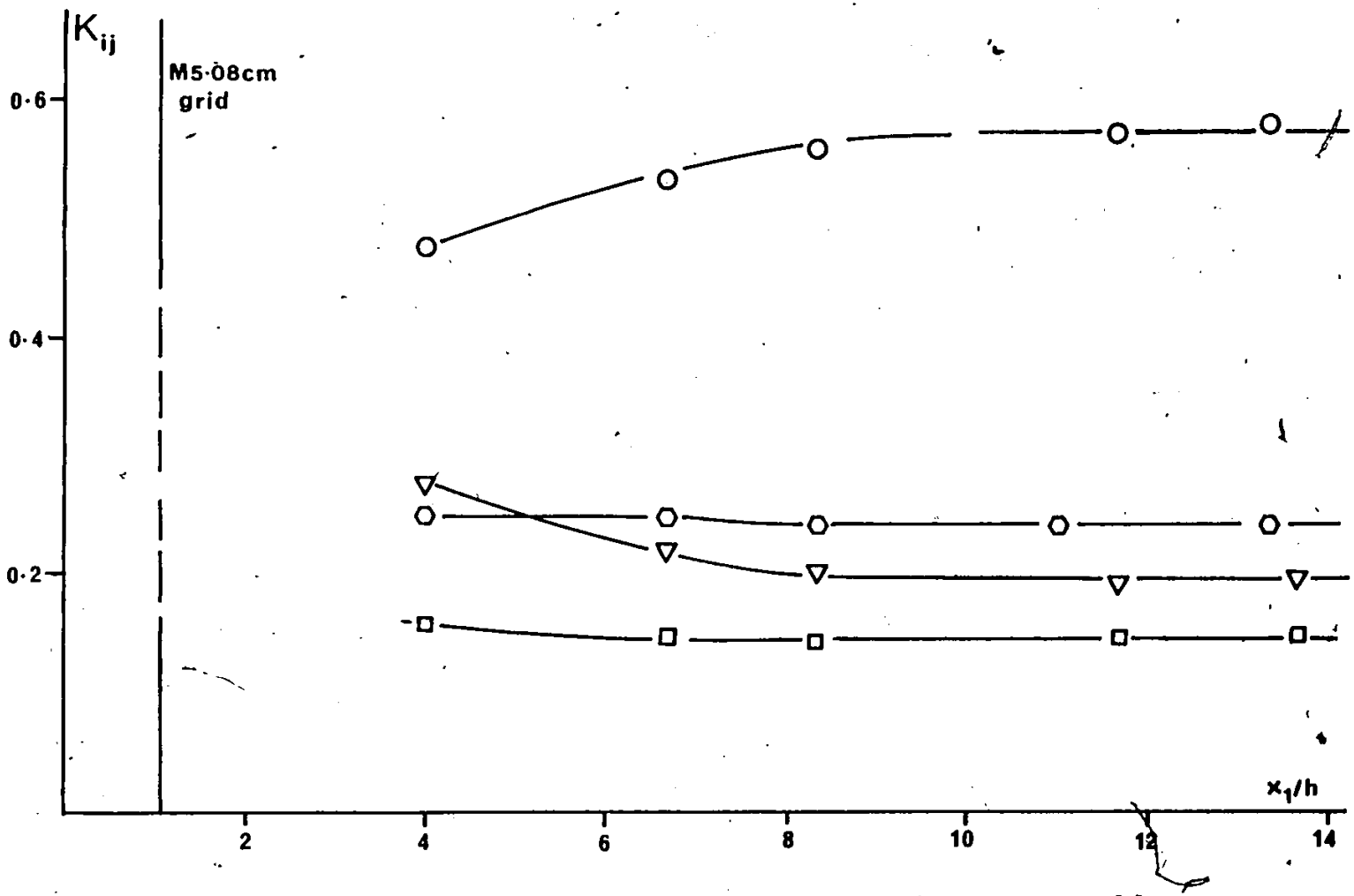

Figure 54. Asymptotic development of dimensionless Reynolds stresses; $\bar{U}c$=6m/s; with M5.08 cm grid; symbols as in Figure 48.

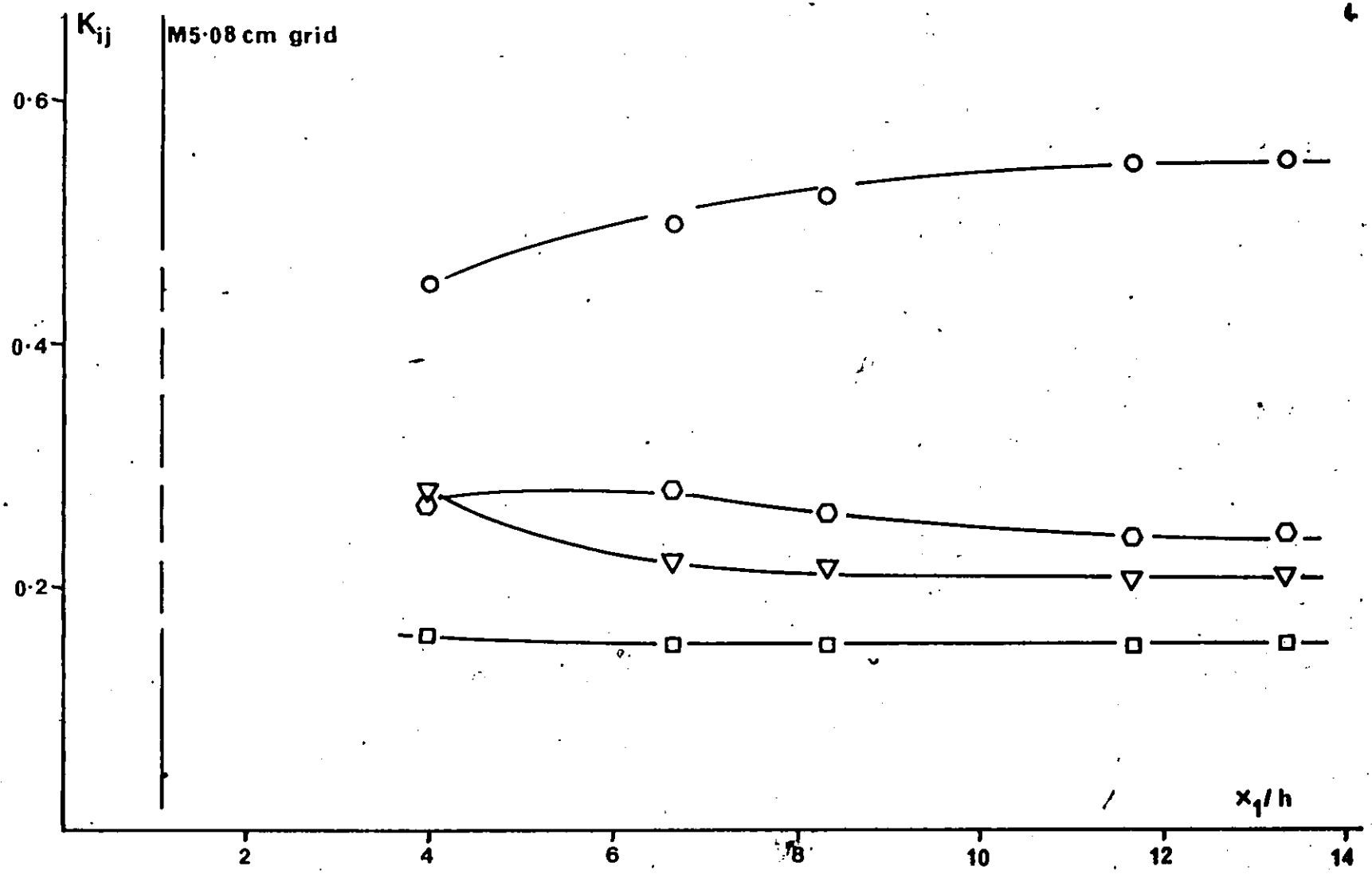

Figure 55. Asymptotic development of dimensionless Reynolds stresses; $\bar{U}c$=9m/s; with M5.08 cm grid; symbols as in Figure 48.

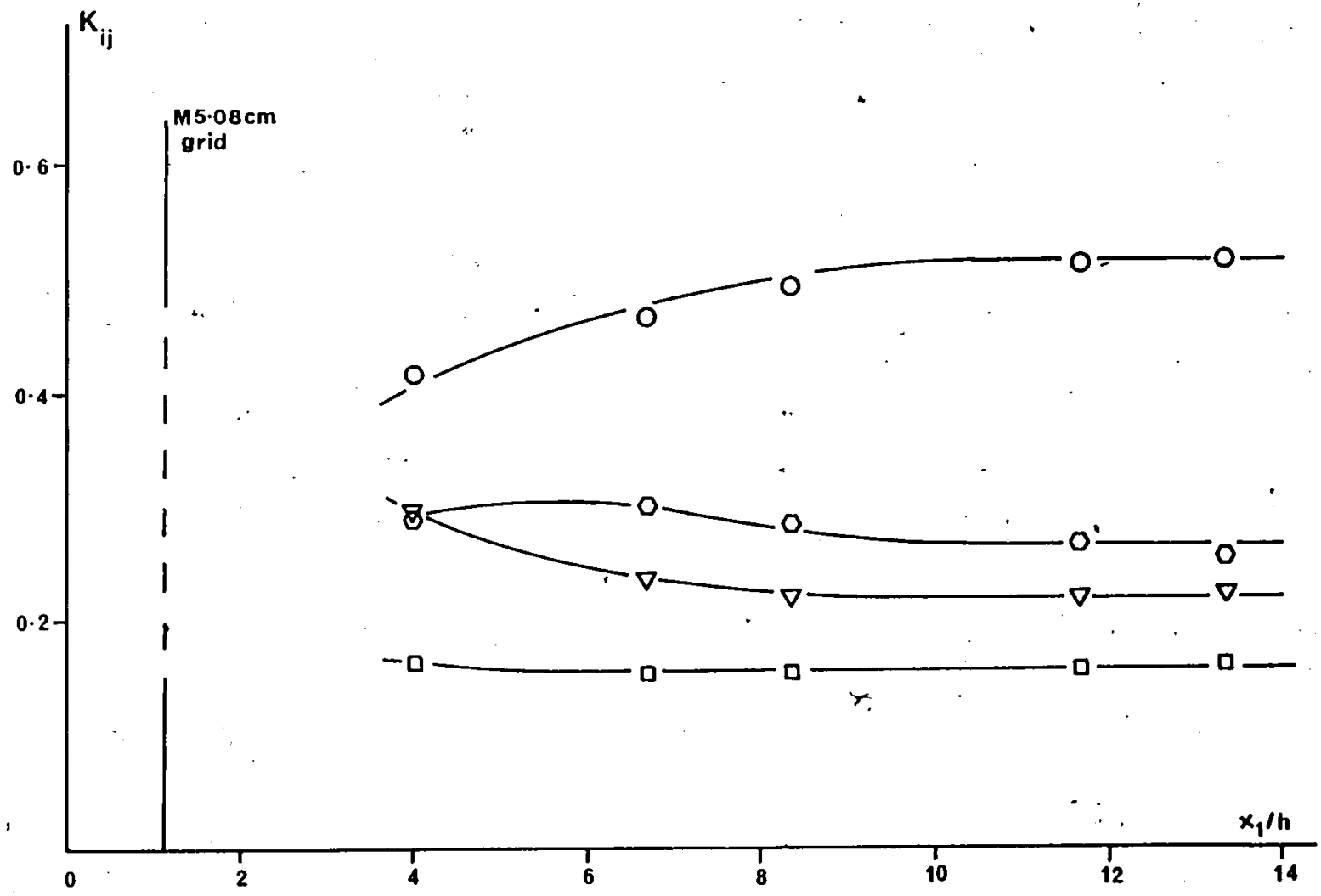

Figure 56. Asymptotic development of dimensionless Reynolds stresses; Uc=13m/s; with M5.08 cm grid; symbols as in Figure 48.

by the initial shear generator or by the grids, as is demonstrated in the above Figures.

The exact asymptotic values of K_{ij} components present a variation as shown in Table 5, which however does not appear to depend systematically on the mean shear and could result partially from measurement errors and partially from transverse inhomogeneity and boundary effects. For practical purposes one can summarize all results by the average values. (second numbers correspond to standard deviation of all available experimental values)

$$K_{ij} = \begin{bmatrix} 0{\cdot}54 \pm 0{\cdot}038 & -0{\cdot}16 \pm 0{\cdot}008 & 0 \\ -0{\cdot}16 \pm 0{\cdot}008 & 0{\cdot}21 \pm 0{\cdot}018 & 0 \\ 0 & 0 & 0{\cdot}26 \pm 0{\cdot}025 \end{bmatrix}$$

	unobstructed flow			M2.54 cm grid at $x_1/h = 4.5$			M5.08 cm grid at $x_1/h = 1.04$			T-C	Ch. et al	Rose	M & L	Units
$\bar{U}_c$	6	9	13	6	9	13	6	9	13	12.4	12.21	15.15	4.5	ms^{-1}
$d\bar{U}_1/dx_2$	43.5	60	84	18.4	28	38.8	14.2	20.8	29.3	48	12.9	13.7	5.45	s^{-1}
K_{11}	0.59	0.56	0.55	0.58	0.55	0.53	0.57	0.55	0.52	0.53	0.49	0.50	0.47	
K_{22}	0.19	0.20	0.20	0.19	0.20	0.20	0.20	0.19	0.21	0.22	0.19	0.25	0.22	
K_{33}	0.22	0.24	0.25	0.23	0.25	0.27	0.24	0.24	0.26	0.28	0.28	0.28	0.31	
K_{12}	0.165	0.165	0.165	0.17	0.17	0.17	0.155	0.155	0.155	0.14	0.165	0.16	0.165	
ℓ	3.02	3.32	3.18	5.75	4.54	4.44	∞	∞	∞	4.36	∞	∞	∞	m
ε/P	0.72	0.72	0.71	0.66	0.58	0.55	1	1	1	0.57	1	1	1	
L_{in}	0.0254	0.0254	0.0254	0.0254	0.0254	0.0254	0.0508	0.0508	0.0508	0.0305	0.0305	-	0.006	m
U_c	6.5	7.2	8.1	5.0	5.6	6.2	3.5	4.0	4.5	6.3	4.1	-	5.0	ms^{-1}
x_1	1.5	1.5	1.5	2.5	2.5	2.5	2.5	2.5	2.5	2.25	3.15	3.0	2.4	m
q_r^2	0.182	0.359	0.686	0.232	0.542	1.999	0.400	1.012	2.230	0.536	0.098	0.055	0.047	m^2s^{-2}

TABLE 5. SUMMARY OF RESULTS

6.3 . STABILITY CRITERIA

Depending on the value of the ratio P/ϵ three possibilities exist for the downstream evolution of the turbulent kinetic energy q^2 : an exponential growth for $P > \epsilon$, a constant value for $P = \epsilon$, and an exponential decay for $P < \epsilon$. These three cases correspond to positive, zero, and negative values of the inverse characteristic length scale $1/\ell$. The first two cases have been observed experimentally; the third case probably corresponds to extremely weakly sheared turbulence (see also computations of on weakly sheared turbulence by Deissler, 1961 and Fox, 1964).

By analogy to Hasen's (1967) prediction, an attempt has been made to correlate the value of $1/\ell$ with a characteristic velocity $\left\{(1/L_{in})(d\bar{U}_1/dx_2)\right\}^{1/3}\nu^{2/3}$ (Figure 57) and predict a "barrier velocity" which would categorize the growth, constancy and decay of the turbulent kinetic energy. From this figure it appears that in flows with $3.5 < u_c < 5$ q^2 reaches a constant asymptotic state while in flows with $u_c > 5$, q^2 grows exponentially. It is probable that for sufficiently small values of u_c, (certainly smaller than 3.5 as Figure shows) q^2 may decay exponentially. This aspect has yet to be investigated.

Correlation of $1/\ell$ with $(1/\bar{U}c)(d\bar{U}_1/dx_2)$, an inverse length scale, (Figure 58) also distingushes two groups of experimental results : those with exponential growth and

those with approximate constancy of turbulent kinetic energy.

Attempts to correlate $1/\ell$ with the mean shear and the total strain were unsuccessful as illustrated in Figures 59, 60 and 61.

6.4 TABULATION OF RESULTS

Measurements and results of past and present experiments are summarized in Table 4. Reference values of the turbulent kinetic energy in the asymptotic state are also listed to facilitate the calculation of the Reynolds stresses and the turbulent kinetic energy at any downstream position in the asymptotic state using the exponential law.

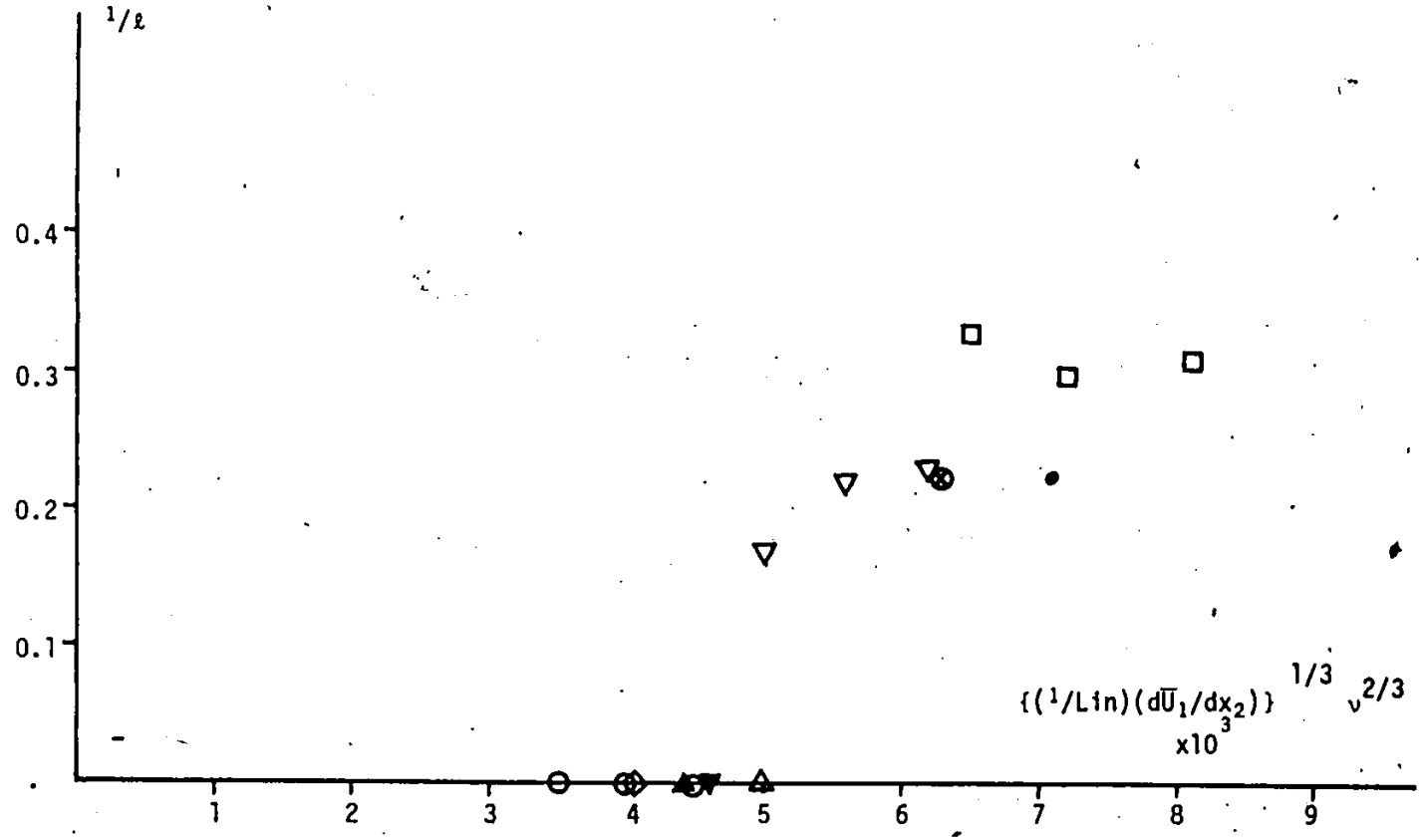

Figure 57:

Correlation of $^1/_\ell$ with the characteristic velocity.
□ - unobstructed flow; ▽ m2.54; O m5.08, ● m1.27,
⊗ Tavoularis & Corrsin, x Rose, ◇ Champagne et al,
△ Mulhearn & Luxton, ▲ m5.08, m2.54, ▼ m5.08, m2.54, m1.27.

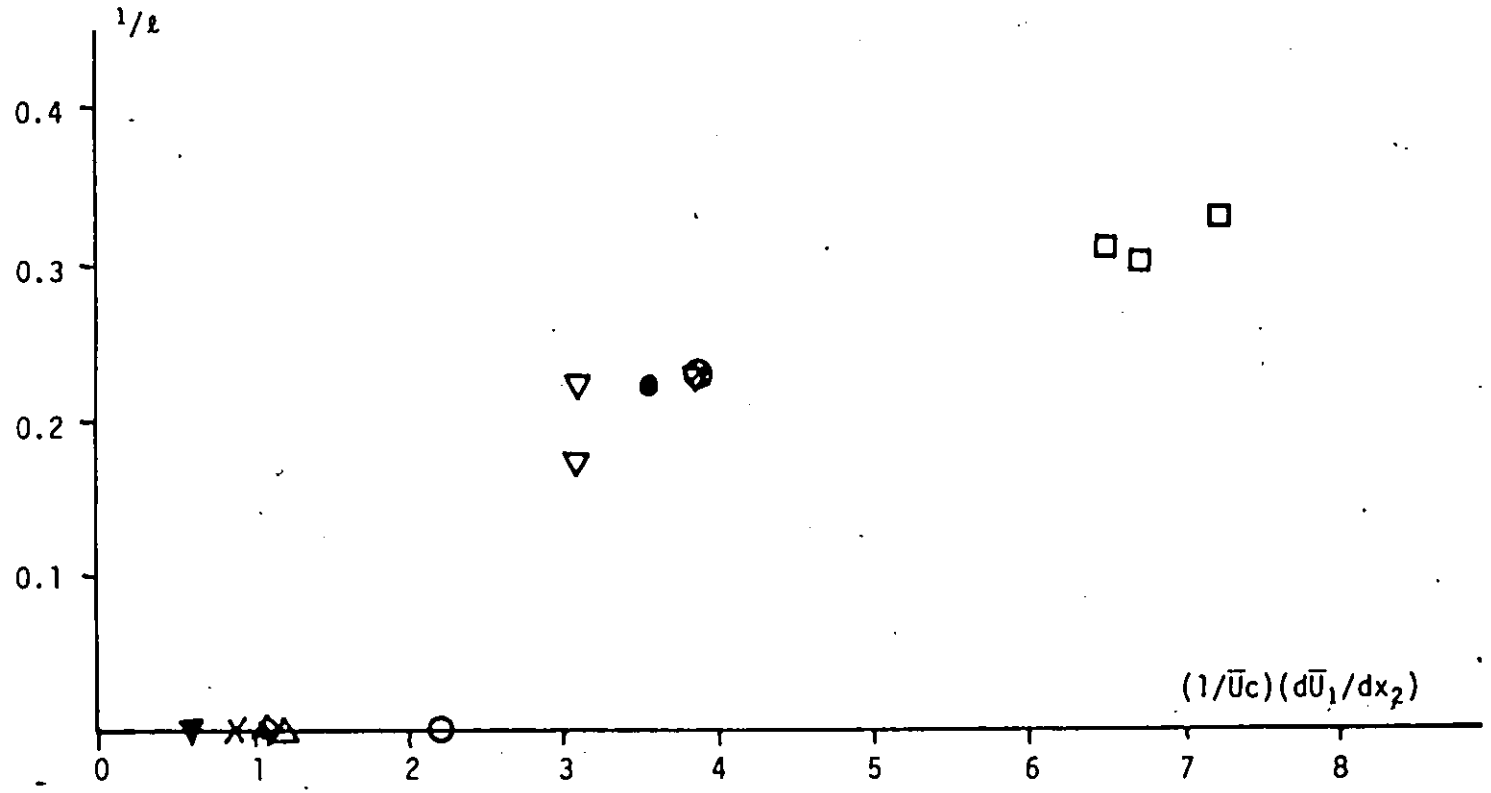

Figure 58:

Inverse characteristic length v/s $(1/\bar{U}c)(d\bar{U}_1/dx_2)$. Symbols as in Figure 57.

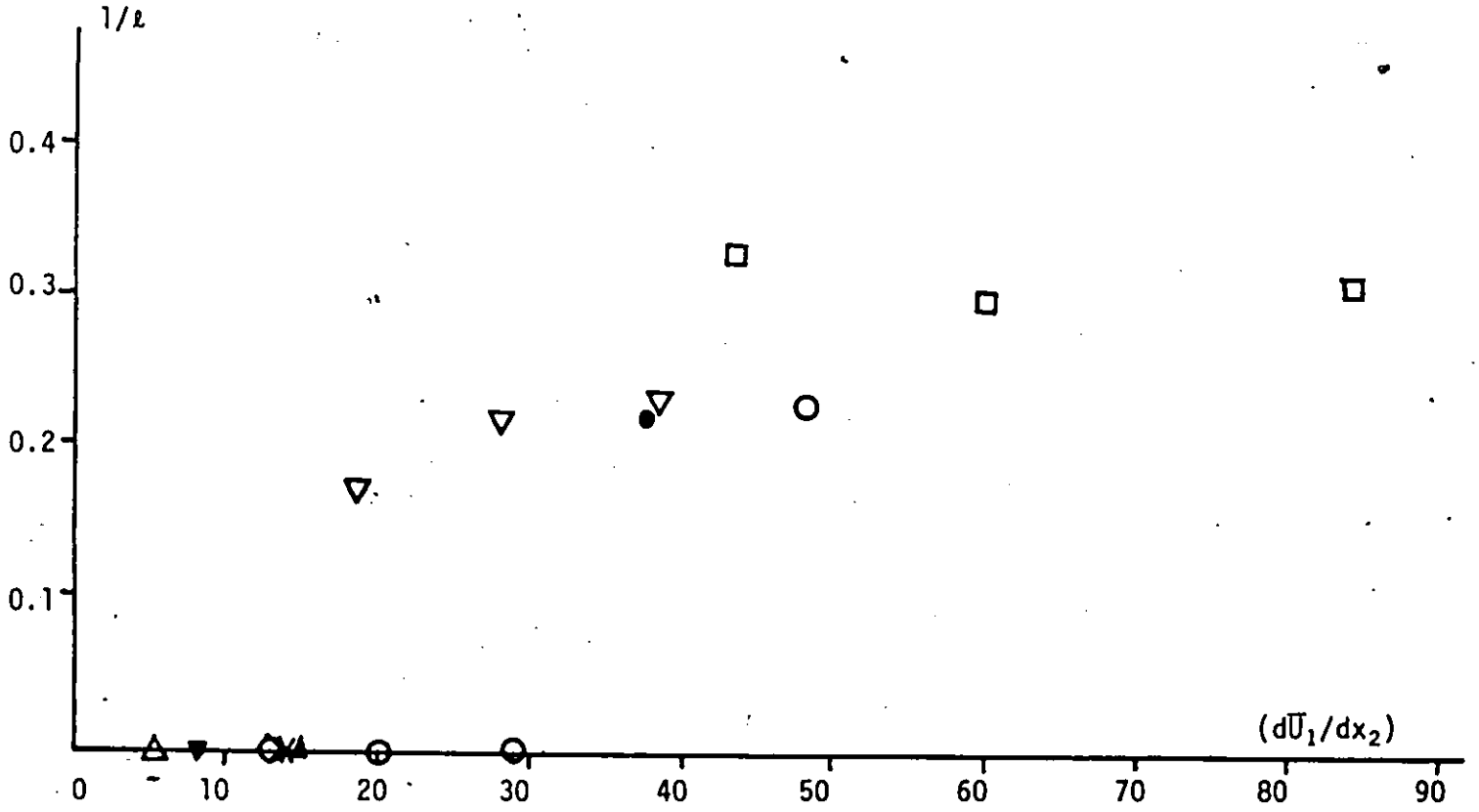

Figure 59:

Inverse characteristic length v/s mean shear. Symbols as in Figure 57.

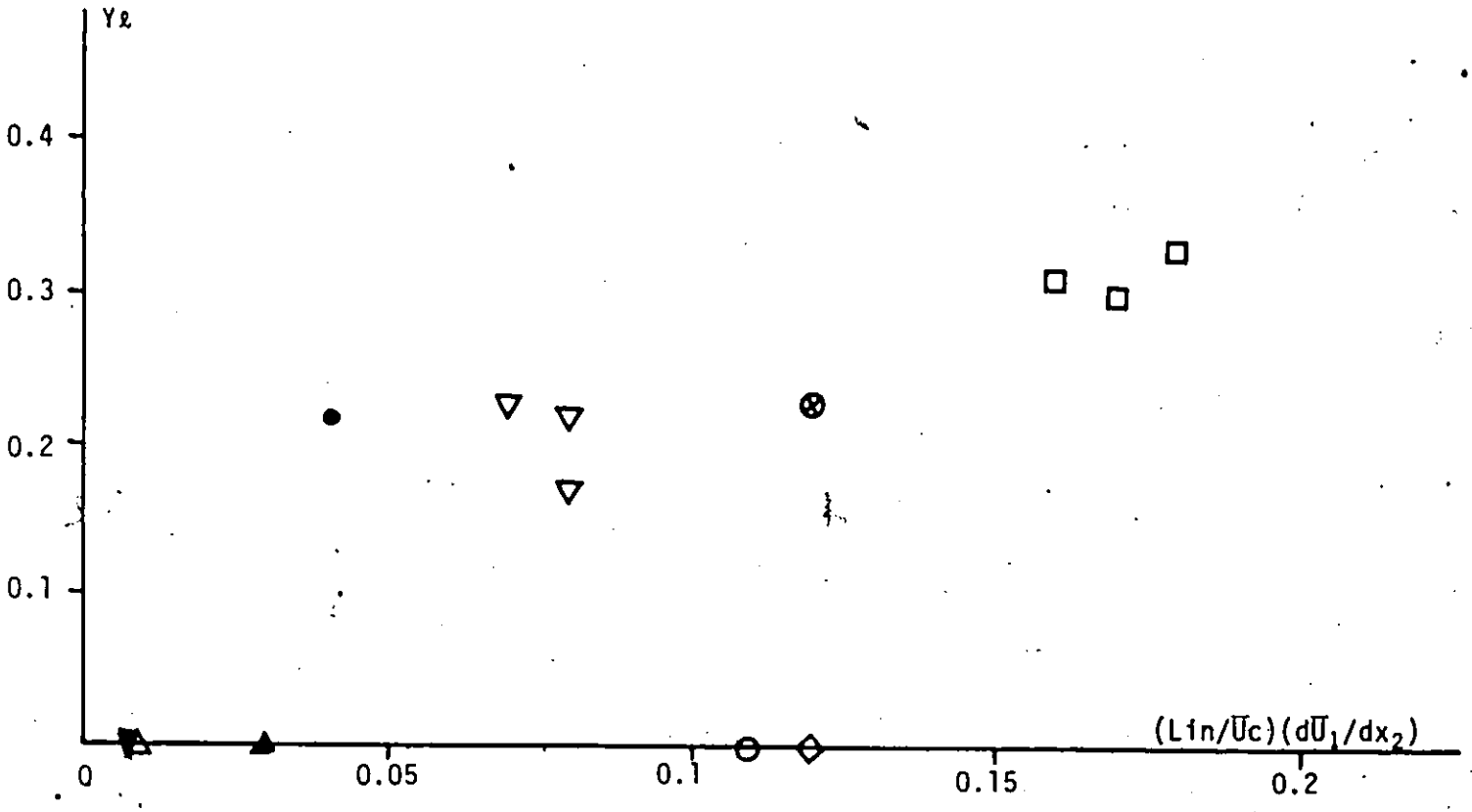

Figure 60:

Inverse characteristic length v/s total strain. Symbols as in Figure 57.

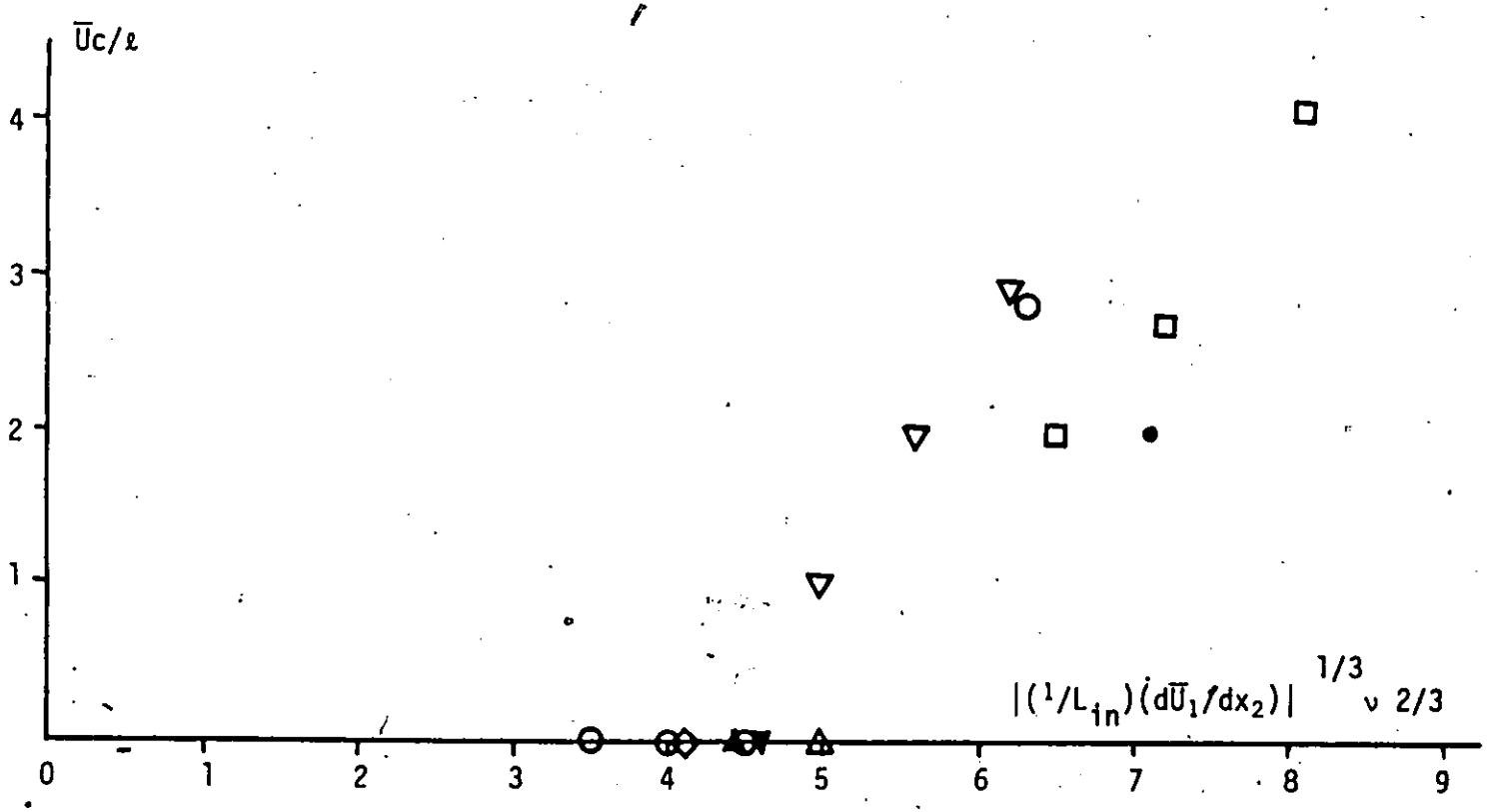

Figure 61:

Time constant v/s characteristic velocity. Symbols as in Figure 57.

Chapter VII

CONCLUSIONS

The present study has investigated universal features and brought into focus some interesting observations of uniformly sheared turbulence. Briefly, the following could be concluded

1. Introduction of a grid into a uniformly sheared turbulent flow reduced the magnitude of the incoming shear by a constant value depending on the rod spacing of the grid. This value was independent of the position of insertion of the grid.

2. The turbulent kinetic energy and the Reynolds stress tensor components either grew exponentially or reached an asymptotic constant value depending on whether the value of the characteristic velocity (u_c) was greater or smaller than a barrier velocity (u_b); the characteristic velocity (Hasen, 1966) was a function of the initial length scale and the mean shear.

3. The dimensionless Reynolds stress tensor was approximately constant in the asymptotic state and had quasi - universal values for all investigations of uniformly sheared turbulent shear flows.

4. The streamwise velocity integral length scales grew nearly exponentially but not at the same rate as the turbulent kinetic energy. Interestingly however, the length scale growth rate for a given geometry was independent of the value of the mean shear.

BIBLIOGRAPHY

Batchelor,G.K., 1956, The theory of homogeneous turbulence, Cambridge Univ. Press, Cambridge.

Benedict, R.P., 1977, Fundamentals of temperature, pressure and flow measurements (2nd edition), Wiley & Sons, New York.

Bradshaw, P., 1971, Introduction to turbulence and its measurements, Pergamon Press, New York.

Burgers, J.M., and Mitchner, M., 1953, On homogeneous non-isotropic turbulence connected with a mean motion having a constant velocity gradient', Konik. Ned. Akad. v. Wet.B, 15, 228(Part , 383).

Champagne, F.H., Harris, V.G.,and Corrsin, S., 1970, Experiments on nearly homogeneous turbulent shear flow, J. Fluid Mech., 8, 209.

Comte-Bellot, G., 1976, Hot-wire anémometry, Ann. Rev. Fluid Mech., 8, 209.

Corrsin, S., 1963, Turbulence : Experimental methods, Handbuch der Physik, 8(2), 525.

Craya, A., 1958, Contribution a l'analyse de la turbulence associee a dse vitesses moyennes, Publ. Scien. et Tech. du Ministere de l'air, No. 345.

Deissler, R.G., 1961, Phys. Fluids, 4, 1187.

Elder, J.W., 1959, Steady flow through non-uniform gauzes of arbitrary shape, J. Fluid Mech., 5, 355.

Feiereisen, W.J., Shirani, E., Ferziger, J.H., and Reynolds, W.C., 1982, Direct simulation of homogeneous turbulent shear flow on ILLIAC IV computer, Third international symposium on turbulent shear flows 3.

Fox, J, 1964, Phys. Fluids, 7, 562.

Harris, V.G., Graham, J.A., and Corrsin, S., 1977, Further experiments in nearly homogeneous turbulent shear flow, J. Fluid Mech., 81, 657.

Hasen, E.M., 1966, A non-linear theory of turbulence onset in a shear flow, J. Fluid Mech., 29, 721.

Hinze, J.O., 1975, Turbulence (2nd edition), McGraw-Hill, New York.

Marton, L., and Marton, C., 1981, Methods of experimental physics -Fluid dynamics, vol. 18 part A, Academic Press, New York.

Mulhearn, P.J., and Luxton, R.E., 1975, The development of turbulence structure in a uniform shear flow, J.Fluid Mech., 68, 577.

Ower, E., and Pankhurst, R.C., 1966, The measurement of air flow, (4th edition), Pergamon Press, Oxford.

Perry, A.E., 1982, Hot-wire anemometry, Oxford univ. press, New York.

Reis, F.B., 1952, Studies of correlation and spectra in homogeneous turbulence, PhD Dissertation, M.I.T., Cambridge, Mass.

Reynolds, A.J, 1974, Turbulent flows in engineering, Wiley & Sons, New York.

Reynolds, O., 1894, On the dynamical theory of incompressible fluids and the determination of the criterion, Phil. Trans. Roy. Soc. London, 186, 123.

Richards, B.E., 1977, Measurement of unsteady fluid dynamic phenomena, Hemisphere Publishing Corporation.

Rogallo, R.S., 1977, An ILLIAC program for the numerical simulation of homogeneous incompressible turbulence, NASA Tech. Memo., 73, 203.

Rose, W.G., 1966, Results of an attempt to generate a homogeneous turbulent shear flow, J. Fluid Mech., 25, 97.

Rose, W.G., 1970, Interaction of grid turbulence with a uniform mean shear, J. Fluid Mech., 44, 767.

Shaanan, S., Mixing of a passive scalar in homogeneous turbulent shear flows, PhD thesis, Eng. dept., Stanford University.

Tavoularis, S., 1978, Experiments in turbulent transport and mixing, PhD Dissertation, Johns Hopkins Univ., Baltimore, Maryland.

Tavoularis, S., 1982, Theory of turbulence, lecture notes for a Graduate course, Univ. of Ottawa, Ontario.

Tavoularis, S., 1983, Asymptotic laws for transversely homogeneous turbulent shear flows, submitted for publication.

Tavoularis, S., and Corrsin, S., 1981, Experiments in nearly homogeneous turbulent shear flow with a uniform mean temperature gradient, J. Fluid Mech., 104, 311.

Tennekes, H., and Lumley, J.L., 1972, A first course in turbulence M.I.T. press, Massachusettes.

TSI Manual, General syatem information for 1050 series.

TSI Manual, Instructions for models 1050, 1051 and 1052.

TSI, Technical Bulletin no.5, Hot film and hot wire anemometry, theory and application.

Schubauer, G.B., and Tchen, C.M., 1961, Turbulent flow, Princeton Univ. Press, New Jersey.

Appendix A

PROCEDURE FOR HOT-WIRE MANUFACTURING

A.1 APPARATUS AND MATERIALS

30 percent concentration nitric acid, flexible tubing, glass tube with regulating valve and platinum electrode, glass nozzles of diameters 0.5 mm amd 1 mm, 6V battery, connecting wires, vise, microscope, stand, stainless tubes (30.5 cm long), steel broaches (0.07 cm diameter tapered to a sharp point), two- and four-way thermocouple ceramic tubes (30.5 cm long), epoxy, Wollaston wire (5 um diameter, 10% rhodium-platinum core and 1.2 um diameter, platinum core, both silver coated).

A.2 PROBE BODY FABRICATION

Steel prongs were soldered to wire leads which were inserted into the bores of the ceramic tube, such that the prong tips were exposed over about 2 cm and the wire leads protruded from the other end. The entire assembly was inserted into the stainless steel tube and both ends were epoxied.

In the case of the cross-wire, the prongs and the leads were made of one piece namely a copper wire (0.07 cm in diameter). Four such wires inserted into the bores of a ceramic tube were exposed at one end by about 2 cm to serve as prongs and protruded from the other end in the form of leads. The prongs were shaped such that they were perfectly aligned in three mutually perpendicular planes. The distance between a pair of prongs in a plane perpendicular to that of the wire was 1-2 mm whereas in the plane of the wire the distance between the prongs was 4-5 mm.

A.3 WIRE MOUNTING

(a) The probe holder was fastened in a small portable vise.

(b) Old solder and rust were removed from the prongs with the use of a smooth file and fine sand paper.

(c) A small amount of flux paste (Mastercraft solder paste) was applied to the prong tips.

(d) With the use of a soldering gun (Weller 140/100 Watts) a small bead of solder was applied to each prong tip.

(e) A small, slightly arched piece of Wollasten wire was cut and clamped on one end in a pincher clamp.

(f) A minute amount of flux paste was re-applied to the prongs tips and the wire was positioned across the prongs in bare contact with both prong tips.

(g) The prongs were heated with a temperature controlled (650 F) soldering pencil (Weller) until the solder engulfed the wire ends. A test for proper mounting was that the bit of wire extending beyond the prongs should snap and break when bent.

(h) Reheating of the soldered ends was occasionally done to relieve stresses in the wire.

In the case of the cross-wire, the pair of prongs in the plane of the wire were notched at the tips, such that the wire, when placed along these notches made an angle of 45 with the prongs. The other pair of prongs were notched similarly such that the wire placed along these notches was perpendicular to the first wire.

A special paste (Alpha microcream) was used as a solder to facilitate quick and easy soldering, avoid the possibility of large beads and eliminate the need for a flux.

A.4 WIRE ETCHING

(a) The acid jet was set up as shown in Figure 57. To avoid hazardous evaporation of acid, the acid container was filled just before use and emptied afterwards.

(b) The probe was connected to th positive pole and the acid to the negative pole of a 6V battery through a 200,000 ohm resistor. Hence, the current through the unetched wire was about 0.03 mA and dropped slightly after etching.

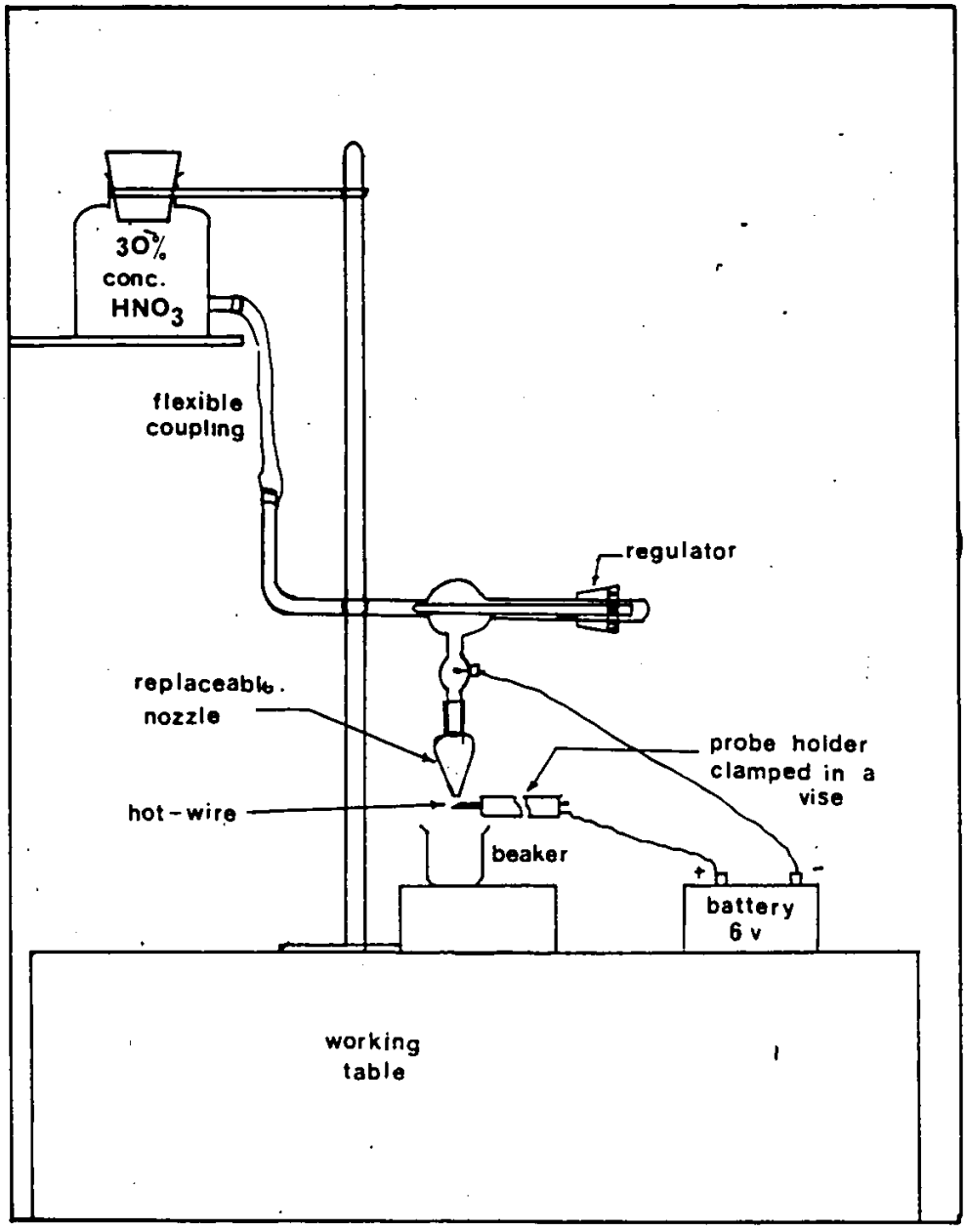

Figure 57. Set up of wire etching apparatus

(c) The regulator was adjusted to produce a stable laminar jet through the nozzle. The nozzle diameter choice was determined by the desired length of the sensor.

(d) The middle section of the wire was immersed into the laminar jet stream and held steady for about 1 to 2 minutes until the silver coating was completely etched and the platinum core exposed.

(e) The wire was inspected under a microscope to confirm that the etching was complete and that the sensing element was intact.

(f) The wire resistance was measured with the TSI anemometer bridge.

(g) Unused probes were stored in a locking cabinet equipped with shockless mounts.

Appendix B

MATHEMATICAL ANALYSIS FOR CROSS-WIRE RESPONSE

In order to obtain the transverse velocity fluctuations by direct addition and subtraction of the two signals of a cross-wire, it is essential that the slopes of their calibration curves be identical. The following analysis demonstrates this fact.

B.1 WIRE RESPONSE NEGLECTING TANGENTIAL HEAT TRANSFER

B.1.1 Non-linearized anemometer output

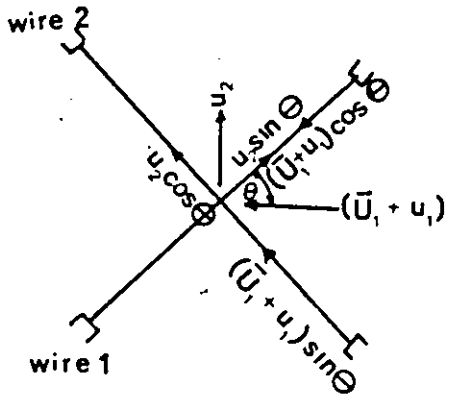

Consider the response of wire 2. It is cooled by an effective velocity Ueff given by

$$U_{eff} = (\bar{U}_1 + u_1)\cos\theta + u_2 \sin\theta \qquad (1.1)$$

where $\bar{U}_1$ is the mean velocity in the x_1 direction, u_1 u_2 are the fluctuating velocities in the x_1 and x_2 direction respectively, and θ is the angle made by the wire with the x_1 - axis.

The anemometer output of this wire is related to the effective velocity by

$$E_2^2 = A_2 + B_2 U_{eff}^n \tag{1.2}$$

where E_2 is the instantaneous anemometer output in volts, A B and n are constants.

Equation (1.2) can be written as

$$E_2^2 = A_2 + B_2[U_1 cos\theta + u_1 cos\theta - u_2 sin\theta]^n$$

Decomposing the instantaneous values into their mean and fluctuating parts we obtain

$$(E_2 + e_2)^2 = A_2 + B_2[U_1 cos\theta + u_1 cos\theta - u_2 sin\theta]^n$$

Expanding binomially and neglecting the higher order terms

$$E_2^2 + 2E_2 e_2 - A_2 = B_2(U_1 cos\theta)^n\left[1 + \frac{u_1}{U_1} - \frac{u_2}{U_1} tan\theta\right] \tag{1.3}$$

Averaging equation (1.3) we get

$$E_2^2 = A_2 + B_2(\bar{U}_1 cos\theta)^n \tag{1.4}$$

Subtracting equation (1.4) from equation (1.3) we obtain

$$e_2 = \frac{B_2}{E_2} \frac{\bar{U}_1^{n-1}(cos\theta)^n n}{2}[u_1 - u_2 tan\theta] \tag{1.5}$$

A similar analysis for wire 1 would yield

$$e_1 = \frac{B_1}{E_1} \frac{\bar{U}_1^{n-1}(sin\theta)^n n}{2}[u_1 + u_2 cot\theta] \tag{1.6}$$

Thus from equations (1.5) and (1.6) it is evident that if the slopes $B_1 = B_2$ and $\theta = 45^0$ then,

$$u_1 = (e_1 + e_2)\frac{1}{2k}$$

$$u_2 = (e_1 - e_2)\frac{1}{2k}$$

B.1.2 Linearized anemometer output

In this case the instantaneous output in volts is linearly related to the effective velocity as

$$E_2 = C_2 U_{eff}$$

$$E_2 = C_2[(U_1 + u_1)\cos\theta - u_2 \sin\theta] \tag{2.1}$$

Decomposing the instantaneous values into their mean and fluctuating parts and simplifying as in section B 1.1 we get

$$e_2 = C_2 \cos\theta (u_1 - u_2 \tan\theta) \tag{2.3}$$

$$e_1 = C_1 \cos\theta (u_1 + u_2 \cot\theta) \tag{2.4}$$

If $\theta = 45^{\circ}$ and the slopes C_1 and C_2 are equal then

$$u_1 = \frac{(e_1 + e_2)}{2c}$$

$$u_2 = \frac{(e_1 - e_2)}{2c}$$

B.2 . WIRE RESPONSE INCLUDING TANGENTIAL HEAT TRANSFER

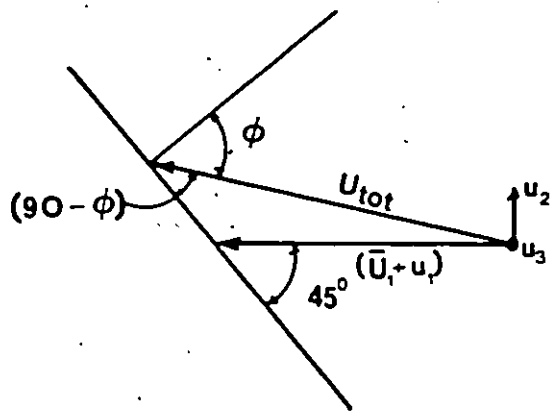

When considering the heat lost from the hot wire by means other than direct cooling by the flow velocity e.g. conduction through the prongs also known as end losses, Champagne and Sleicher proposed an expression for the effective velocity given by

$$U_{eff}^2 = U_{tot}^2[\cos^2\phi + k^2\sin^2\phi]$$

$$U_{eff}^2 = U_{tot}^2[1-(1-k^2)\sin^2\phi] \qquad (1)$$

Assume that the wire forms an angle of 45 with the -axis. Then

$$U_{tot}^2 = (\bar{U}_1 + u_1)^2 + u_2^2 + u_3^2$$

where $\bar{U}_1$ is the mean velocity in the x_1-direction, u_1, u_2, u_3 are fluctuating velocities in the x_1, x_2, x_3 direction and $\bar{U}_{tot}$ is the total velocity

and

$$45^\circ = 90^\circ - \phi + \sin^{-1}\frac{u_2}{\sqrt{(U_1+u_1)^2+u_2^2+u_3^2}}$$

$$\phi = 45^\circ + \sin^{-1}(\xi)$$

$$\sin\phi = \frac{\sqrt{2}}{2}\left[\sqrt{1-\xi^2}+\xi\right]$$

$$\sin\phi \approx \frac{\sqrt{2}}{2}\left[1+\frac{u_2}{\sqrt{(U_1+u_1)^2+u_2^2+u_3^2}}\right]$$

substituting in equation (1) we obtain

$$U_{eff}^2 = [(U_1+u_1)^2+u_2^2+u_3^2]\left[1-\frac{1}{2}(1-k^2)\left(1+\frac{2u_2}{\sqrt{(U_1+u_1)^2+u_2^2+u_3^2}}\right)\right] \qquad (2)$$

On neglecting higher order terms and simplifying we get

$$U_{eff} \approx \frac{U_1}{\sqrt{2}}(1+k^2)^{1/2}\left[1+\frac{(u_1-u_2)}{U_1(1+k^2)}+\frac{K^2(u_1+u_2)}{U_1(1+k^2)}\right] \qquad (3)$$

B.2.1 Non-linearized anemometer output

From Kings law we have

$$E_1^2 = A_1 + B_1 U_{eff}^n$$

where E_1, A_1, B_1 have the usual meaning.

Substituting the value of $\bar{U}_{eff}$, decomposing the instantaneous values into their corresponding mean and fluctuating parts, expanding and neglecting higher order terms, and following a similar simplification as in section B 1.1, we get

$$e_1 = \frac{1}{2E_1}\frac{B_1}{(\sqrt{2})^n}(1+k^2)^{\frac{n}{2}-1}U_1^{n-1}n[(u_1-u_2)+k^2(u_1+u_2)]$$

$$e_2 = \frac{1}{2E_2}\frac{B_2}{(\sqrt{2})^n}(1+k^2)^{\frac{n}{2}-1}U_1^{n-1}n[(u_1+u_2)+k^2(u_1-u_2)]$$

It can be seen that if $\theta = 45^\circ$ and slopes B_1 and B_2 are identical then

$$u_1 = \frac{1}{2p(k^2+1)}(e_1+e_2)$$

$$u_2 = \frac{1}{2p(k^2-1)}(e_1-e_2)$$

B.2.2 Linearized anemometer output

In this case the instantaneous anemometer output in volts is related to the effective velocity as

$$E_1 = C_1 U_{eff}$$

Once again following a similar analysis as in section B 1.1 we get

$$e_1 = C_1 \frac{1}{[2(1+k^2)]^{1/2}}[(u_1 - u_2) + k^2(u_1 + u_2)]$$

$$e_2 = C_2 \frac{1}{[2(1+k^2)]^{1/2}}[(u_1 + u_2) + k^2(u_1 - u_2)]$$

If slopes C_1 and C_2 are identical and if $\theta = 45^\circ$ then

$$u_1 = \frac{1}{2m(k^2+1)}(e_1 + e_2)$$

$$u_2 = \frac{1}{2m(k^2+1)}(e_1 - e_2)$$